CELL SCAFFOLD- AND DRUG-BASED STRATEGIES FOR IMPROVING THE INTEGRATION OF NEURAL PROSTHESES INTO BRAIN TISSUE

by

Erin Kay Purcell

A dissertation submitted in partial fulfillment
of the requirements for the degree of
Doctor of Philosophy
(Biomedical Engineering)
in The University of Michigan
2008

Doctoral Committee:

Professor Daryl R. Kipke, Chair
Professor David C. Martin
Associate Professor Jack M. Parent
Associate Professor Shuichi Takayama

DEDICATION

To my wonderful loving and supportive family: my husband Jake, my daughter Scarlett, and Baby #2

ACKNOWLEDGEMENTS

Daryl Kipke has been an incredibly supportive advisor. He allowed me to freely design and pursue the research studies that I found the most interesting. He helped me allocate the resources needed to complete my work; I am especially thankful for the trip to Dr. David Mooney's lab at Harvard that he arranged for me to gain cell encapsulation expertise. I am very grateful for the support he showed for me through my pregnancies and maternity leave while in his lab, and the understanding he has shown for work/family life balance. In addition, my committee has provided wonderful support and feedback to me, and I would like to thank Dr. Takayama, Dr. Parent, and Dr. Martin for all of their time and effort.

Several individuals worked on the research described in this dissertation. Aparna Singh and Soumya Yandamuri were hard-working and dedicated undergraduate students who are co-authors on the research described in chapters 2 and 4. Jackie Gauthier worked on developing initial *in vitro* methods used for cell encapsulation. Elizabeth Nunamaker, a former graduate student in our lab, initiated the study described in Chapter 3, and is the first author on the manuscript published from that work. John Seymour, a fellow graduate student in the lab, fabricated the probes and developed the quantification techniques for analyzing tissue response used in Chapters 4 and 5. He is a co-author on the Chapter 4 work. Dave Thompson is a co-author on the Chapter 5 research; he was

a first year graduate student who assisted with surgeries, recordings, and MatLab coding. I was very lucky to work with all of these individuals, who not only made such terrific contributions to the projects, but were also so enjoyable to work with.

There are several other people who have likewise added immeasurably to my graduate experience. Members of the Neural Engineering Lab provided valuable feedback, insightful discussions, and necessary training on so many occasions, and made for a fun and dynamic work environment. I particularly would like to thank Rachel Miriani, Kip Ludwig, Taegyun Moon, Liz Nunamaker, John Seymour, and Jey Subbaroyan. Jess Kemppainen, Elisa Cosgrove, and Alexandra Teuscher have been great friends during my time in the program. Members of my "old lab", headed by Dr. James Russell, helped me learn numerous techniques and have been great friends as well, and I would particularly like to acknowledge Dr. Rita Cowell and Dr. Alison Berent-Spillson. These two women also showed me that it is possible to have children and earn a PhD. Sarah Richardson-Burns and Jeff Hendricks from Dr. David Martin's lab have provided many helpful discussions. The wonderful core facilities at the University, including the MIL and Organogenesis cores, have been instrumental in the research reported here. I would like to thank Marta Dzaman and Shelley Almburg for their assistance. Finally, thanks to the staff in the Biomedical Engineering offices, especially Maria Steele, Tonya Thompson, and Vera Williams for all of their assistance over the years.

My family has supported me throughout my graduate career, and I am especially grateful to my husband, Jake. He made many sacrifices so that I could pursue my goals. When I

was discouraged, he gave me the confidence to keep going. He supported me in so many ways, whether it was through encouraging words, taking care of the household when I needed to work or study, or listening to me practice talks or reviewing papers and proposals for me. He has been the best partner I could hope for. My extended family has always been there for me as well; especially my father, brother, grandmother, aunt Jean, step-mom and in-laws. I would finally like to thank my late mother, Jane, for being a wonderful mother, teaching me to work hard and be a good student, and to have compassion for those who suffer from neurological disease.

TABLE OF CONTENTS

LIST OF FIGURES

LIST OF TABLES

LIST OF APPENDICES

ABSTRACT

Neuroprosthetic devices record extracellular cortical signals which may then be used to place exterior devices under a patient's direct control. Therefore, these systems have the potential to restore function to individuals immobilized by paralysis or neurodegenerative disease. For neuroprosthetics to be useful in clinical and research settings, long-term, stable recordings must be achieved. However, these devices are plagued by recording instability, and the reactive tissue response that occurs after insertion into the brain is a likely cause. Specifically, neuronal density is reduced surrounding devices, and glial encapsulation (composed of microglia and astrocytes) isolates neuroprostheses from their neuronal signal sources.

The research presented describes the development and evaluation of two strategies to improve the tissue response to neuroprostheses: (1) a neural stem cell (NSC)-seeded scaffold and (2) a cell cycle-inhibiting drug. NSCs were hypothesized to secrete factors, such as neurotrophins, which would improve device-tissue integration. The cells were encapsulated in an alginate hydrogel and seeded into a well on the neural prostheses. Two studies were conducted to develop the cell-seeded device. In the first study, *in vitro* testing identified the alginate composition which provided optimal scaffold mechanical stability as well as support of neurotrophic factor release from encapsulated NSCs. The second study characterized the relationship between alginate composition, degradation, and biocompatibility *in vivo*. The third study evaluated the effects of the NSC scaffold

on the tissue response to implanted probes *in vivo*. Quantitative histological examination revealed that the NSC-seeded alginate scaffold mitigated the early tissue response to an implanted prosthesis, but exacerbated it by six weeks post-implantation. Based on research showing a link between central nervous system injury and cell-cycle re-entry by neurons, astrocytes, and microglia, the final study of the dissertation investigated the role of cell cycle re-entry in the tissue response to neural prostheses. Specifically, the study explored the effects of a cell cycle-inhibiting drug (flavopiridol) on electrophysiology and tissue response metrics. Flavopiridol reduced the appearance of a cell cycle protein (cyclin D1) in microglia surrounding probes three days after implantation and decreased impedance over the 28 day study period. Additionally, the data revealed several novel, significant correlations between recording quality, impedance, and endpoint histology measurements.

In conclusion, the studies demonstrate significant effects of two intervention strategies on tissue response and electrophysiology measurements, characterize alginate stability and its use as a NSC scaffold, and add insight into the relationship between the tissue-device interface and recording quality.

CHAPTER 1
INTRODUCTION

Neural Prostheses: Development, Therapeutic Potential, and Performance

The discovery in 1870 by Fritsch and Hitzig that the cerebral cortex was electrically excitable, and that stimulation of defined regions within it produced contralateral movement in dogs, provided the basis for decades of neurophysiology studies and dismissed the prevailing notion that the cortex was an insignificant "rind" (the Latin meaning of "cortex") (Gross 2007). Gasser and Erlanger used a cathode ray oscilloscope to measure conduction velocities and describe action potential waveforms in the sciatic nerve of mammals and frogs beginning in the 1920's, and were awarded the Nobel Prize in 1944 for this work (Perl 1994). In 1939, Hodgkin and Huxley directly recorded action potentials intracellularly from the giant axon of the squid, representing the first time this feat was achieved (Hodgkin and Huxley 1939). Nearly 20 years later, the first long-term extracellular recordings from an unrestrained animal were reported using microwires (Strumwasser 1958).

Since then, the current designs for cortical prostheses have been developed, namely microwires, microelectrode arrays, and the planar Michigan probe (Figure 1.1) (Schwartz 2004; Polikov, Tresco et al. 2005). Microwires were the first microelectrodes produced, and typically are composed of rows of eight or more 30–50 micron diameter stainless steel or tungsten wires spaced 200-300 microns apart. They are insulated with

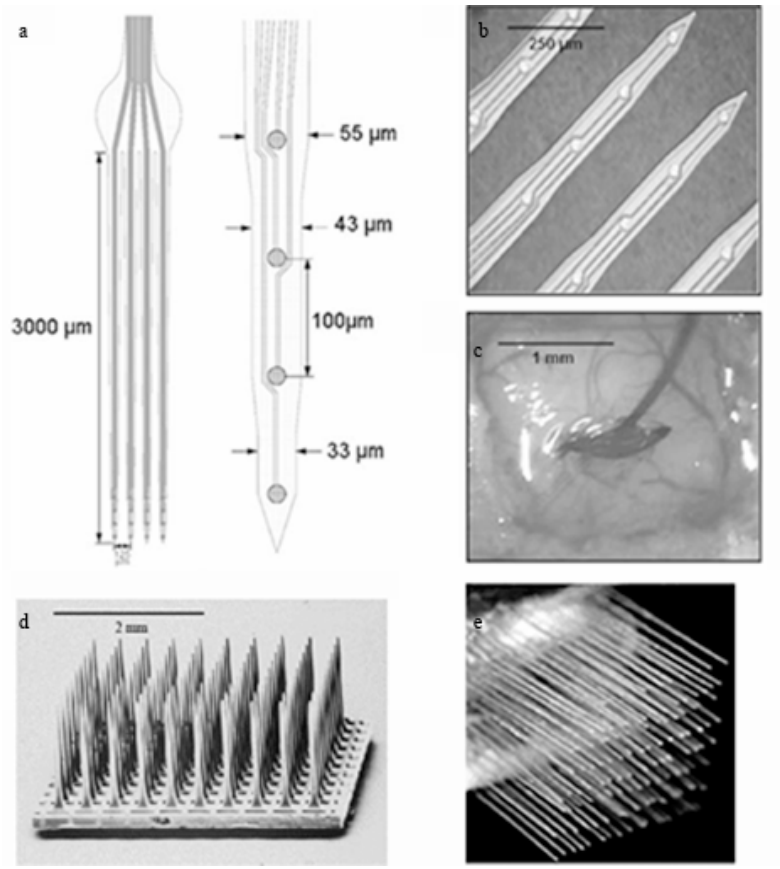

Figure 1.1. Neural probe designs. The schematic and dimensions of an example of a Michigan probe design (a), close-up of a four shank, sixteen site Michigan probe (b), and its insertion into the rat cortex (c) (Vetter, Williams et al. 2004). The Utah microelectrode array (d) (Rousche and Normann 1998). Microwires with a 50 micron diameter used by Nicolelis *et al.* (e) (Nicolelis, Dimitrov et al. 2003).

Teflon or polyimide (Figure 1.1e). Silicon microelectrode arrays developed at the University of Utah have a 10x10 array of microneedles protruding 1.0-1.5 millimeters from a 4x4 squared millimeter area (Figure 1.1d). Platinum or iridium recording sites on the tip of each needle are 25-50 microns in length, and the base of each microneedle is insulated from its neighbors by a glass coating. Planar silicon recording electrodes such as those developed at the University of Michigan use photolithography techniques to create a variety of probe geometries, site sizes and spacings (Figure 1.1a-c). The devices have iridium sites and silicon dioxide/nitride insulation. Available designs vary from 1-4

shanks, 16-32 channels, 2-6 mm shank lengths, and 400-1250 squared micron site sizes (NeuroNexus, http://www.neuronexustech.com/). Unlike microwires and microelectrode arrays, the Michigan probe allows for recordings at varying depths within the cortex. For a review of current probe technologies, see (Schwartz, Cui et al. 2006).

Neural probes, in their varied designs, record extracellular signals from a patient's uninjured cortex. Through oxidation and reduction reactions, charge is transferred from ions in the extracellular space produced during neuronal firing to free electrons in the electrode, resulting in current crossing the electrode-electrolyte interface (Webster 1998). The recordings include low frequency signals (<300 Hz) produced by cell aggregates (local field potentials, LFPs) and single and multi-unit activity ("units," 300 Hz-10 kHz filter setting) resulting from neuronal action potentials. Single and multi-unit signals, and possibly LFPs to a lesser extent, may then be used to place an exterior assistive device under the patient's direct control. Thus, motor function is restored while effectively circumventing impaired neural circuits that have been damaged by traumatic injury or neurodegenerative disease (Schwartz, Cui et al. 2006). These systems are commonly termed "brain-machine interfaces" (BMIs), "brain-controlled interfaces" (BCIs), or, more commonly, neural prostheses (Lebedev and Nicolelis 2006; Schwartz, Cui et al. 2006). Neural prostheses rely on the property of cortical neurons to change their activity in relation to movement parameters (i.e. direction, force, and velocity), as well as the ability to operantly condition subjects to voluntarily modulate their cortical firing rates (Evarts 1968; Fetz 1969; Humphrey, Schmidt et al. 1970; Georgopoulos, Kalaska et al. 1982; Georgopoulos, Schwartz et al. 1986). The feasibility of this strategy was demonstrated in

the last decade when monkeys were shown to able to successfully control a cursor on a computer screen or a robotic arm using voluntary cortical signals (Taylor, Tillery et al. 2002; Carmena, Lebedev et al. 2003). Recent work in tetraplegic humans has shown that neural recordings from motor cortex are possible even years after spinal cord injury, and those spikes were readily modulated when patients imagined making movements (Hochberg, Serruya et al. 2006; Donoghue, Nurmikko et al. 2007). The ability to use these signals to control robotic devices and computer interfaces was confirmed. Further, a recent study has demonstrated cortical control of a complex, multi-jointed robotic arm with a gripper by monkeys during a self-feeding task (Velliste, Perel et al. 2008). Thus, these technologies have the potential to restore some level of function to the 200,000 patients currently suffering from full or partial paralysis in the U.S. (Polikov, Tresco et al. 2005).

While these results are encouraging, these devices are currently plagued by inconsistent performance in terms of recording longevity and stability (Rousche and Normann 1998; Liu, McCreery et al. 1999; Williams, Rennaker et al. 1999; Nicolelis, Dimitrov et al. 2003; Polikov, Tresco et al. 2005; Liu, McCreery et al. 2006; Schwartz, Cui et al. 2006). Rousche and Normann reported that 60% of microelectrode arrays were functional (detected units) after a six month implantation period in cats (Rousche and Normann 1998). Nicolelis *et al.* showed a 58% to 35% drop in the percentage of microwires which recorded units from one month to eighteen months after implantation in a monkey (Nicolelis, Dimitrov et al. 2003). Vetter *et al*. demonstrated that 13/14 implanted Michigan probes were functional over a 127 day study period; however, anecdotal

evidence suggests variable success with this probe type as well (Vetter, Williams et al. 2004). Liu and McCreery *et al.* have shown that microelectrode array recordings tend to be highly variable within the first two months of implantation in cats, and then generally stabilize (Liu, McCreery et al. 1999; Liu, McCreery et al. 2006). However, in some cases recordings became increasingly unstable with time, to the point where no neural activity could be recorded (Liu, McCreery et al. 1999). The longevity of individual electrodes was widely variable (Figure 1.2) (Liu, McCreery et al. 2006). In order for neural prostheses to be clinically useful, stable, long-term recordings from large populations of neurons in multiple brain areas must be reliably and reproducibly achieved (Lebedev and Nicolelis 2006).

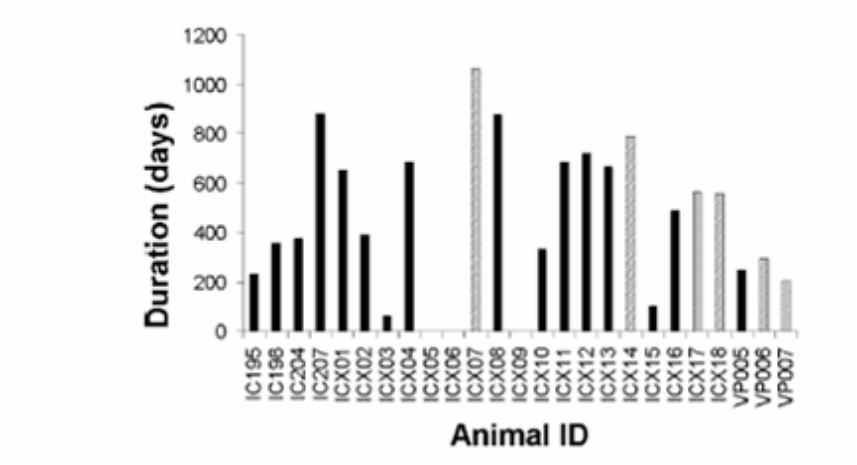

Figure 1.2. The maximum number of days during which neuronal spikes could be resolved on any sites of implanted electrode arrays (Liu, McCreery et al. 2006).

The Reactive Tissue Response to Neural Probes

Following implantation into the brain, a reactive tissue response occurs to probes which is believed to be a major contributing factor to their inconsistent performance. Glia encapsulate the devices, and neuronal density is reduced within the effective recording radius of the probe (Edell, Toi et al. 1992; Turner, Shain et al. 1999; Szarowski, Andersen et al. 2003; Kim, Hitchcock et al. 2004; Biran, Martin et al. 2005; Polikov, Tresco et al. 2005) (Figure 1.3). Thus, there is a loss of the signal source (neurons) surrounding neural prostheses, as well as the formation of a glial sheath which creates a barrier to signal transmission.

The glial sheath is composed of a thin inner coating of microglia surrounded by a thicker layer of astrocytes. Microglia constitute 5-10% of the cells in the brain in number, and are active surveillants of their surrounding environment, sensing injury and displaying immune functions (Polikov, Tresco et al. 2005; Hanisch and Kettenmann 2007). They may be implicated in either the exacerbation or mitigation of central nervous system (CNS) injury depending on the pathology or disease state (Hanisch and Kettenmann 2007). These cells have a "ramified" or branched morphology in their surveilling state, and take on an amoeboid configuration when shifted into an activated state. Activated microglia phagocytose foreign material, proliferate, and produce lytic enzymes to degrade foreign material (Polikov, Tresco et al. 2005). Astrocytes are the second key component of reactive gliosis, and comprise 30-65% of brain cells. They provide structural support for neurons and modulate the environment around them, releasing

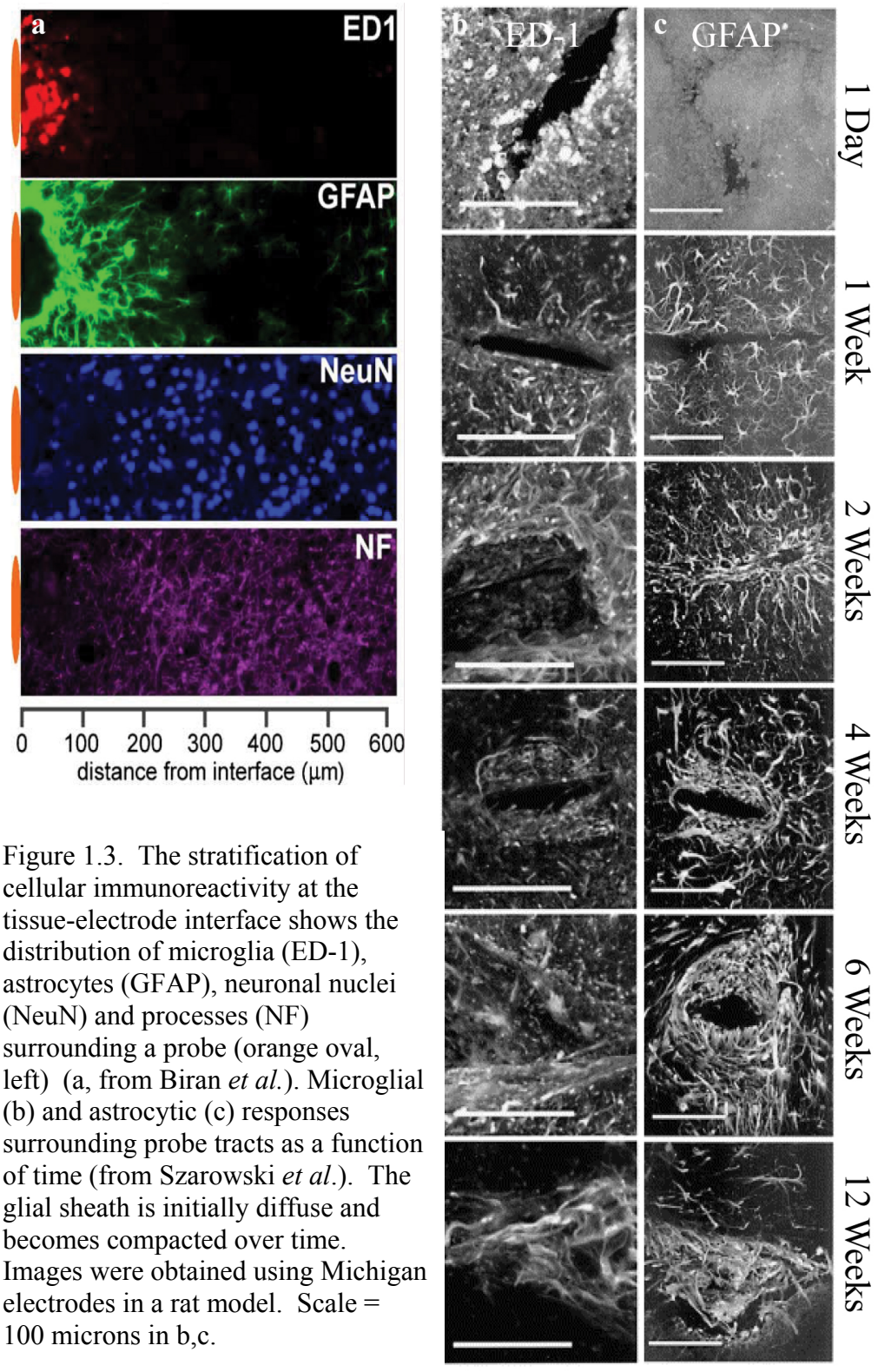

Figure 1.3. The stratification of cellular immunoreactivity at the tissue-electrode interface shows the distribution of microglia (ED-1), astrocytes (GFAP), neuronal nuclei (NeuN) and processes (NF) surrounding a probe (orange oval, left) (a, from Biran *et al.*). Microglial (b) and astrocytic (c) responses surrounding probe tracts as a function of time (from Szarowski *et al.*). The glial sheath is initially diffuse and becomes compacted over time. Images were obtained using Michigan electrodes in a rat model. Scale = 100 microns in b,c.

growth factors and buffering neurotransmitters and ions released during neuronal firing (Svendsen 2002; Polikov, Tresco et al. 2005). They may also regulate synapse production and have a role in neurogenesis (Svendsen 2002). Reactive astrocytes proliferate, migrate, hypertrophy, and upregulate the production of glial fibrillary acidic protein (GFAP, an intermediate filament specific to this cell type) following injury (Polikov, Tresco et al. 2005). Together, microglia and astrocytes form an encapsulation layer around probes which is initially diffuse one week after implantation and later becomes a compact sheath by six weeks in rats (Figure 1.3b-c) (Szarowski, Andersen et al. 2003). Long-term glial encapsulation was also demonstrated in rhesus macaques implanted with microwires at three month and three year time points; microglial reactivity surrounding implants was apparent at the three month time point only, while a robust astrocyte response was observed at both time points (Griffith and Humphrey 2006).

Reduced neuronal density surrounding probes is a potential cause of a loss of signal quality over time. Large amplitude, reliably separated neuronal spikes (or "units") are typically found within 50 microns of recording sites, and no extracellular signals are recorded from neurons located at distances greater than 140 microns from the probe (Henze, Borhegyi et al. 2000). Therefore, the reported 40% loss of neuronal density within 100 microns of the device surface in the first month after implantation is particularly concerning (Biran, Martin et al. 2005). Whether reduced neuronal density indicates a "kill zone," or displacement of neurons by the glial sheath, is debatable (Edell, Toi et al. 1992; Biran, Martin et al. 2005). However, it is clear that this effect is not due to initial insertion trauma, but rather prolonged device-tissue interactions (Biran, Martin

et al. 2005). It has also been demonstrated that the neuronal and glial responses are intertwined; there is an inverse relationship between neurofilament and microglial staining intensity as a function of distance from the probe surface (Biran, Martin et al. 2005). The time course of neuronal density reductions has not been fully characterized; Biran *et al.* report similar reductions at the two and four week post-implant time points (Biran, Martin et al. 2005).

In addition to the more thoroughly investigated glial and neuronal responses, other histological features accompanying probe implantation have been described. Vasculature is severed and dragged upon device insertion, and damage extends several hundred microns from the implant site (Bjornsson, Oh et al. 2006). Implanted probes are associated with an increase in extracellular matrix molecules such as collagen, fibronectin, and laminin around the device (Kim, Hitchcock et al. 2004). Cells attached to explanted probes were shown to secrete detectable quantities of inflammatory cytokines (Biran, Martin et al. 2005). Vimentin staining associated with reactive astrocytes has been shown to follow a similar pattern and time course to GFAP staining (Szarowski, Andersen et al. 2003). The body of evidence regarding the tissue response to implanted neural probes reinforces the conclusion presented by Szarowski *et al*: "active intervention is needed to control the reactive response, heal the vasculature and rescue neurons" to improve the tissue-device interface (Szarowski, Andersen et al. 2003).

While a cause-and-effect relationship between tissue response and recording quality is a widely held belief in the field of neural engineering, explicit evidence and

characterization of this association remains very limited. The glial scar is known to be a potential diffusion barrier to the transmission of ions, neurotransmitters, and growth factors through the extracellular space (Roitbak and Sykova 1999). This may affect not only normal signal transmission, but neural recording by a probe. Additionally, impedance magnitude at 1 kHz (the fundamental frequency of the neuronal action potential) is increased at recording sites with "extensive" glial reactivity (Williams, Hippensteel et al. 2007). While it is reasonable to believe that reductions in neuronal density would result in a loss of signal quality, this has not yet been proven. Likewise, the relative contributions of gliosis and neuronal loss to recording instability, as well as the role of neuronal plasticity and function, have not been explored. Further understanding these issues will result in improved probe modifications to integrate devices with surrounding tissue.

Probe Modifications for Improved Tissue Integration

Various strategies have been used to modify the probe surface with the ultimate goal of improving the device-tissue interface. These include the use of protein-based coatings (Buchko, Kozloff et al. 2001; Cui, Lee et al. 2001; Cui, Wiler et al. 2003; He and Bellamkonda 2005; He, McConnell et al. 2006) , conductive polymers (Cui, Lee et al. 2001; Cui, Wiler et al. 2003; Kim, Abidian et al. 2004; Ludwig, Uram et al. 2006; Richardson-Burns, Hendricks et al. 2007; Richardson-Burns, Hendricks et al. 2007; Abidian and Martin 2008), and hydrogels (Kim, Abidian et al. 2004). These strategies respectively aim to improve or attract neuronal adhesion to recording sites, reduce impedance and increase charge transfer through an effective increase in recording site

surface area, and buffer the mismatch in mechanical properties between the probe and surrounding brain tissue. Relatively few studies have been conducted which implement soluble-molecule releasing scaffolds onto the probe to intervene in this response, and no available published work describes cell-seeded coatings. An *in vitro* study has described the use of BDNF-seeded hydrogels to coat microelectrode arrays (Jun, Hynd et al. 2008). Multiple groups have reported the use of anti-inflammatory drugs such as dexamethasone and minocycline to attenuate the tissue response to neural implants (Shain, Spataro et al. 2003; Spataro, Dilgen et al. 2005; Kim and Martin 2006; Rennaker, Miller et al. 2007; Zhong and Bellamkonda 2007). Dexamethasone released from nanoparticles entrapped in alginate hydrogel probe coatings reduced impedance compared to control probes over a two week implantation period (Kim and Martin 2006). Probes treated with a nitrocellulose-dexamethasone coating reduced astroglial response and neuronal loss over four weeks *in vivo* (Zhong and Bellamkonda 2007). Probes coated with nitrocellulose containing the anti-inflammatory neuropeptide a-melanocyte stimulating hormone (a-MSH) had reduced impedance at 1 kHz *in vitro*, although *in vivo* results were not reported (Zhong and Bellamkonda 2005). Nerve growth factor (NGF)-incorporating polypyrrole coatings reduced impedance on microelectrode recording sites and caused PC-12 cell differentiation *in vitro*, indicating retention of NGF bioactivity (Kim 2005). Kennedy reports the use of a segment of sciatic nerve placed inside a cone electrode to encourage axonal growth into the electrode (Kennedy 1989). In the cone electrode study, recordings were taken over 200 days, although the sample size was very small (2 rats). Interestingly, the authors believe the effectiveness of this approach may have resulted from secretion of nerve growth factor (NGF) and other chemoattractant molecules to the

surrounding neurons. A later study in rats and monkeys revealed central myelinated axons and dendrites penetrating the cone electrode (Kennedy, Mirra et al. 1992). A human ALS patient was implanted with the cone electrode, where NGF-seeded Matrigel was used in place of sciatic nerve. The patient was able to modulate his cortical signals to control a cursor for typing, and the implant was functional for at least 16 months (Kennedy, Bakay et al. 2000). While the approach in these studies showed promise, the methods were complex and somewhat unclear (i.e., NGF dosage is not stated), and the release characteristics of the neurotrophins *in vitro* and *in vivo* are not described. Neurotrophic factor-secreting and cell-seeded scaffolds remain largely unexplored as probe modification techniques. Additionally, pharmaceutical interventions have been limited to anti-inflammatory drugs. In this dissertation, we describe the development and evaluation of two novel strategies to improve the device-tissue interface: a neural stem cell-seeded alginate scaffold, as well as the administration of a cell-cycle inhibiting drug.

Alginate and Cell Encapsulation

Alginate is a polysaccharide polymer derived from brown seaweed. It is composed of D-mannuronic (M) and L-guluronic acid (G) residues in varying proportions (Figure 1.4a). Cross-linking and gel formation takes place when divalent cations (usually calcium) ionically bind carboxylic acid groups of blocks of guluronic acid residues between chains. This is typically illustrated by an eggbox model of binding (Figure 1.4b-c). Alginate is a versatile biocompatible polymer used in a wide range of applications, including endovascular embolization, wound dressings, nerve regeneration grafts, and drug delivery (Thomas 2000; Becker, Kipke et al. 2001; Tonnesen and Karlsen 2002;

Hashimoto, Suzuki et al. 2005). Recent work in our laboratory has explored its use as a dural sealant (Nunamaker 2006). Alginate is also commonly used to encapsulate cells and provide an immuno-isolating barrier between the engrafted cells and the host tissue (Figure 1.4d).

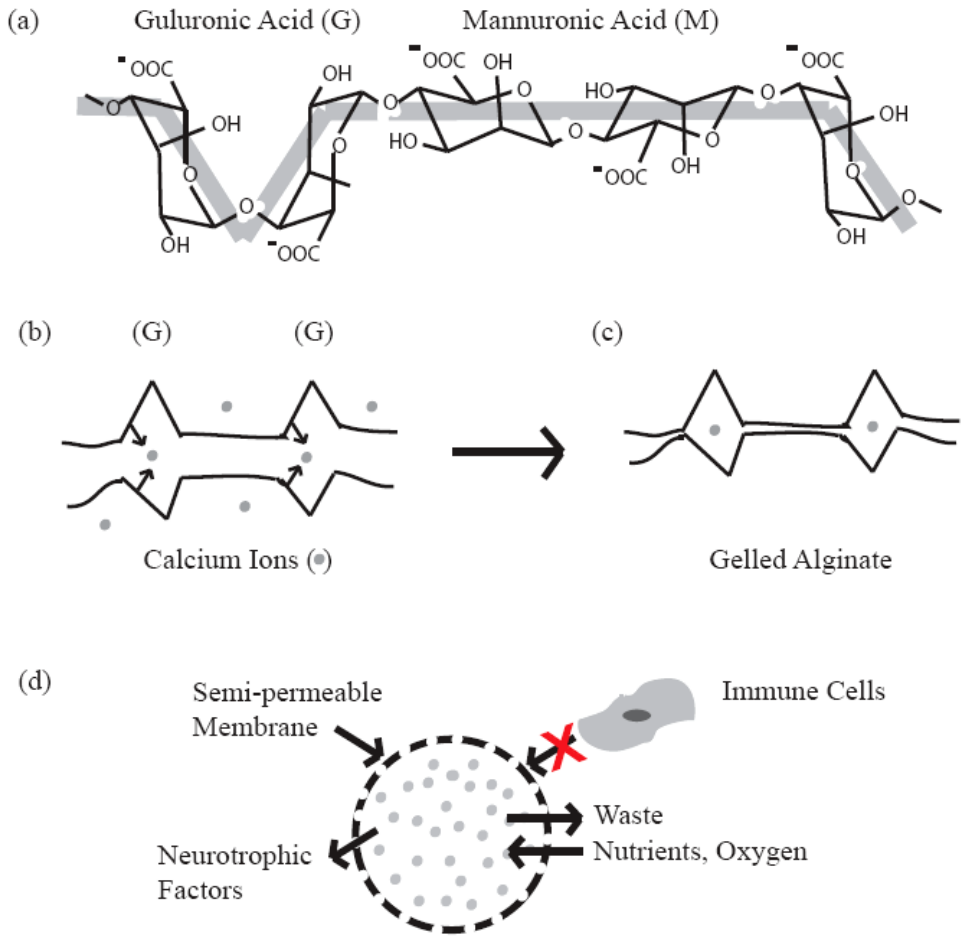

Figure 1.4. Alginate structure (a) and cross-linking mechanism (b-c). Alginate encapsulation is frequently used to protect secretory cells from an immune response while allowing the desired factors to freely pass through the membrane (d).

Pancreatic islets and insulin-secreting cells are the most well characterized alginate-encapsulated cells, where treatment of diabetic patients is the ultimate goal. The literature surrounding this subject is extensive, with ground-breaking work published by Lim and

Sun in 1980. Here, reversal of diabetes in rats implanted with alginate-encapsulated islets was demonstrated for a period of 2-3 weeks (Lim and Sun 1980). Numerous groups have pursued alginate-encapsulated cells for the treatment of a variety of disease states since then (de Vos, Faas et al. 2006).

A relationship between alginate composition and the function of the graft has been demonstrated in numerous studies. Alginate cross-linking ion and concentration, weight percentage, polycation coating, molecular weight, and proportion of G and M residues have been reported to affect cell viability, scaffold stability, diffusion through the gel, and biocompatibility *in vitro* and *in vivo*. Cross-linking ion choice and concentration, as well as alginate molecular weight, may affect a variety of scaffold variables, but these are typically negligible factors in scaffold function at the values used for cell encapsulation studies. Specifically, divalent cations have varying affinities for alginate, and those with higher affinities than calcium (such as lead, cadmium, barium, and strontium) are less sensitive to chelating compounds which may break cross-links and reduce gel mechanical integrity (Strand, Morch et al. 2000). However, these heavy metals are cytotoxic and generally not useful for cell encapsulation. Increasing calcium chloride concentration up to 0.02M during cross-linking increases gel strength, but gel strength is constant with additional increases in $CaCl_2$ concentration and is usually used at a 0.1 M concentration for cell encapsulation (Martinsen, Skjak-Baek et al. 1989). Greater calcium chloride concentration also contributes to increased gel porosity and diffusion (Strand, Morch et al. 2000). Gels with a higher weight percentage of alginate have improved stability, but this may coincide with reduced cell proliferation and viability (Martinsen, Skjak-Baek et

al. 1989; Stabler, Wilks et al. 2001). Increasing molecular weight reduces diffusion through the gel and contributes to increased stability; however, this is a factor only when comparing relatively low molecular weight alginates (Martinsen, Skjak-Baek et al. 1989; Stabler, Wilks et al. 2001). Above a molecular weight of approximately 240,000, alginate stability is determined primarily by G/M content alone (Martinsen, Skjak-Baek et al. 1989; Strand, Morch et al. 2000).

There are reported tradeoffs in the effects of G/M content and the use of polycation coatings in graft stability, function, and biocompatibility, and these metrics must be investigated for new applications and cell types on an individual basis. Poly-L-lysine (PLL), as well as other less common polycation coatings, are often used to stabilize the alginate bead and provide a barrier to immune system components such as IgG (Kulseng, Thu et al. 1997; Gugerli, Cantana et al. 2002). However, the PLL coating layer may itself incite inflammation and toxicity to encapsulated cells (King, Sandler et al. 2001; Strand, Ryan et al. 2001; Rokstad, Holtan et al. 2002; King, Lau et al. 2003). Alginates with high G content are more mechanically stable and permissive to diffusion of proteins than those with a high M content (Martinsen, Skjak-Baek et al. 1989; Martinsen, Storro et al. 1992; Strand, Morch et al. 2000). However, high G alginate has been shown to initially inhibit the metabolic and secretory activity of cells due to growth inhibition, theoretically because a higher strength gel is more difficult for proliferating cells to displace (Constantinidis, Rask et al. 1999; Stabler, Wilks et al. 2001). Therefore, the effects of G/M content and PLL coating should be investigated for new alginate cell encapsulation applications, such as the entrapment of neural stem cells.

Neural Stem Cell Therapy for Central Nervous System Injury

Neural stem cells are self-renewing, multipotent cells capable of producing neurons, astrocytes, and oligodendrocytes (Kornblum 2007). In 1992, Reynolds and Weiss reported the culture of "neurospheres" (heterogenous masses of stem and progenitor cells) derived from single mouse CNS cells and propagated with epidermal growth factor (EGF) (Reynolds and Weiss 1992) (Figure 1.5). The stem cell characteristics of these cells, which were defined as the ability to proliferate, retain multi-lineage potential over time, and generate a large number of progeny, were reported in a later publication (Reynolds and Weiss 1996). In addition to this groundbreaking work, neural stem cells have been discovered and described from a variety of sources: both endogenous and exogenous; adult, fetal, and embryonic; and from CNS regions including the cortex, striatum, cerebellum, hippocampus, subventricular zone, and spinal cord (Ryder, Snyder et al. 1990; Reynolds and Weiss 1992; Weiss, Dunne et al. 1996; Lindvall, Kokaia et al. 2004; Martino and Pluchino 2006; Gaillard, Prestoz et al. 2007; Kornblum 2007; Singec, Jandial et al. 2007; Zhao, Deng et al. 2008). Importantly, neural stem cells have been researched extensively as a source of regeneration or repair for CNS tissue damaged by injury or degenerative disease.

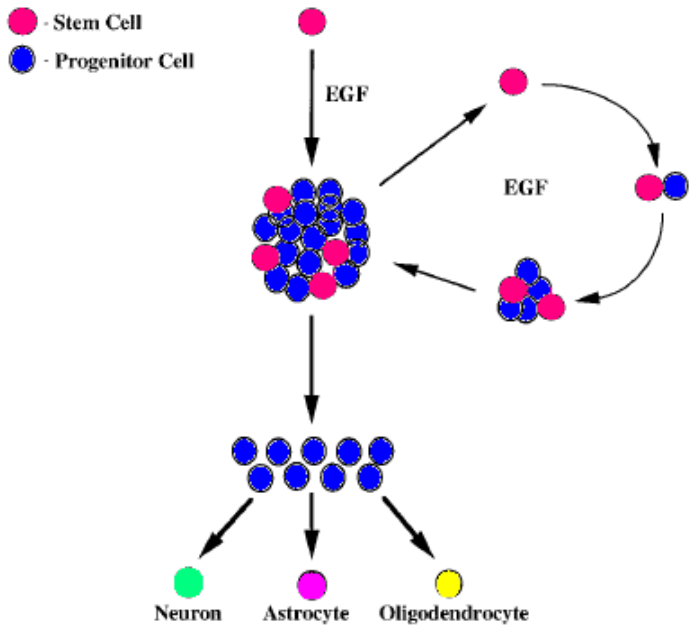

Figure 1.5 (From Reynolds and Weiss, 1996). The EGF-responsive stem cell generates a neurosphere composed of more stem cells (close to 20%, shown in pink) and progenitor cells (blue). The secondary stem cells, when replated alone or in populations, generate new, clonally derived spheres. Both primary and secondary spheres contain progenitor cells that proliferate and differentiate into neurons, astrocytes, and oligodendrocytes.

Administration of exogenous stem and progenitor cells to sites of CNS injury may be used as a means of *replacing* lost tissue, where the focus is on directing the differentiation of implanted cells into neurons and reinnervation of the appropriate targets. This strategy has its roots in fetal tissue grafting for Parkinson's Disease (PD) patients, which showed evidence of amelioration of symptoms in early clinical trials and generated much excitement in the medical community (Lindvall, Brundin et al. 1990; Freed, Greene et al. 2001). However, several issues subsequently arose with the procedure, including availability of tissue, variability in functional outcome, evidence of dyskinesia in transplant patients, ethical considerations in using cells derived from aborted fetuses and, very recently, reports of PD pathology in long-term grafted neurons (Lindvall, Kokaia et al. 2004; Miller 2008). Additionally, allodynia associated with

aberrant graft-induced sprouting has been reported in rats receiving NSCs to treat spinal cord injury (Hofstetter, Holmstrom et al. 2005). Nonetheless, tissue replacement with stem and progenitor cell grafts has been used to intervene in numerous sources of CNS pathology, and positive outcomes also have been reported in animal models of stroke, ALS, Huntington's Disease, spinal cord injury, traumatic brain injury, and multiple sclerosis (Lindvall, Kokaia et al. 2004; Martino and Pluchino 2006). Lending further support to this approach, Gaillard *et al.* recently reported reestablishment of cortical circuitry by grafted embryonic cortical neurons into damaged mouse cortex, where transplanted tissue developed efferent projections to the thalamus and spinal cord (Gaillard, Prestoz et al. 2007).

Separate from a cell replacement mechanism, several studies suggest that neural stem cells have an innate ability to promote healing and axonal regeneration of host neurons as well as reduction in glial scar formation. These effects may explain the numerous reports of restoration of functional recovery in the absence of effective replacement of damaged neurons or reinnervation by transplanted tissue (Ourednik, Ourednik et al. 2002; Teng, Lavik et al. 2002; Lu, Jones et al. 2003; Pluchino, Quattrini et al. 2003; Heine, Conant et al. 2004; Lindvall, Kokaia et al. 2004; Llado, Haenggeli et al. 2004; Pluchino, Zanotti et al. 2005; Richardson, Broaddus et al. 2005; Martino and Pluchino 2006; Lee, Jeyakumar et al. 2007). Additionally, *in vitro* studies have shown a neuroprotective effect of NSC-conditioned medium in models of Huntington's disease, PD, and serum withdrawal-induced PC-12 cell death (Yasuhara, Matsukawa et al. 2006; Li, Liu et al. 2007; Lim, Lee et al. 2008). This "bystander" or "chaperone" effect is believed to be due to the

constitutive secretion of multiple neurotrophic factors, as well as factors that degrade molecules which are inhibitory to axonal growth. Specifically, NSCs have been found to elute or express nerve growth factor (NGF), brain derived neurotrophic factor (BDNF), glial derived neurotrophic factor (GDNF), neurotrophin-3 (NT3), stem cell factor (SCF), and matrix metalloprotease-2 (MMP-2), which degrades chondroitin sulfate proteoglycan (a molecule inhibitory to axonal growth) (Ourednik, Ourednik et al. 2002; Lu, Jones et al. 2003; Heine, Conant et al. 2004; Llado, Haenggeli et al. 2004; Ryu, Kim et al. 2004; Yasuhara, Matsukawa et al. 2006; Redmond, Bjugstad et al. 2007). Importantly, these neurotrophic factors are known to support neuronal survival and plasticity in various models of axonopathy and neuropathy (Kolb, Gorny et al. 1997; Han and Holtzman 2000; Nicole, Ali et al. 2001; Lu, Pang et al. 2005; Wilkins and Compston 2005). While the mechanism is unclear, studies have also reported reduced gliosis in injured CNS tissue associated with NSC transplantation (Teng, Lavik et al. 2002; Lee, Jeyakumar et al. 2007). Studies by Pluchino *et al*. have highlighted the ability of exogenous neurosphere-derived neural precursor cells to display immune functions that result in neuroprotection in a model of multiple sclerosis, providing evidence for another potential mechanism underlying the bystander effect (Pluchino, Quattrini et al. 2003; Pluchino, Zanotti et al. 2005). Thus, implanted neural stem cells may rescue compromised host neurons and reduce glial scar formation through a variety of potential mechanisms, both known and yet to be elucidated. These cells may exert similar effects on the tissue response to implanted neural probes. This dissertation explores this possibility, as well as the efficacy of using a cell cycle inhibiting drug to improve the integration of the probe with brain tissue.

Cell Cycle Inhibition as Therapy for Central Nervous System Injury

The cell cycle is a complex process involved in the growth and proliferation of cells, and is regulated by numerous proteins. Cells are most often in a quiescent or resting phase termed G0, but may become mitotic after successfully passing through the necessary phases and checkpoints of the cycle: a growth phase during which RNA synthesis and protein production take place (G1), a DNA synthesis step (S), and a final preparatory stage (G2) prior to cellular division (M) (Figure 1.6a). To complete this process, the cells must pass two important checkpoints that are regulated by cyclin-dependent kinases (CDKs), which occur during G1 and G2. Cyclins are regulatory subunits of CDKs, and control these transitions. Binding to cyclins is necessary for CDKs to achieve the appropriate phosphorylation state and become activated (Schafer 1998). The G1 to S phase transition is regulated by CDK4,6 binding to cyclin D, which in turn results in the transcription of genes necessary for cell cycle progression (Schafer 1998).

Following central nervous system injury, cell cycle proteins are upregulated in mitotic cells (namely, astrocytes and microglia) and non-mitotic cells (differentiated neurons). Mitotic cells proliferate upon re-entry into the cell cycle, while non-mitotic cells undergo caspase-mediated apoptosis (Cernak, Stoica et al. 2005). Cell cycle inhibitors prevent cellular re-entry into the cell cycle, and have been shown to prevent glial proliferation and neuronal death in models of brain injury *in vitro* and *in vivo*.

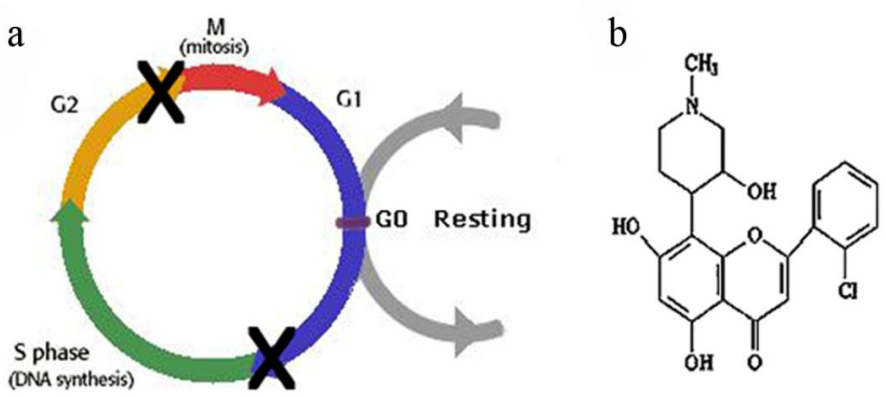

Figure 1.6. The stages of the cell cycle (a), with X's marking transitions inhibited by flavopiridol. The structure of flavopiridol is shown in (b).

Specifically, flavopiridol (Figure 1.6b) is a flavonoid cell cycle inhibiting drug which has shown efficacy in attenuating CNS damage in several injury models, and has completed Phase II trials for cancer treatment (Morris, Bramwell et al. 2006). Flavopiridol is a broad CDK inhibitor, reduces cyclin D1 transcription, and arrests the cell cycle in G1 or at the G2/M interface (Swanton 2004). Di Giovanni *et al.* showed that a one-time intracerebroventricular injection of flavopiridol reduced cyclin D1 expression, decreased neuronal cell death, reduced glial activation, and improved motor and cognitive recovery following traumatic brain injury in rats (Di Giovanni, Movsesyan et al. 2005). Flavopiridol administration to rats with spinal cord injury reduced cell cycle protein expression, improved functional recovery, reduced lesion volume, decreased astrocyte activation, and reduced neuronal apoptosis (Byrnes, Stoica et al. 2007). Flavopiridol attenuated excitotoxic cell death and reduced the expression of cell cycle proteins in kainic acid-treated neurons *in vitro* (Verdaguer, Jimenez et al. 2004). It is also neuroprotective in neurons exposed to the parkinsonian neurotoxin 1-methyl-4-phenylpyridinium *in vitro* (Alvira, Tajes et al. 2007). In an *in vitro* model of apoptotic

motoneurons, flavopiridol administration reduced cell death associated with cell cycle (cyclin D1 and E) expression following neurotrophic factor withdrawal (Appert-Collin, Hugel et al. 2006). A combination of flavopiridol and minocycline was neuroprotective in an ischemic rat model for the ten week study period (Iyirhiaro, Brust et al. 2008). Thus, there are several lines of evidence that flavopiridol administration reduces the effects of CNS injury. As such, flavopiridol is a candidate for mitigation of the tissue response to neural prostheses.

Dissertation Organization

This dissertation includes four research studies which are either in press, revision, submission, or preparation for submission to peer-reviewed journals. Chapters two through five describe this work. The first chapter of the dissertation is an introduction, which familiarizes the reader with general background information. The last chapter of the dissertation reviews the significance of the conclusions of the described research, and discusses future directions for the work.

Chapter 2 investigates the effects of alginate composition on the neurotrophic factor secretion of encapsulated neural stem cells, as well as the stability of the scaffold itself. The results indicate that alginate with a high guluronic acid content, and no poly-L-lysine coating layer, provided superior stability and support of neurotrophic factor release amongst the conditions tested. Further, medium conditioned by neural stem cells encapsulated in this material increased PC-12 survival in an *in vitro* model of cell death. This chapter is in revision in the journal *Tissue Engineering*.

Chapter 3 examines the stability and biocompatibility of alginate disks of various compositions ($CaCl_2$-crosslinked, $CaCl_2$-crosslinked with poly-L-lysine coating, and $CaCO_3$-crosslinked) implanted subcutaneously in rats for a period of three months. We hypothesized that $CaCO_3$-crosslinking and poly-L-lysine coating may improve the *in vivo* mechanical stability of alginate, and that poly-L-lysine may enhance the inflammatory response to implanted gels. The results indicated no clear differences in biocompatibility between the conditions, and little evidence for improved mechanical stability with poly-L-lysine coating. Chapter 3 is in press in *The Journal of Biomedical Materials Research – Part A*.

Chapter 4 studies the impact of neural stem cell-seeding a non-functional parylene neural prosthesis on the tissue response to the devices over a three month time period. Cell-seeding improved the tissue response within the first week of implantation, and had a negative impact on device-tissue integration by six weeks. The time course of altered neuronal and non-neuronal densities surrounding the implants is also described. Chapter 4 has been submitted to *Experimental Neurology*.

Chapter 5 explores the role of cell cycle re-entry in the tissue response to neural probes. The use of a cell cycle-inhibiting drug, flavopiridol, decreased electrode impedance over the four week study period, and reduced expression of a cell cycle protein (cyclin D1) in activated microglia at the three day time point. No effects on recording metrics were observed, although the time course of these measurements corresponded well with the evolving tissue reaction to the devices. Significant correlations between endpoint

histology, impedance, and recording quality were demonstrated. Chapter 5 is in preparation for submission to the *Journal of Neural Engineering*.

Chapter 6 summarizes the conclusions of the previous chapters, as well as their impacts to the field of neural engineering. Additionally, several opportunities for future work are discussed, including quantitative immunohistochemistry with *in situ* probes, functionalization of neural stem cell-seeded prostheses, and investigating neuronal function around the devices.

The dissertation provides several novel results characterizing the device-tissue interface, as well as the development and evaluation of two new intervention strategies to improve upon it. This work impacts the fields of neural engineering, biomaterials, and neuroscience, and provides a foundation for future discovery in these areas.

References

Abidian, M. R. and D. C. Martin (2008). "Experimental and theoretical characterization of implantable neural microelectrodes modified with conducting polymer nanotubes." Biomaterials **29**(9): 1273-83.

Alvira, D., M. Tajes, et al. (2007). "Inhibition of cyclin-dependent kinases is neuroprotective in 1-methyl-4-phenylpyridinium-induced apoptosis in neurons." Neuroscience **146**(1): 350-65.

Appert-Collin, A., B. Hugel, et al. (2006). "Cyclin dependent kinase inhibitors prevent apoptosis of postmitotic mouse motoneurons." Life Sci **79**(5): 484-90.

Becker, T. A., D. R. Kipke, et al. (2001). "Calcium alginate gel: a biocompatible and mechanically stable polymer for endovascular embolization." J Biomed Mater Res **54**(1): 76-86.

Biran, R., D. C. Martin, et al. (2005). "Neuronal cell loss accompanies the brain tissue response to chronically implanted silicon microelectrode arrays." Exp Neurol **195**(1): 115-26.

Bjornsson, C. S., S. J. Oh, et al. (2006). "Effects of insertion conditions on tissue strain and vascular damage during neuroprosthetic device insertion." J Neural Eng **3**(3): 196-207.

Buchko, C. J., K. M. Kozloff, et al. (2001). "Surface characterization of porous, biocompatible protein polymer thin films." Biomaterials **22**(11): 1289-300.

Byrnes, K. R., B. A. Stoica, et al. (2007). "Cell cycle activation contributes to post-mitotic cell death and secondary damage after spinal cord injury." Brain **130**(Pt 11): 2977-92.

Carmena, J. M., M. A. Lebedev, et al. (2003). "Learning to control a brain-machine interface for reaching and grasping by primates." PLoS Biol **1**(2): E42.

Cernak, I., B. Stoica, et al. (2005). "Role of the cell cycle in the pathobiology of central nervous system trauma." Cell Cycle **4**(9): 1286-93.

Constantinidis, I., I. Rask, et al. (1999). "Effects of alginate composition on the metabolic, secretory, and growth characteristics of entrapped beta TC3 mouse insulinoma cells." Biomaterials **20**(21): 2019-27.

Cui, X., V. A. Lee, et al. (2001). "Surface modification of neural recording electrodes with conducting polymer/biomolecule blends." J Biomed Mater Res **56**(2): 261-72.

Cui, X., J. Wiler, et al. (2003). "In vivo studies of polypyrrole/peptide coated neural probes." Biomaterials **24**(5): 777-87.

de Vos, P., M. M. Faas, et al. (2006). "Alginate-based microcapsules for immunoisolation of pancreatic islets." Biomaterials **27**(32): 5603-17.

Di Giovanni, S., V. Movsesyan, et al. (2005). "Cell cycle inhibition provides neuroprotection and reduces glial proliferation and scar formation after traumatic brain injury." Proc Natl Acad Sci U S A **102**(23): 8333-8.

Donoghue, J. P., A. Nurmikko, et al. (2007). "Assistive technology and robotic control using motor cortex ensemble-based neural interface systems in humans with tetraplegia." J Physiol **579**(Pt 3): 603-11.

Edell, D. J., V. V. Toi, et al. (1992). "Factors influencing the biocompatibility of insertable silicon microshafts in cerebral cortex." IEEE Trans Biomed Eng **39**(6): 635-43.

Evarts, E. V. (1968). "Relation of pyramidal tract activity to force exerted during voluntary movement." J Neurophysiol **31**(1): 14-27.

Fetz, E. E. (1969). "Operant conditioning of cortical unit activity." Science **163**(870): 955-8.

Freed, C. R., P. E. Greene, et al. (2001). "Transplantation of embryonic dopamine neurons for severe Parkinson's disease." N Engl J Med **344**(10): 710-9.

Gaillard, A., L. Prestoz, et al. (2007). "Reestablishment of damaged adult motor pathways by grafted embryonic cortical neurons." Nat Neurosci **10**(10): 1294-9.

Georgopoulos, A. P., J. F. Kalaska, et al. (1982). "On the relations between the direction of two-dimensional arm movements and cell discharge in primate motor cortex." J Neurosci **2**(11): 1527-37.

Georgopoulos, A. P., A. B. Schwartz, et al. (1986). "Neuronal population coding of movement direction." Science **233**(4771): 1416-9.

Griffith, R. W. and D. R. Humphrey (2006). "Long-term gliosis around chronically implanted platinum electrodes in the Rhesus macaque motor cortex." Neurosci Lett **406**(1-2): 81-6.

Gross, C. G. (2007). "The discovery of motor cortex and its background." J Hist Neurosci **16**(3): 320-31.

Gugerli, R., E. Cantana, et al. (2002). "Quantitative study of the production and properties of alginate/poly-L-lysine microcapsules." J Microencapsul **19**(5): 571-90.

Han, B. H. and D. M. Holtzman (2000). "BDNF protects the neonatal brain from hypoxic-ischemic injury in vivo via the ERK pathway." J Neurosci **20**(15): 5775-81.

Hanisch, U. K. and H. Kettenmann (2007). "Microglia: active sensor and versatile effector cells in the normal and pathologic brain." Nat Neurosci **10**(11): 1387-94.

Hashimoto, T., Y. Suzuki, et al. (2005). "Review Peripheral nerve regeneration using non-tubular alginate gel crosslinked with covalent bonds." J Mater Sci Mater Med **16**(6): 503-9.

He, W. and R. V. Bellamkonda (2005). "Nanoscale neuro-integrative coatings for neural implants." Biomaterials **26**(16): 2983-90.

He, W., G. C. McConnell, et al. (2006). "Nanoscale laminin coating modulates cortical scarring response around implanted silicon microelectrode arrays." J Neural Eng **3**(4): 316-26.

Heine, W., K. Conant, et al. (2004). "Transplanted neural stem cells promote axonal regeneration through chronically denervated peripheral nerves." Exp Neurol **189**(2): 231-40.

Henze, D. A., Z. Borhegyi, et al. (2000). "Intracellular features predicted by extracellular recordings in the hippocampus in vivo." J Neurophysiol **84**(1): 390-400.

Hochberg, L. R., M. D. Serruya, et al. (2006). "Neuronal ensemble control of prosthetic devices by a human with tetraplegia." Nature **442**(7099): 164-71.

Hodgkin, A. L. and A. F. Huxley (1939). "Action potentials recorded from inside a nerve fibre." Nature **144**: 710-711.

Hofstetter, C. P., N. A. Holmstrom, et al. (2005). "Allodynia limits the usefulness of intraspinal neural stem cell grafts; directed differentiation improves outcome." Nat Neurosci **8**(3): 346-53.

Humphrey, D. R., E. M. Schmidt, et al. (1970). "Predicting measures of motor performance from multiple cortical spike trains." Science **170**(959): 758-62.

Iyirhiaro, G. O., T. B. Brust, et al. (2008). "Delayed combinatorial treatment with flavopiridol and minocycline provides longer term protection for neuronal soma but not dendrites following global ischemia." J Neurochem.

Jun, S. B., M. R. Hynd, et al. (2008). "Modulation of cultured neural networks using neurotrophin release from hydrogel-coated microelectrode arrays." J Neural Eng **5**(2): 203-13.

Kennedy, P. R. (1989). "The cone electrode: a long-term electrode that records from neurites grown onto its recording surface." J Neurosci Methods **29**(3): 181-93.

Kennedy, P. R., R. A. Bakay, et al. (1992). "Behavioral correlates of action potentials recorded chronically inside the Cone Electrode." Neuroreport **3**(7): 605-8.

Kennedy, P. R. and R. A. E. Bakay (1997). "Activity of single action potentials in monkey motor cortex during long-term task learning." Brain Research **760**(1-2): 251-254.

Kennedy, P. R., R. A. E. Bakay, et al. (2000). "Direct control of a computer from the human central nervous system." Ieee Transactions on Rehabilitation Engineering **8**(2): 198-202.

Kennedy, P. R., S. S. Mirra, et al. (1992). "The cone electrode: ultrastructural studies following long-term recording in rat and monkey cortex." Neurosci Lett **142**(1): 89-94.

Kim, D. (2005). Surface Modification of Neural Prosthetic Devices By Functional Polymers Incorporating Neurotrophic and Pharmacological Agents. Biomedical Engineering. Ann Arbor, Michigan.

Kim, D. H., M. Abidian, et al. (2004). "Conducting polymers grown in hydrogel scaffolds coated on neural prosthetic devices." J Biomed Mater Res A **71**(4): 577-85.

Kim, D. H. and D. C. Martin (2006). "Sustained release of dexamethasone from hydrophilic matrices using PLGA nanoparticles for neural drug delivery." Biomaterials **27**(15): 3031-7.

Kim, Y. T., R. W. Hitchcock, et al. (2004). "Chronic response of adult rat brain tissue to implants anchored to the skull." Biomaterials **25**(12): 2229-37.

King, A., J. Lau, et al. (2003). "The effect of capsule composition in the reversal of hyperglycemia in diabetic mice transplanted with microencapsulated allogeneic islets." Diabetes Technol Ther **5**(4): 653-63.

King, A., S. Sandler, et al. (2001). "The effect of host factors and capsule composition on the cellular overgrowth on implanted alginate capsules." J Biomed Mater Res **57**(3): 374-83.

Kolb, B., G. Gorny, et al. (1997). "Nerve growth factor stimulates growth of cortical pyramidal neurons in young adult rats." Brain Res **751**(2): 289-94.

Kornblum, H. I. (2007). "Introduction to neural stem cells." Stroke **38**(2 Suppl): 810-6.

Kulseng, B., B. Thu, et al. (1997). "Alginate polylysine microcapsules as immune barrier: permeability of cytokines and immunoglobulins over the capsule membrane." Cell Transplant **6**(4): 387-94.

Lebedev, M. A. and M. A. Nicolelis (2006). "Brain-machine interfaces: past, present and future." Trends Neurosci **29**(9): 536-46.

Lee, J. P., M. Jeyakumar, et al. (2007). "Stem cells act through multiple mechanisms to benefit mice with neurodegenerative metabolic disease." Nat Med **13**(4): 439-47.

Li, X., T. Liu, et al. (2007). "Effect of neural stem cells on apoptosis of PC12 cells induced by serum deprivation." Biotechnol Prog **23**(4): 952-7.

Lim, F. and A. M. Sun (1980). "Microencapsulated islets as bioartificial endocrine pancreas." Science **210**(4472): 908-10.

Lim, H. C., S. T. Lee, et al. (2008). "Neuroprotective effect of neural stem cell-conditioned media in in vitro model of Huntington's disease." Neurosci Lett **435**(3): 175-80.

Lindvall, O., P. Brundin, et al. (1990). "Grafts of fetal dopamine neurons survive and improve motor function in Parkinson's disease." Science **247**(4942): 574-7.

Lindvall, O., Z. Kokaia, et al. (2004). "Stem cell therapy for human neurodegenerative disorders-how to make it work." Nat Med **10 Suppl**: S42-50.

Liu, X., D. B. McCreery, et al. (2006). "Evaluation of the stability of intracortical microelectrode arrays." IEEE Trans Neural Syst Rehabil Eng **14**(1): 91-100.

Liu, X., D. B. McCreery, et al. (1999). "Stability of the interface between neural tissue and chronically implanted intracortical microelectrodes." IEEE Trans Rehabil Eng **7**(3): 315-26.

Llado, J., C. Haenggeli, et al. (2004). "Neural stem cells protect against glutamate-induced excitotoxicity and promote survival of injured motor neurons through the secretion of neurotrophic factors." Mol Cell Neurosci **27**(3): 322-31.

Lu, B., P. T. Pang, et al. (2005). "The yin and yang of neurotrophin action." Nat Rev Neurosci **6**(8): 603-14.

Lu, P., L. L. Jones, et al. (2003). "Neural stem cells constitutively secrete neurotrophic factors and promote extensive host axonal growth after spinal cord injury." Exp Neurol **181**(2): 115-29.

Ludwig, K. A., J. D. Uram, et al. (2006). "Chronic neural recordings using silicon microelectrode arrays electrochemically deposited with a poly(3,4-ethylenedioxythiophene) (PEDOT) film." Journal of Neural Engineering **3**: 59.

Martino, G. and S. Pluchino (2006). "The therapeutic potential of neural stem cells." Nat Rev Neurosci **7**(5): 395-406.

Martinsen, A., G. Skjak-Baek, et al. (1989). "Alginate as Immobilization Material: I. Correlation between Chemical and Physical Properties of Alginate Gel Beads." Biotechnol Bioeng **33**(1): 79-89.

Martinsen, A., I. Storro, et al. (1992). "Alginate as Immobilization Material .3. Diffusional Properties." Biotechnology and Bioengineering **39**(2): 186-194.

Miller, G. (2008). "Parkinson's disease. Signs of disease in fetal transplants." Science **320**(5873): 167.

Morris, D. G., V. H. Bramwell, et al. (2006). "A Phase II Study of Flavopiridol in Patients With Previously Untreated Advanced Soft Tissue Sarcoma." Sarcoma **2006**: 64374.

Nicole, O., C. Ali, et al. (2001). "Neuroprotection mediated by glial cell line-derived neurotrophic factor: involvement of a reduction of NMDA-induced calcium influx by the mitogen-activated protein kinase pathway." J Neurosci **21**(9): 3024-33.

Nicolelis, M. A., D. Dimitrov, et al. (2003). "Chronic, multisite, multielectrode recordings in macaque monkeys." Proc Natl Acad Sci U S A **100**(19): 11041-6.

Nunamaker, E. A. (2006). Alginate as a Novel Material for Duraplasty: Investigations of the Material Properties, In Vivo Stability, and Sealing Strength. Biomedical Engineering. Ann Arbor, University of Michigan. **PhD**.

Ourednik, J., V. Ourednik, et al. (2002). "Neural stem cells display an inherent mechanism for rescuing dysfunctional neurons." Nat Biotechnol **20**(11): 1103-10.

Perl, E. (1994). "The 1944 Nobel Prize to Erlanger and Gasser." Faseb J **8**(10): 782-3.

Pluchino, S., A. Quattrini, et al. (2003). "Injection of adult neurospheres induces recovery in a chronic model of multiple sclerosis." Nature **422**(6933): 688-94.

Pluchino, S., L. Zanotti, et al. (2005). "Neural stem cells and their use as therapeutic tool in neurological disorders." Brain Res Brain Res Rev **48**(2): 211-9.

Pluchino, S., L. Zanotti, et al. (2005). "Neurosphere-derived multipotent precursors promote neuroprotection by an immunomodulatory mechanism." Nature **436**(7048): 266-71.

Polikov, V. S., P. A. Tresco, et al. (2005). "Response of brain tissue to chronically implanted neural electrodes." J Neurosci Methods **148**(1): 1-18.

Redmond, D. E., Jr., K. B. Bjugstad, et al. (2007). "Behavioral improvement in a primate Parkinson's model is associated with multiple homeostatic effects of human neural stem cells." Proc Natl Acad Sci U S A **104**(29): 12175-80.

Rennaker, R. L., J. Miller, et al. (2007). "Minocycline increases quality and longevity of chronic neural recordings." J Neural Eng **4**(2): L1-5.

Reynolds, B. A. and S. Weiss (1992). "Generation of neurons and astrocytes from isolated cells of the adult mammalian central nervous system." Science **255**(5052): 1707-10.

Reynolds, B. A. and S. Weiss (1996). "Clonal and population analyses demonstrate that an EGF-responsive mammalian embryonic CNS precursor is a stem cell." Dev Biol **175**(1): 1-13.

Richardson-Burns, S. M., J. L. Hendricks, et al. (2007). "Polymerization of the conducting polymer poly(3,4-ethylenedioxythiophene) (PEDOT) around living neural cells." Biomaterials **28**(8): 1539-52.

Richardson-Burns, S. M., J. L. Hendricks, et al. (2007). "Electrochemical polymerization of conducting polymers in living neural tissue." J Neural Eng **4**(2): L6-L13.

Richardson, R. M., W. C. Broaddus, et al. (2005). "Grafts of adult subependymal zone neuronal progenitor cells rescue hemiparkinsonian behavioral decline." Brain Res **1032**(1-2): 11-22.

Roitbak, T. and E. Sykova (1999). "Diffusion barriers evoked in the rat cortex by reactive astrogliosis." Glia **28**(1): 40-8.

Rokstad, A. M., S. Holtan, et al. (2002). "Microencapsulation of cells producing therapeutic proteins: optimizing cell growth and secretion." Cell Transplant **11**(4): 313-24.

Rousche, P. J. and R. A. Normann (1998). "Chronic recording capability of the Utah Intracortical Electrode Array in cat sensory cortex." J Neurosci Methods **82**(1): 1-15.

Ryder, E. F., E. Y. Snyder, et al. (1990). "Establishment and characterization of multipotent neural cell lines using retrovirus vector-mediated oncogene transfer." J Neurobiol **21**(2): 356-75.

Ryu, J. K., J. Kim, et al. (2004). "Proactive transplantation of human neural stem cells prevents degeneration of striatal neurons in a rat model of Huntington disease." Neurobiol Dis **16**(1): 68-77.

Schafer, K. A. (1998). "The cell cycle: a review." Vet Pathol **35**(6): 461-78.

Schwartz, A. B. (2004). "Cortical neural prosthetics." Annu Rev Neurosci **27**: 487-507.

Schwartz, A. B., X. T. Cui, et al. (2006). "Brain-controlled interfaces: movement restoration with neural prosthetics." Neuron **52**(1): 205-20.

Shain, W., L. Spataro, et al. (2003). "Controlling cellular reactive responses around neural prosthetic devices using peripheral and local intervention strategies." IEEE Trans Neural Syst Rehabil Eng **11**(2): 186-8.

Singec, I., R. Jandial, et al. (2007). "The leading edge of stem cell therapeutics." Annu Rev Med **58**: 313-28.

Spataro, L., J. Dilgen, et al. (2005). "Dexamethasone treatment reduces astroglia responses to inserted neuroprosthetic devices in rat neocortex." Exp Neurol **194**(2): 289-300.

Stabler, C., K. Wilks, et al. (2001). "The effects of alginate composition on encapsulated betaTC3 cells." Biomaterials **22**(11): 1301-10.

Strand, B. L., Y. A. Morch, et al. (2000). "Alginate as immobilization matrix for cells." Minerva Biotecnologica **12**(4): 223-233.

Strand, B. L., T. L. Ryan, et al. (2001). "Poly-L-Lysine induces fibrosis on alginate microcapsules via the induction of cytokines." Cell Transplant **10**(3): 263-75.

Strumwasser, F. (1958). "Long-term recording' from single neurons in brain of unrestrained mammals." Science **127**(3296): 469-70.

Svendsen, C. N. (2002). "The amazing astrocyte." Nature **417**(6884): 29-32.

Swanton, C. (2004). "Cell-cycle targeted therapies." Lancet Oncol **5**(1): 27-36.

Szarowski, D. H., M. D. Andersen, et al. (2003). "Brain responses to micro-machined silicon devices." Brain Res **983**(1-2): 23-35.

Taylor, D. M., S. I. Tillery, et al. (2002). "Direct cortical control of 3D neuroprosthetic devices." Science **296**(5574): 1829-32.

Teng, Y. D., E. B. Lavik, et al. (2002). "Functional recovery following traumatic spinal cord injury mediated by a unique polymer scaffold seeded with neural stem cells." Proc Natl Acad Sci U S A **99**(5): 3024-9.

Thomas, S. (2000). "Alginate dressings in surgery and wound management--Part 1." J Wound Care **9**(2): 56-60.

Tonnesen, H. H. and J. Karlsen (2002). "Alginate in drug delivery systems." Drug Dev Ind Pharm **28**(6): 621-30.

Turner, J. N., W. Shain, et al. (1999). "Cerebral astrocyte response to micromachined silicon implants." Exp Neurol **156**(1): 33-49.

Velliste, M., S. Perel, et al. (2008). "Cortical control of a prosthetic arm for self-feeding." Nature.

Verdaguer, E., A. Jimenez, et al. (2004). "Inhibition of cell cycle pathway by flavopiridol promotes survival of cerebellar granule cells after an excitotoxic treatment." J Pharmacol Exp Ther **308**(2): 609-16.

Vetter, R. J., J. C. Williams, et al. (2004). "Chronic neural recording using silicon-substrate microelectrode arrays implanted in cerebral cortex." IEEE Trans Biomed Eng **51**(6): 896-904.

Webster, J. G. (1998). Medical Instrumentation: Application and Design. New York, Wiley.

Weiss, S., C. Dunne, et al. (1996). "Multipotent CNS stem cells are present in the adult mammalian spinal cord and ventricular neuroaxis." J Neurosci **16**(23): 7599-609.

Wilkins, A. and A. Compston (2005). "Trophic factors attenuate nitric oxide mediated neuronal and axonal injury in vitro: roles and interactions of mitogen-activated protein kinase signalling pathways." J Neurochem **92**(6): 1487-96.

Williams, J. C., J. A. Hippensteel, et al. (2007). "Complex impedance spectroscopy for monitoring tissue responses to inserted neural implants." J Neural Eng **4**(4): 410-23.

Williams, J. C., R. L. Rennaker, et al. (1999). "Long-term neural recording characteristics of wire microelectrode arrays implanted in cerebral cortex." Brain Res Brain Res Protoc **4**(3): 303-13.

Yasuhara, T., N. Matsukawa, et al. (2006). "Transplantation of human neural stem cells exerts neuroprotection in a rat model of Parkinson's disease." J Neurosci **26**(48): 12497-511.

Zhao, C., W. Deng, et al. (2008). "Mechanisms and functional implications of adult neurogenesis." Cell **132**(4): 645-60.

Zhong, Y. and R. V. Bellamkonda (2005). "Controlled release of anti-inflammatory agent alpha-MSH from neural implants." J Control Release **106**(3): 309-18.

Zhong, Y. and R. V. Bellamkonda (2007). "Dexamethasone-coated neural probes elicit attenuated inflammatory response and neuronal loss compared to uncoated neural probes." Brain Res **1148**: 15-27.

CHAPTER 2
IN VITRO DEVELOPMENT AND CHARACTERIZATION OF A CORTICAL NEURAL STEM CELL-SEEDED ALGINATE SCAFFOLD

Abstract

The purpose of this study was to evaluate the effects of alginate composition on the neurotrophic factor release, viability, and proliferation of encapsulated NSCs, as well as on the mechanical stability of the scaffold itself. Four compositions were tested: a high guluronic acid (68%) and a high mannuronic acid (54%) content alginate, with or without a poly-L-lysine (PLL) coating layer. Enzyme-linked immunosorbent assay (ELISA) was used to quantify the release of brain derived neurotrophic factor (BDNF), glial derived neurotrophic factor (GDNF) and nerve growth factor (NGF) from the encapsulated cells. All three factors were detected from encapsulated cells only when a high G alginate without PLL was used. Additionally, capsules with this composition remained intact more frequently when exposed to solutions of low osmolarity, potentially indicating superior mechanical stability. NSCs survived and proliferated in all alginate matrices similarly over the 21 day study course irrespective of scaffold condition. NSC-seeded alginate beads with a high G, non-PLL coated composition may be useful in the repair of injured nervous tissue, where the mechanism is the secretion of neuroprotective factors. We verify the neuroprotective effects of medium conditioned by NSC-seeded alginate beads on the serum-withdrawal mediated death of PC-12 cells here.

Introduction

Alginate is a biocompatible hydrogel that has been used to encapsulate many types of cells with the purpose of immuno-isolation from the host (Lim and Sun 1980; Joki, Machluf et al. 2001; Borlongan, Skinner et al. 2004; Wikstrom, Elomaa et al. 2008). Encapsulation protects graft cells from potential damage caused by an immune response while allowing the secretion of therapeutic agents from the cells into the surrounding host tissue. Small molecules such as glucose, oxygen and waste products freely pass through the gel matrix. Recent studies have investigated the use of alginate as a neural stem cell (NSC) scaffold (Li, Liu et al. 2006; Ashton, Banerjee et al. 2007; Li, Liu et al. 2007). However, the effect of alginate composition on NSC function has not been investigated.

Administration of stem cells to sites of central nervous system (CNS) injury may be used as a means of replacing damaged or diseased tissue, where the focus is on directing the differentiation of implanted cells into neurons and subsequent reinnervation of host tissue. This strategy has been used to intervene in numerous models of CNS injury, including Parkinson's Disease, stroke, ALS, spinal cord injury, traumatic brain injury, and Huntington's Disease (Lindvall, Kokaia et al. 2004; Martino and Pluchino 2006; Gaillard, Prestoz et al. 2007). However, in many studies the degree of functional recovery following NSC transplantation is not explained by the quantity of differentiated graft cells alone, lending credence to a "bystander" or supporting role of NSCs (Ourednik, Ourednik et al. 2002; Pluchino, Zanotti et al. 2005; Martino and Pluchino 2006). Several studies suggest that NSCs have an innate ability to promote neuroprotection and axonal regeneration of host tissue (Ourednik, Ourednik et al. 2002; Teng, Lavik et al. 2002; Lu,

Jones et al. 2003; Heine, Conant et al. 2004; Llado, Haenggeli et al. 2004). Potential mechanisms include constitutive secretion of multiple neurotrophic factors (Ourednik, Ourednik et al. 2002; Teng, Lavik et al. 2002; Lu, Jones et al. 2003; Llado, Haenggeli et al. 2004), as well as degrading molecules which are inhibitory to axonal growth (Heine, Conant et al. 2004). NSCs derived from various sources have been found to elute nerve growth factor (NGF), brain derived neurotrophic factor (BDNF), glial derived neurotrophic factor (GDNF), and matrix metalloprotease-2 (MMP-2), which degrades chondroitin sulfate proteoglycan (a molecule inhibitory to axonal growth)(Lu, Jones et al. 2003; Heine, Conant et al. 2004; Llado, Haenggeli et al. 2004; Li, Liu et al. 2007). Thus, neural stem and progenitor cells may be exploited as a sort of miniature drug factory, releasing factors which result in the desired healing response in injured nervous tissue. Encapsulation of these cells in alginate may further enhance their therapeutic utility by localizing the cells to the site of injury and isolating them from a host immune response.

Alginate is a biocompatible polysaccharide polymer composed of D-mannuronic (M) and L-guluronic acid (G) residues in varying proportions. Cross-linking and gel formation takes place when divalent cations, such as calcium, ionically bind carboxylic acid groups of blocks of guluronic residues between chains. Alginate has been used widely to encapsulate cells following ground-breaking work published by Lim and Sun in 1980, which demonstrated reversal of diabetes in rats implanted with alginate-encapsulated pancreatic islets for a period of 2-3 weeks (Lim and Sun 1980). Several studies have sought to understand the relationship between alginate composition and the function of the graft (Soon-Shiong, Otterlie et al. 1991; De Vos, De Haan et al. 1997; Constantinidis,

Rask et al. 1999; King, Sandler et al. 2001; Stabler, Wilks et al. 2001; Strand, Ryan et al. 2001; Rokstad, Holtan et al. 2002; King, Lau et al. 2003; Wikstrom, Elomaa et al. 2008). Two common themes emerge in the literature regarding alginate composition and graft performance: the effect of the M/G content of the alginate and the importance of a polycation coating layer. These two variables have been related to gel mechanical stability, viability of encapsulated cells, *in vivo* biocompatibility, and diffusion through the alginate gel. In terms of mechanical stability, alginates with a high G content are more mechanically stable than those with a high M content (Strand, Morch et al. 2000). However, high G alginate has been shown to initially inhibit the metabolic and secretory activity of cells due to growth inhibition, theoretically because a higher strength gel is more difficult for proliferating cells to displace (Constantinidis, Rask et al. 1999; Stabler, Wilks et al. 2001). Beads composed of high G alginate are also known to be more porous than high M alginate, thus enhancing diffusion of molecules into and out of the matrix (Martinsen, Storro et al. 1992). Poly-L-lysine (PLL) coating is commonly employed as a means of strengthening the alginate bead and providing a barrier to immune system components such as IgG (Kulseng, Thu et al. 1997; Gugerli, Cantana et al. 2002). However, the PLL coating layer may itself cause an unfavorable foreign body response and slight toxicity to encapsulated cells, and its use remains controversial (King, Sandler et al. 2001; Strand, Ryan et al. 2001; Rokstad, Holtan et al. 2002; van Raamsdonk, Cornelius et al. 2002; King, Lau et al. 2003; Orive, Hernandez et al. 2003; Orive, Tam et al. 2006).

In light of the extensive research indicating a relationship between alginate composition and encapsulated cell function, as well as the limited amount of data on NSC encapsulation in alginate, the effects of M/G content and PLL coating on entrapped cortical NSCs were investigated. We show that neurotrophic factor release and mechanical stability in response to an osmotic challenge were optimal in a high G scaffold without a PLL coating layer. NSCs survived and proliferated in alginate regardless of the compositions tested. Neurotrophic factor release and bioactivity assay data substantiated the use of NSCs encapsulated in alginate to heal injured nervous tissue via a bystander mechanism. These scaffolded cells have therapeutic potential in treating nervous system injuries in future studies, and current work in our lab is investigating their ability to repair a cortical lesion in the adult rat brain (Purcell, Seymour et al. 2007).

Materials and Methods

Materials

Cortical NSCs, nestin antibody, neuronal class III β-tubulin (TUJ-1) antibody, and all NSC cell culture reagents were purchased from StemCell Technologies (Vancouver, BC). MTS assay and ELISA kits were obtained from Promega Corporation (Madison, WI). Alginate was from NovaMatrix (Drammen, Norway). Live/Dead Assay and PC-12 medium reagents were from Invitrogen Corporation (Carlsbad, CA). BD Biocoat collagen-coated plates were from BD Biosciences (San Jose, CA). Centricon filters and NG-2 antibody were from Millipore Corporation (Billerica, MA). Secondary antibodies were from Molecular Probes (Eugene, OR). PC-12 cells were obtained from the

American Type Culture Collection (ATCC) (Manassas, VA). All other reagents were from Sigma-Aldrich (St. Louis, MO).

Cortical NSC Culture and Encapsulation in Alginate

E14 murine cortical neural stem cells were cultured and expanded with 20 ng/mL epidermal growth factor (EGF) according to the supplier's protocol with a penicillin/streptomycin antibiotic supplement. The culture and stem cell characteristics of these cells have been described (Reynolds and Weiss 1992; Reynolds and Weiss 1996). Cell encapsulation was achieved by mixing a cell slurry with alginate 50:50 and dropping into a 0.1 M calcium chloride solution for 10 minutes. The encapsulation yielded beads with a final concentration of 500,000 cells/mL in 1% w/v alginate (approximately 200 cells per bead). The weight percentage was chosen based on a recommendation reported in the literature (Stabler, Wilks et al. 2001). Cells were approximately 90% viable as assessed by trypan blue staining prior to encapsulation. Bead size was approximately 1 mm in diameter and controlled by parallel air flow through a glass atomizer. Four different conditions were employed to optimize the encapsulation procedure: a high guluronic (G) alginate (68% G content, molecular weight = 219,000 g/mol) or a high mannuronic (M) alginate (54% M content, molecular weight = 222,000 g/mol), with or without a PLL coating layer. The conditions chosen have been shown to have differing mechanical strengths based on M/G content, and molecular weights were closely matched to eliminate this factor as an experimental variable (Martinsen, Skjak-Baek et al. 1989; Strand, Morch et al. 2000). These conditions are abbreviated as G, M, G-PLL, and M-PLL. All alginates were highly purified and sterile.

PLL coating was achieved as previously described (Strand, Gaserod et al. 2002). Briefly, beads were rinsed in physiological saline prior to a ten minute incubation in 0.1% PLL-HCl (15,000-30,000 MW) in saline. Following additional saline rinsing, beads were incubated for 10 minutes in 0.1% alginate in saline. Beads received a final rinse prior to being returned to medium. Beads were cultured in static transwell dishes containing 500,000 cells (encapsulated or unencapsulated) which were allowed to proliferate in the presence of EGF over time.

ELISA

At 1, 4, 7, 14, and 21 day time points, media samples were collected for quantification of growth factor release with enzyme linked immunosorbent assay (ELISA) (*n*=5 per condition). Untreated media and supernatant from non-encapsulated cells were used as controls. Supernatant was concentrated with YM-3 Centricon filters at 4°C. Promega Emax ELISA kits for NGF, BDNF, and GDNF were used according to the manufacturer's protocol. Average values below the lowest dilution above zero of the standard curve for each kit were considered to be non-detectable (ND).

Alginate Mechanical Stability

The mechanical stability of the alginate beads was assessed using a semi-quantitative osmotic pressure test (Van Raamsdonk and Chang 2001). Testing was conducted at 1, 7, 14 and 21 day time points. Alginate beads were exposed to solutions of low osmolarity (0, 2.8, and 11.1 mOsm saline with media used as a control) for a period of 3 hours, as previously described (Van Raamsdonk and Chang 2001). Thirty beads per condition were

assessed visually for breakage at each time point. The number of intact capsules was compared between conditions by an observer blinded to the experimental condition.

NSC Proliferation and Viability in Alginate

Beads were collected for quantification of proliferation with an MTS assay and viability with propidium iodide staining at the same time points as ELISA. In the MTS assay, a tetrazolium compound is bioreduced by metabolically active cells into a formazan product which is quantified by a plate reader. Twenty beads per well (n=4 wells per condition per day) were assayed for each condition in accordance with previously published methods and sample sizes in similar studies (Bunger, Jahnke et al. 2002).

To assess the viability of the cells in the alginate, beads were exposed to propidium iodide for 1.5 hours and counterstained with Hoechst for the final 10 minutes (n=4 per condition). Results were assessed by obtaining the percentage of propidium iodide positive nuclei by counting under a Zeiss Axioplan microscope. Slides were evaluated by an observer blinded to the experimental condition.

Immunocytochemistry of Cells in Alginate

Beads were collected at the same time points as ELISA for histology (n=4 per condition). For all staining applications, beads were briefly fixed in PBS-buffered 4% paraformaldehyde for 10 minutes followed by dehydration in graded washes of ethanol up to 70%. The samples were embedded in paraffin and sectioned on a microtome at a 5 μm thickness. Sections were de-paraffinized, rehydrated, blocked with 10% normal goat

serum and stained with markers of differentiation. Specifically, immunocytochemistry for TUJ-I (neuronal precursors), GFAP (astrocytes), NG-2 (oligodendrocyte precursors), and nestin (undifferentiated NSCs) were performed based on a previously described method at 1:500, 1:80, 1:500, and 1:80 concentrations respectively (Cowell, Plane et al. 2003). Tris buffered saline (TBS) was used in place of phosphate buffered saline (PBS) to improve bead stability during staining by avoiding phosphate binding of calcium cross-links. Nuclei were counterstained with Hoechst. As a negative control, TBS was used in place of primary antibody. Analysis of results was a qualitative assessment of histology.

Bioactivity of Conditioned Medium from NSC-Seeded Beads

To verify the potential ability of cortical NSCs to exert neuroprotective effects via a bystander mechanism when encapsulated in alginate, a serum-withdrawal model of apoptosis in PC-12 cells was used (Li, Liu et al. 2007). PC-12 cells were cultured in RPMI-1640 medium supplemented with 10% heat-inactivated horse serum and 5% fetal bovine serum on type IV collagen-coated 96-well plates, based on methods previously described (Greene and Tischler 1976). To obtain conditioned medium, NSCs were encapsulated in 1% high G alginate, and medium was collected 48 hours later. The high G alginate scaffold was chosen for this experiment based on its improved mechanical stability and support of neurotrophic factor release as demonstrated in this study. Non-seeded alginate beads conditioned the control medium. Fifty percent of serum-containing medium was removed and replaced with either NSC-conditioned or control medium (from empty capsules). Control cells were given a media change only. Twenty-four and forty-eight hours later, PC-12s were evaluated for viability with a Live/Dead kit. The

center of each well was imaged with the 20X objective of a Leica inverted microscope, and live and dead cells were counted by an observer blinded to the experimental condition with ImageJ software (U. S. National Institutes of Health, Bethesda, MD). The experiment was repeated, and a univariate ANOVA model which factored in time and trial was used to evaluate the combined data. Cell viability was evaluated as a percent of control.

Statistical Analysis

Differences between controls and experimental conditions for ELISA, MTS values, NSC and PC-12 viability were analyzed with standard ANOVA techniques, and a Tukey post-hoc test where significance was noted. Osmotic pressure test data was analyzed with logistic regression due to the binary response variable (1 = intact bead, 0 = broken bead). Histology was evaluated on a qualitative basis. Statistical significance was defined at the 0.05 level.

Results

ELISA

The amount of NGF secreted from the unencapsulated cells (roughly between 10 and 90 pg/million cells/day depending on time point, Table 2.1) was similar to that previously reported from the C17.2 NSC line derived from cerebellum (approximately 10 pg/million cells/day), and NGF secreted from cells in G capsules also fell within this range (Lu, Jones et al. 2003). GDNF secretion from unencapsulated and G encapsulated cells on day fourteen was somewhat higher than the value reported for the C17.2 clone (70

pg/million cells/day) (Table 2.1) (Lu, Jones et al. 2003). No secretion of NGF or GDNF was detected at any time point from cells encapsulated in other scaffold conditions. NGF was detected on fewer days from G encapsulated cells compared to unencapsulated cells (Table 2.1). BDNF was detected from all conditions, both encapsulated and unencapsulated, at the four day time point, and values were generally higher than that reported for C17.2 cells (10 pg/million cells/day) (Table 2.1) (Lu, Jones et al. 2003). The four day time point is also when cell viability tended to be at its lowest levels for scaffold conditions; it is unknown if the two phenomena are related (Figure 2.2a). NGF

		1	4	7	14	21	Days
Cells	*NGF*	30.98 +/- 5.64	19.18 +/- 8.17	74.19 +/- 26.01†	44.76 +/- 9.25	89.20 +/- 11.87‡	
	GDNF	ND	ND	ND	156.47 +/- 39.47	ND	
	BDNF	ND	141.89 +/- 82.99	ND	ND	ND	
G	*NGF*	33.52 +/- 10.34	ND	26.67 +/- 12.23	ND	ND	
	GDNF	ND	ND	ND	296.19 +/- 175.72	ND	
	BDNF	ND	173.98 +/- 36.52	ND	ND	ND	
M	*NGF*	ND	ND	ND	ND	ND	
	GDNF	ND	ND	ND	ND	ND	
	BDNF	ND	50.96 +/- 9.07	ND	ND	ND	
G/PLL	*NGF*	ND	ND	ND	ND	ND	
	GDNF	ND	ND	ND	ND	ND	
	BDNF	ND	161.74 +/- 52.07	ND	ND	ND	
M/PLL	*NGF*	ND	ND	ND	ND	ND	
	GDNF	ND	ND	ND	ND	ND	
	BDNF	ND	102.30 +/- 59.86	ND	ND	ND	

Table 2.1. Neurotrophic factor release varies with scaffold condition and time. Values are given in pg/million cells/day. Unencapsulated cells secrete NGF, BDNF, and GDNF at various time points throughout the study, whereas all three factors were detected from encapsulated cells only when a high G alginate scaffold was used. BDNF was detected from all conditions at the four day time point, and GDNF was detected at the fourteen day time point from G encapsulated and unencapsulated cells. NGF secretion from unencapsulated cells at 21 days was significantly greater than 1 day and 4 day values (‡), and secretion at 7 days was greater than 4 day values (†) ($p < 0.05$, ANOVA). Non-detectable values are denoted "ND." Mean ± s.e.m. is shown.

levels for unencapsulated cells were higher at 7 and 21 days compared to initial time points; no other significant differences were found.

Alginate Mechanical Stability

G beads were significantly more stable than all other conditions when exposed to solutions of low osmolarity (Figure 2.1a, $p < 0.001$). The odds of beads remaining intact was increased by at least 18-fold in comparison to other conditions when a high G composition was used. Representative images of beads exposed to 0 mOsm solutions after 7 days *in vitro* further highlight the improved stability of high G beads compared to other alginate compositions during this test (Figure 2.1b-e). High M beads were more stable than PLL-coated beads (Figure 2.1a, $p < 0.001$). The data shows that PLL coating resulted in increased incidence of bead breakage, with no significant difference between G-PLL and M-PLL beads. The presence of a PLL coating layer was visually confirmed in a separate investigation using the same coating protocol with FITC-labeled PLL and fluorescence microscopy (data not shown). There was a significant reduction of alginate stability after 24 hours; the odds of beads being intact decreased 9-fold after this time point (Figure 2.1a, $p < 0.001$). No further significant changes in stability over time were observed. Similar results were found when beads were exposed to solutions of 2.8 and 11.1 mOsm saline (data not shown).

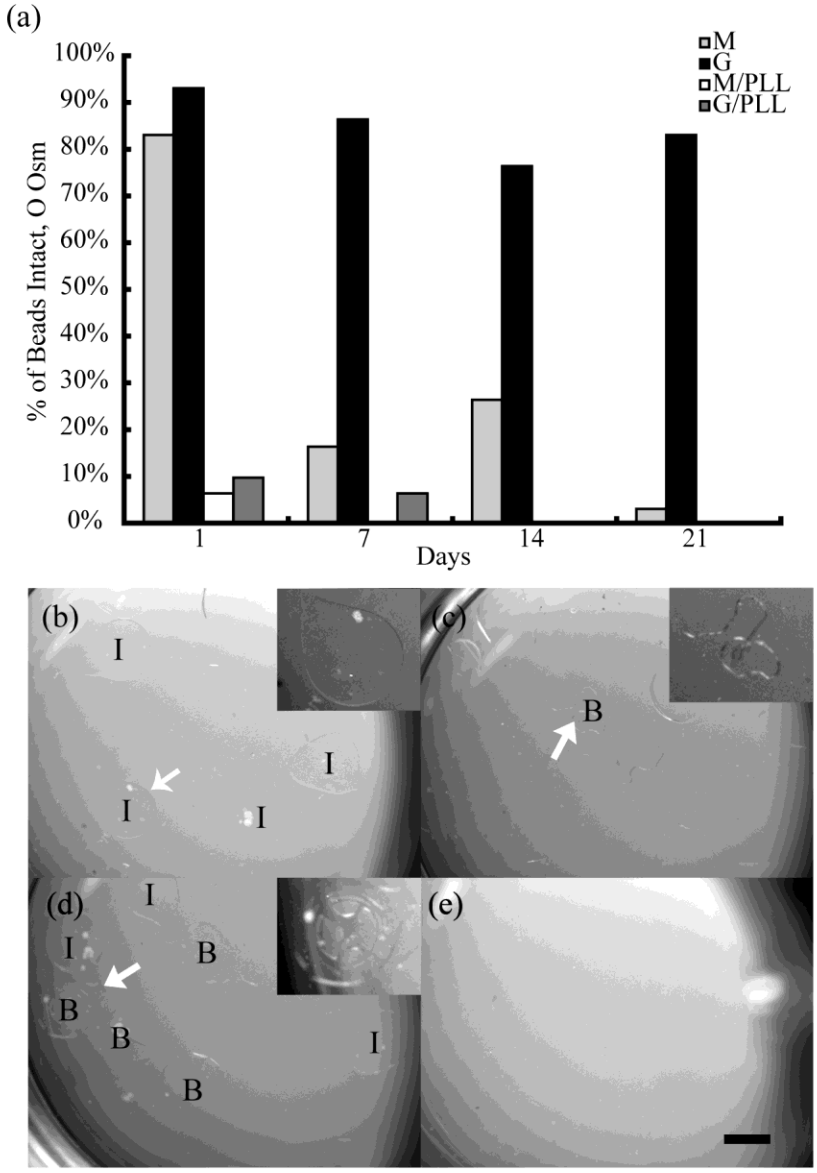

Figure 2.1. NSC-seeded alginate microcapsules with a G composition have superior stability in comparison to all other conditions. G beads remain intact more frequently than M capsules after exposure to 0 mOsm 7 days after seeding (a) ($p < 0.001$, logistic regression). PLL-coated capsules break more frequently than uncoated capsules ($p < 0.001$, logistic regression). Representative images of G (b), G-PLL (c), M (d), and M-PLL (e) capsules in solution illustrate the stability of G capsules (intact beads are labeled "I") and breakage (broken beads are denoted "B") of M and G-PLL beads. M-PLL beads are completely dissolved. Insets in (b)-(d) highlight representative beads (arrows) to improve visualization. Error bars are not shown due to the nature of the data analysis. Scale = 1 mm.

Proliferation and Viability in Alginate

NSCs survive and proliferate in all alginate matrices regardless of composition (Figure 2.2a-d). M-PLL capsules were too mechanically unstable to assay after the first week. After an initial drop in viability at 4 days to the 20-40% range, cell viability rebounds to over 70% thereafter regardless of encapsulation condition (Figure 2.2a, $p < 0.05$). Cell death levels were high immediately following encapsulation, mainly due to necrosis with many cells appearing to be lysed by the procedure. Representative pictures of healthy and propidium iodide positive cells from the same sample of high G-encapsulated neurospheres are shown in Figure 2.2b-c. Cells at the interior of larger encapsulated neurospheres are particularly vulnerable to necrosis, presumably due to reduced nutrient and oxygen diffusion (Figure 2.2c). At later time points, chromatin clumping possibly indicating apoptosis was seen in a few cells, and much lower levels of necrosis occurred. There were no significant differences in viability between alginate conditions. An MTS assay revealed cell proliferation in all alginate matrices irrespective of composition, and cell number was significantly increased over initially low or non-detectable values beginning at 4 days (Figure 2.2d, $p < 0.05$). Previous experiments visually validated the MTS assay of alginate beads with toluidene blue staining of paraffin sections (data not shown). The data indicate that NSCs survive and proliferate within alginate matrices following an initial drop in viability regardless of composition, likely due to the physiological challenge the encapsulation procedure presents to the cells.

Figure 2.2. NSCs survive (a-c) and proliferate (d) in alginate regardless of the compositions tested. Viability of the cells is initially reduced following encapsulation, but significantly improves for all conditions after one week (a). Cells are labeled with Hoechst (blue), and propidium iodide (red) stains nuclei of cells with compromised membranes indicative of cell death (b-c). Representative pictures of G-encapsulated cells at 21 days illustrate the vulnerability of cells in the center of larger proliferating neurospheres to necrosis, presumably due to reduced nutrient and oxygen diffusion (b-c). NSCs proliferate irrespective of alginate composition, with significantly increased cell numbers detected beginning at 4 days compared to initially low or non-detectable values 1 day after encapsulation (d). A further increase occurs at 21 days post-encapsulation. M-PLL capsules were too mechanically unstable to assay after the first week. †, ‡ = significantly increased versus 1 day, or 1 and 4 days respectively at the 0.05 level (ANOVA). Mean ± s.e.m. is shown. Scale = 100 microns.

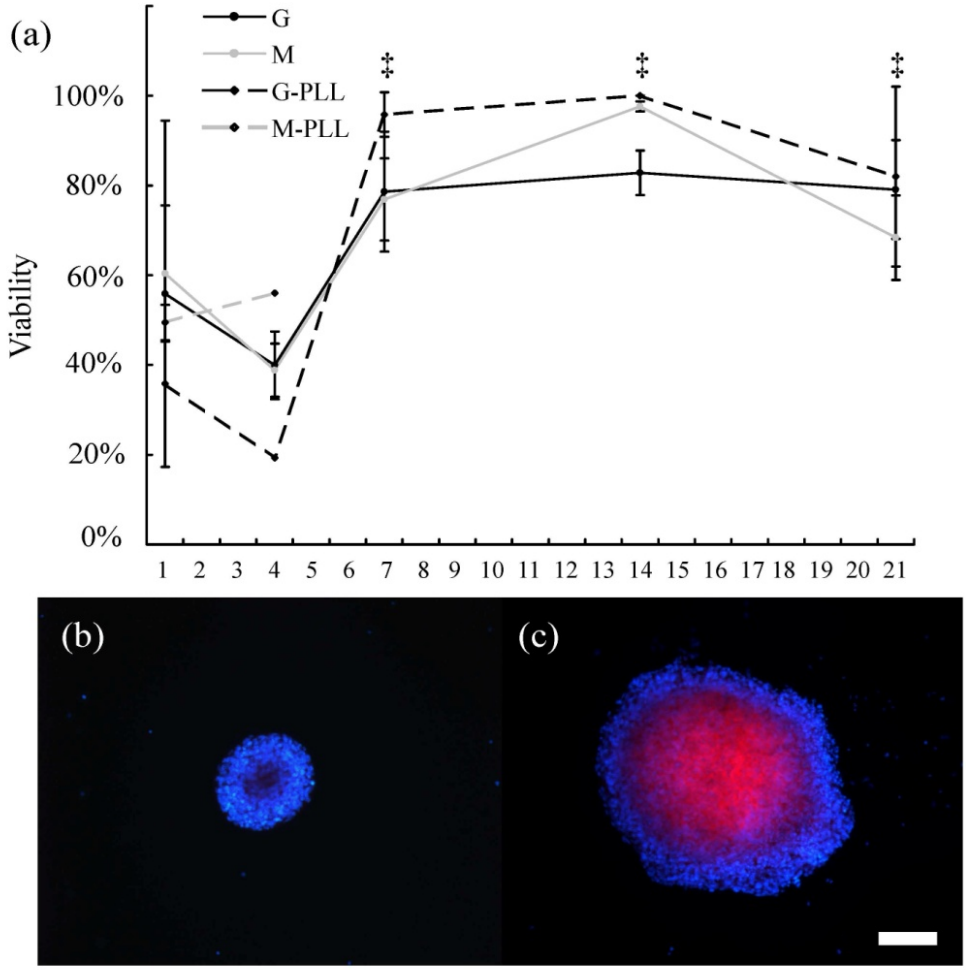
(a)
G
M
G-PLL
M-PLL
Viability
100%
80%
60%
40%
20%
0%
1 2 3 4 5 6 7 8 9 10 11 12 13 14 15 16 17 18 19 20 21
‡
(b)
(c)
(d)
Cell Number per 20 Beads
20,000
18,000
16,000
14,000
12,000
10,000
8,000
6,000
4,000
2,000
0
†

Immunocytochemistry of Cells in Alginate

Results of immunocytochemistry were limited due to bead instability during staining, and dehydration and processing seemed to affect tissue appearance. However, preliminary results revealed that encapsulated NSCs express nestin on the periphery and GFAP in the center of larger proliferating cell masses after entrapment in alginate (Figure 2.3a-b). Smaller neurospheres were often nestin positive and largely GFAP negative (data not shown). This profile of expression is typical for that observed with similar neurosphere-derived cells in culture (Campos, Leone et al. 2004). No expression of TUJ-1 was observed. Interestingly, some evidence of limited NG-2 expression was observed in one bead, indicating oligodendrocyte precursors (Figure 2.3c).

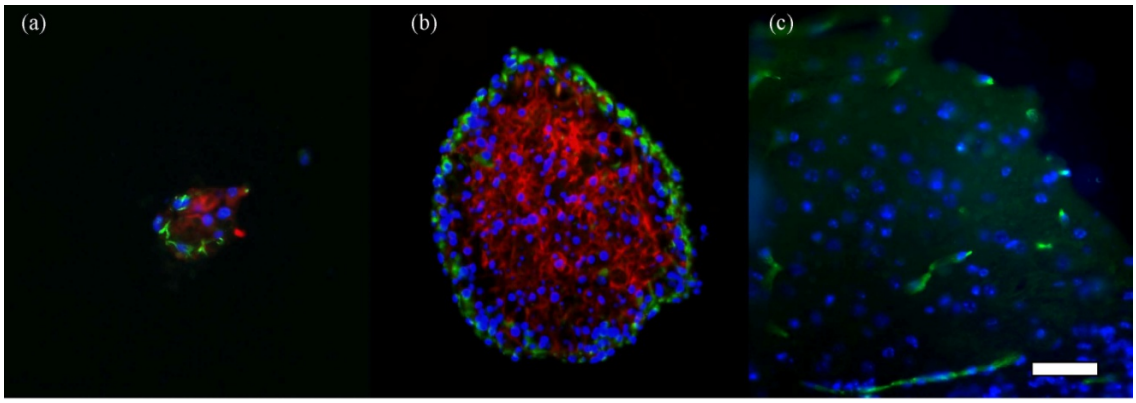

Figure 2.3. Encapsulated NSCs express nestin (green) on the periphery and GFAP (red) in the center of cell masses after entrapment in alginate (a-b). Interestingly, some evidence of limited NG-2 expression (green) was observed in one bead, indicating oligodendrocyte progenitors (c). All nuclei were counterstained with Hoechst (blue). Images are from (a) G, 14 day, (b) M-PLL, 14 day, and (c) G-PLL, 4 day, scaffolds and time points. Scale = 50 microns.

Bioactivity of Conditioned Medium from NSC-Seeded Beads

Results of a viability assay revealed a significant protective effect of conditioned medium collected from NSCs encapsulated in G beads against serum withdrawal-mediated PC-12 cell death over 48 hours (Figure 2.4a, $p < 0.05$). These results are novel for cortical

NSCs, and corroborate a similar study done with hippocampal NSCs (Li, Liu et al. 2007). Representative images of live and dead PC-12 cells are shown for NSC-conditioned and control medium treatments in Figure 2.4b and c, respectively.

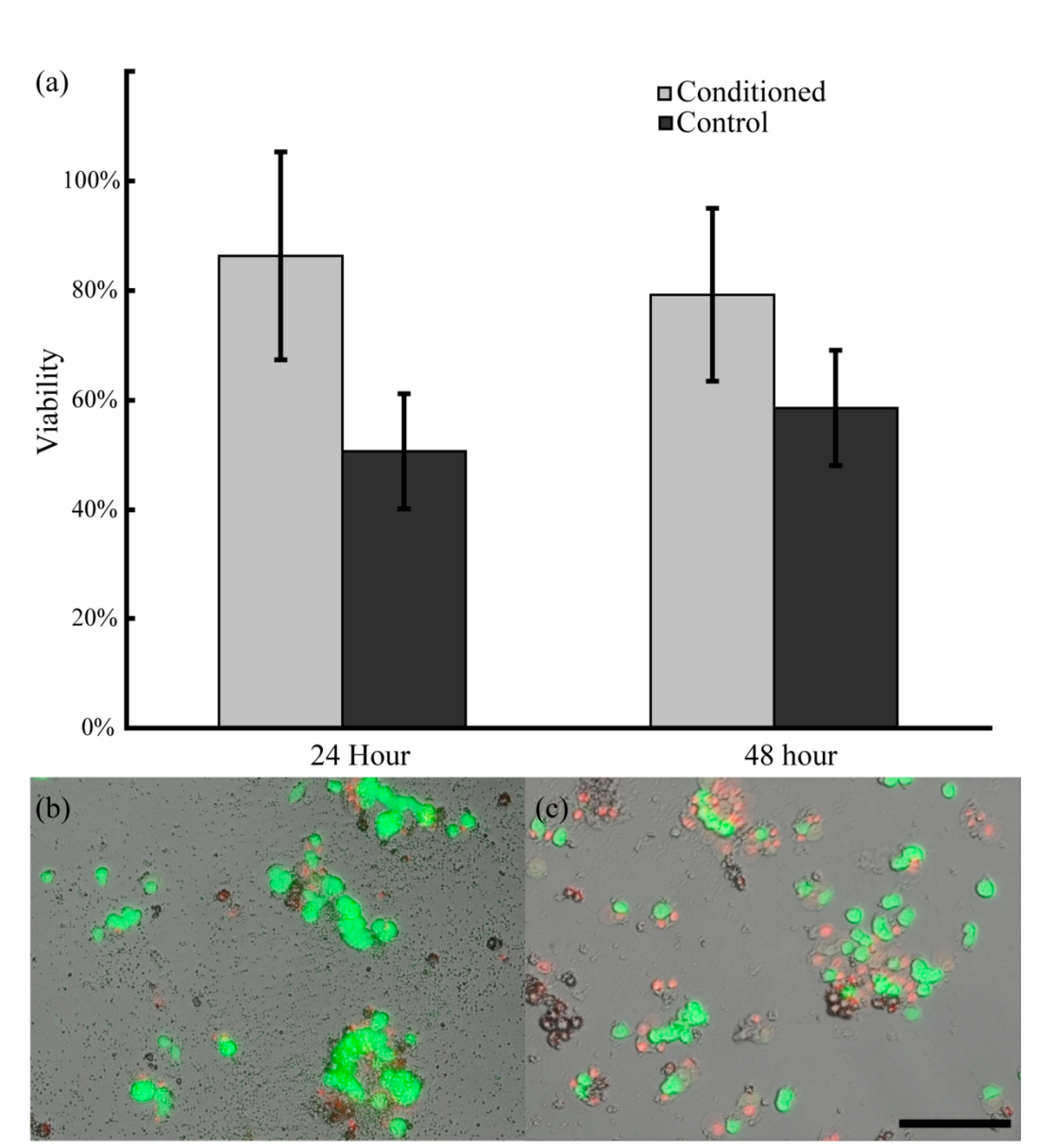

Figure 2.4. NSC-conditioned medium from G encapsulated cells protects PC-12 cells from serum withdrawal-mediated cell death (a) ($p < 0.05$, ANOVA). Representative images of live (green) and dead (red) PC-12 cells after a 50% serum withdrawal and treatment with medium conditioned by NSC-seeded (b, 75.6% viable) or unseeded (c, 49.5% viable) alginate microspheres. Results are reported as a percentage of control PC-12 cell viability. Mean ± s.e.m. is shown. Scale = 100 microns.

Discussion

Alginate composition has been shown to affect encapsulated cell proliferation and secretion of therapeutic proteins, as well as the mechanical stability of the scaffold (Constantinidis, Rask et al. 1999; Strand, Morch et al. 2000; Stabler, Wilks et al. 2001). We sought to characterize the effects composition may have on NSCs, as alginate is largely unstudied as a carrier for these cells. NSCs survive and proliferate in alginate irrespective of the scaffold compositions tested in this study. Among the conditions tested, a high G content alginate without a PLL coating layer was the optimal composition based on its mechanical stability during the osmotic pressure test and support of neurotrophic factor release.

Our data reveal that cortical NSCs, even when encapsulated in alginate, secrete NGF, BDNF and GDNF into the surrounding media. Importantly, these neurotrophic factors are known to support neuronal survival and plasticity in various models of axonopathy and neuropathy (Kolb, Gorny et al. 1997; Han and Holtzman 2000; Nicole, Ali et al. 2001; Lu, Pang et al. 2005; Wilkins and Compston 2005). Quantitative analysis of constitutive neurotrophic factor release from NSCs is relatively rarely reported in the literature, despite the popular theory that release of these proteins and their effects on compromised host tissue is a potential mechanism behind the cells' restorative capacity (Ourednik, Ourednik et al. 2002; Teng, Lavik et al. 2002; Lindvall, Kokaia et al. 2004; Llado, Haenggeli et al. 2004; Martino and Pluchino 2006). Time courses of release are generally lacking, as are release profiles from scaffolded cells. Lu *et al.* reported detection of NGF, BDNF, and GDNF in medium collected from C17.2 neural stem cells

after a 24 hour time point, with levels in the 10-70 pg/million cells/day range (Lu, Jones et al. 2003). GDNF and NGF, but not BDNF, secretion was detected from these cells in a separate report (Llado, Haenggeli et al. 2004). GDNF release from alginate encapsulated and unencapsulated hippocampal NSCs tended to be approximately 500-1,000 pg/million cells after 72 hours, as reported by Li *et al.* (Li, Liu et al. 2007). Our results are consistent with these ranges.

This study revealed that the detection of released neurotrophic factors is influenced by alginate composition and time. BDNF and GDNF are detected at single time points (4 and 14 days, respectively), while NGF release is observed throughout the study by unencapsulated and encapsulated cells. NGF is detected on fewer days (occurring only in the first week post-encapsulation) from encapsulated cells in comparison to unencapsulated cells, possibly due to the initial reduction in viability of the cells by encapsulation, degradation of the NGF protein, or interactions of NGF with the alginate matrix. GDNF and NGF are only detected from encapsulated cells when a high G, non-PLL coated capsule is used. Meanwhile, BDNF is released from cells in all conditions tested. Why the high G alginate capsules seem more permissive to neurotrophic factor release is unclear, given that previous literature for insulin-secreting cells has suggested reduced proliferation and less secretion at early time points for cells encapsulated in high G alginate (Stabler, Wilks et al. 2001). No significant effect of alginate composition on NSC proliferation was demonstrated here, which may be due to the relatively low alginate weight percentage (1%) used, as well as differences in the cell types studied. Additionally, the increased gel porosity of high G alginate (which could be further

enhanced by swelling) and the potential for stabilization of trophic factors by interaction with the alginate matrix are possible explanations (Martinsen, Storro et al. 1992; Peters, Isenberg et al. 1998). Since neurotrophic factors are larger than insulin (approximately 20-30 kDa versus 5 kDa), the increased porosity of high G alginate may be necessary to allow for adequate release. It has been suggested that interaction with alginate may stabilize growth factors (Peters, Isenberg et al. 1998). The release timing of individual neurotrophic factors may be explained by cellular events and their relationship to evolving environmental cues, and the quantities and timing of neurotrophic factor release is likely to vary with culture conditions. BDNF release coincided with low cell viability, while GDNF detection occurred at a time of increased viability and cell number. It is important to note that the initial drop in viability following encapsulation could affect the types and quantities of trophic factors released from the cells. However, elucidating the mechanisms behind the release profile of neurotrophic factors by the NSCs is beyond the scope of the current work.

The mechanical stability of alginate *in vivo* over time remains an important challenge (Orive, Hernandez et al. 2003; Nunamaker, Purcell et al. 2007). In a cell encapsulation application, alginate localizes graft cells to the transplant site and isolates them from the immune response, and loss of mechanical strength may compromise these functions. Alginates with a high G content are known to be more mechanically stable than those with higher M contents, due to stabilization by additional cross-links (Strand, Morch et al. 2000). That result was verified here, where the stability of alginate capsules of varying compositions was semi-quantitatively compared by an osmotic pressure test. High G

capsules remained intact far more frequently when exposed to solutions of low osmolarities compared to M beads and PLL-coated conditions, and no evidence of decreased proliferation and therapeutic factor secretion was observed. A tradeoff between cellular function and scaffold mechanical strength has been reported previously with insulin-secreting cells (Stabler, Wilks et al. 2001). However, this tradeoff was more pronounced for higher weight percentage (2%) alginates than the weight percentage (1%) used here. Additionally, this phenomenon was reported for a markedly different cell type than the one studied here, with presumably substantial impacts on proliferation and secretion characteristics.

It was somewhat surprising that the PLL-coated capsules were more prone to breakage than uncoated beads during the osmotic pressure test, given that PLL has been credited with improving mechanical stability (Benson, Papas et al. 1997; Rokstad, Holtan et al. 2002). This data requires careful interpretation, with consideration for the consequences of saline washing, the potential effects of polycation coating on swelling behavior, the impact of alginate concentration, and the definition of mechanical stability. The results may be affected by the multiple saline washes used in the coating protocol. Monovalent sodium ions may compete with divalent calcium ions for binding sites between G residues, and ultimately break the cross-links and weaken the gel (Wang and Spencer 1998). We have previously reported a study in which uncoated and PLL-coated alginate disks were washed identically in saline, implanted subcutaneously in rats, and monitored over a three month time period for mechanical stability, weight changes related to swelling behavior, and biocompatibility (Nunamaker, Purcell et al. 2007). PLL-coating

resulted in a slight but significant increase in complex modulus seven days after implantation in comparison to non-coated gels; no other significant differences in stability between the two conditions were noted. Therefore, PLL coating may confer a slight advantage, or at least have a non-detrimental role, on gel stability when results are not affected by saline washing. However, saline washing is a prototypic part of PLL coating protocols; thus if coating is pursued, the current results indicate that the potentially destabilizing effects of saline washing should be considered.

In the same study, both PLL and non-coated gels initially dropped in weight following implantation, followed by similar trends in increasing weight (interpreted as swelling) for a period of two weeks. The weight gains were greater for non-coated than PLL-coated samples, potentially indicating greater swelling. Previous research has indicated that osmotic swelling of the bead core against a less elastic polycation membrane may eventually cause capsules to burst (Thu, Bruheim et al. 1996). Therefore, although the G capsules may not burst, they may swell during exposure to an osmotic challenge, likely changing diffusion properties (which may, in turn, be related to their permissiveness to neurotrophic factor release) (Gugerli, Cantana et al. 2002). The capsules in this study may be particularly vulnerable to swelling and saline effects due to the relatively low weight percentage used (1%); increased alginate concentration improves resistance to swelling (Thu, Bruheim et al. 1996). Finally, the way in which mechanical stability is measured (i.e. rheology in the *in vivo* study, osmotic pressure in the *in vitro* study) is likely to affect results. De Castro *et al*. reported PLL-coating to confer superior

resistance to compression, but the lowest resistance to osmotic pressure, in a mechanical stability test of three different polycation coatings (De Castro, Orive et al. 2005).

The authors in the current study hypothesize that alginate beads were initially weakened by saline washes prior to PLL coating, and swelled in response to solutions of low osmolarity against the PLL coating, causing them to burst. Thus, the mechanical stability of uncoated beads was improved compared to coated beads in the current experiment, but consideration for the effects of saline washing, swelling behavior and changes in diffusion characteristics is required. Importantly, PLL coating has been credited with isolating alginate from IgG and complement diffusion into the gel. The coating protocol used in the experiments reported here was recommended to achieve this property (Kulseng, Thu et al. 1997). However, polycation coatings are still controversial after over 25 years of research due to the fact that they may directly elicit a tissue response (King, Sandler et al. 2001; Strand, Ryan et al. 2001; van Raamsdonk, Cornelius et al. 2002; King, Lau et al. 2003; Orive, Hernandez et al. 2003; Orive, Tam et al. 2006). In addition to the questionable effect on *in vivo* biocompatibility, our data demonstrate bead breakage during an osmotic challenge and reduced neurotrophic factor detection associated with PLL coating.

Our results indicate that a high G alginate without PLL coating was the optimal composition for NSC encapsulation amongst the conditions tested based on superior mechanical stability during the osmotic pressure test and support of neurotrophic factor release. However, several opportunities for further development remain. Alternative

polycations or a different polycation coating procedure may allow for tailoring diffusivity properties without a loss in mechanical stability or neurotrophic factor detection (Orive, Hernandez et al. 2003). Alginate weight percentage variation, bead size reduction, and incorporation of interpenetrating networks are additional examples of methods which may improve results (Desai, Sojomihardjo et al. 2000; Stabler, Wilks et al. 2001; Canaple, Rehor et al. 2002; Wang, Childs et al. 2005). We are currently evaluating the ability of a high G, non-PLL coated alginate scaffold seeded with NSCs to repair a cortical lesion *in vivo*, and early results are promising (Purcell, Seymour et al. 2007).

Acknowledgements

Special thanks to Soumya Yandamuri for performing blinded cell counts. The authors gratefully thank Dr. David Mooney and Dr. David Martin and their students for assistance in cell encapsulation training. Thanks to Joe Kazemi and the Center for Statistical Consultation and Research (CSCAR) at the University of Michigan for their assistance with statistical methods. This project was supported by the Center for Neural Communication Technology (NIBIB, P41 EB002030), a NSF Graduate Research Fellowship, and a Rackham Engineering Award from the University of Michigan.

References

Ashton, R. S., A. Banerjee, et al. (2007). "Scaffolds based on degradable alginate hydrogels and poly(lactide-co-glycolide) microspheres for stem cell culture." Biomaterials **28**(36): 5518-25.

Benson, J. P., K. K. Papas, et al. (1997). "Towards the development of a bioartificial pancreas: effects of poly-L-lysine on alginate beads with BTC3 cells." Cell Transplant **6**(4): 395-402.

Borlongan, C. V., S. J. Skinner, et al. (2004). "Intracerebral transplantation of porcine choroid plexus provides structural and functional neuroprotection in a rodent model of stroke." Stroke **35**(9): 2206-10.

Bunger, C. M., A. Jahnke, et al. (2002). "MTS colorimetric assay in combination with a live-dead assay for testing encapsulated L929 fibroblasts in alginate poly-L-lysine microcapsules in vitro." Artif Organs **26**(2): 111-6.

Campos, L. S., D. P. Leone, et al. (2004). "Beta1 integrins activate a MAPK signalling pathway in neural stem cells that contributes to their maintenance." Development **131**(14): 3433-44.

Canaple, L., A. Rehor, et al. (2002). "Improving cell encapsulation through size control." J Biomater Sci Polym Ed **13**(7): 783-96.

Constantinidis, I., I. Rask, et al. (1999). "Effects of alginate composition on the metabolic, secretory, and growth characteristics of entrapped beta TC3 mouse insulinoma cells." Biomaterials **20**(21): 2019-27.

Cowell, R. M., J. M. Plane, et al. (2003). "Complement activation contributes to hypoxic-ischemic brain injury in neonatal rats." J Neurosci **23**(28): 9459-68.

De Castro, M., G. Orive, et al. (2005). "Comparative study of microcapsules elaborated with three polycations (PLL, PDL, PLO) for cell immobilization." J Microencapsul **22**(3): 303-15.

De Vos, P., B. De Haan, et al. (1997). "Effect of the alginate composition on the biocompatibility of alginate-polylysine microcapsules." Biomaterials **18**(3): 273-8.

Desai, N. P., A. Sojomihardjo, et al. (2000). "Interpenetrating polymer networks of alginate and polyethylene glycol for encapsulation of islets of Langerhans." J Microencapsul **17**(6): 677-90.

Gaillard, A., L. Prestoz, et al. (2007). "Reestablishment of damaged adult motor pathways by grafted embryonic cortical neurons." Nat Neurosci **10**(10): 1294-9.

Greene, L. A. and A. S. Tischler (1976). "Establishment of a noradrenergic clonal line of rat adrenal pheochromocytoma cells which respond to nerve growth factor." Proc Natl Acad Sci U S A **73**(7): 2424-8.

Gugerli, R., E. Cantana, et al. (2002). "Quantitative study of the production and properties of alginate/poly-L-lysine microcapsules." J Microencapsul **19**(5): 571-90.

Han, B. H. and D. M. Holtzman (2000). "BDNF protects the neonatal brain from hypoxic-ischemic injury in vivo via the ERK pathway." J Neurosci **20**(15): 5775-81.

Heine, W., K. Conant, et al. (2004). "Transplanted neural stem cells promote axonal regeneration through chronically denervated peripheral nerves." Exp Neurol **189**(2): 231-40.

Joki, T., M. Machluf, et al. (2001). "Continuous release of endostatin from microencapsulated engineered cells for tumor therapy." Nat Biotechnol **19**(1): 35-9.

King, A., J. Lau, et al. (2003). "The effect of capsule composition in the reversal of hyperglycemia in diabetic mice transplanted with microencapsulated allogeneic islets." Diabetes Technol Ther **5**(4): 653-63.

King, A., S. Sandler, et al. (2001). "The effect of host factors and capsule composition on the cellular overgrowth on implanted alginate capsules." J Biomed Mater Res **57**(3): 374-83.

Kolb, B., G. Gorny, et al. (1997). "Nerve growth factor stimulates growth of cortical pyramidal neurons in young adult rats." Brain Res **751**(2): 289-94.

Kulseng, B., B. Thu, et al. (1997). "Alginate polylysine microcapsules as immune barrier: permeability of cytokines and immunoglobulins over the capsule membrane." Cell Transplant **6**(4): 387-94.

Li, X., T. Liu, et al. (2007). "Effect of neural stem cells on apoptosis of PC12 cells induced by serum deprivation." Biotechnol Prog **23**(4): 952-7.

Li, X., T. Liu, et al. (2006). "Culture of neural stem cells in calcium alginate beads." Biotechnol Prog **22**(6): 1683-9.

Lim, F. and A. M. Sun (1980). "Microencapsulated islets as bioartificial endocrine pancreas." Science **210**(4472): 908-10.

Lindvall, O., Z. Kokaia, et al. (2004). "Stem cell therapy for human neurodegenerative disorders-how to make it work." Nat Med **10 Suppl**: S42-50.

Llado, J., C. Haenggeli, et al. (2004). "Neural stem cells protect against glutamate-induced excitotoxicity and promote survival of injured motor neurons through the secretion of neurotrophic factors." Mol Cell Neurosci **27**(3): 322-31.

Lu, B., P. T. Pang, et al. (2005). "The yin and yang of neurotrophin action." Nat Rev Neurosci **6**(8): 603-14.

Lu, P., L. L. Jones, et al. (2003). "Neural stem cells constitutively secrete neurotrophic factors and promote extensive host axonal growth after spinal cord injury." Exp Neurol **181**(2): 115-29.

Martino, G. and S. Pluchino (2006). "The therapeutic potential of neural stem cells." Nat Rev Neurosci **7**(5): 395-406.

Martinsen, A., G. Skjak-Baek, et al. (1989). "Alginate as Immobilization Material: I. Correlation between Chemical and Physical Properties of Alginate Gel Beads." Biotechnol Bioeng **33**(1): 79-89.

Martinsen, A., I. Storro, et al. (1992). "Alginate as Immobilization Material .3. Diffusional Properties." Biotechnology and Bioengineering **39**(2): 186-194.

Nicole, O., C. Ali, et al. (2001). "Neuroprotection mediated by glial cell line-derived neurotrophic factor: involvement of a reduction of NMDA-induced calcium influx by the mitogen-activated protein kinase pathway." J Neurosci **21**(9): 3024-33.

Nunamaker, E. A., E. K. Purcell, et al. (2007). "In vivo stability and biocompatibility of implanted calcium alginate disks." J Biomed Mater Res A **83**(4): 1128-37.

Orive, G., R. M. Hernandez, et al. (2003). "Cell encapsulation: promise and progress." Nat Med **9**(1): 104-7.

Orive, G., S. K. Tam, et al. (2006). "Biocompatibility of alginate-poly-L-lysine microcapsules for cell therapy." Biomaterials **27**(20): 3691-700.

Ourednik, J., V. Ourednik, et al. (2002). "Neural stem cells display an inherent mechanism for rescuing dysfunctional neurons." Nat Biotechnol **20**(11): 1103-10.

Peters, M. C., B. C. Isenberg, et al. (1998). "Release from alginate enhances the biological activity of vascular endothelial growth factor." J Biomater Sci Polym Ed **9**(12): 1267-78.

Pluchino, S., L. Zanotti, et al. (2005). "Neurosphere-derived multipotent precursors promote neuroprotection by an immunomodulatory mechanism." Nature **436**(7048): 266-71.

Purcell, E. K., J. P. Seymour, et al. (2007). In Vivo Evaluation of a Neural Stem Cell-Seeded Chronic Probe. Society for Neuroscience, San Diego, CA.

Reynolds, B. A. and S. Weiss (1992). "Generation of neurons and astrocytes from isolated cells of the adult mammalian central nervous system." Science **255**(5052): 1707-10.

Reynolds, B. A. and S. Weiss (1996). "Clonal and population analyses demonstrate that an EGF-responsive mammalian embryonic CNS precursor is a stem cell." Dev Biol **175**(1): 1-13.

Rokstad, A. M., S. Holtan, et al. (2002). "Microencapsulation of cells producing therapeutic proteins: optimizing cell growth and secretion." Cell Transplant **11**(4): 313-24.

Soon-Shiong, P., M. Otterlie, et al. (1991). "An immunologic basis for the fibrotic reaction to implanted microcapsules." Transplant Proc **23**(1 Pt 1): 758-9.

Stabler, C., K. Wilks, et al. (2001). "The effects of alginate composition on encapsulated betaTC3 cells." Biomaterials **22**(11): 1301-10.

Strand, B. L., O. Gaserod, et al. (2002). "Alginate-polylysine-alginate microcapsules: effect of size reduction on capsule properties." J Microencapsul **19**(5): 615-30.

Strand, B. L., Y. A. Morch, et al. (2000). "Alginate as immobilization matrix for cells." Minerva Biotecnologica **12**(4): 223-233.

Strand, B. L., T. L. Ryan, et al. (2001). "Poly-L-Lysine induces fibrosis on alginate microcapsules via the induction of cytokines." Cell Transplant **10**(3): 263-75.

Teng, Y. D., E. B. Lavik, et al. (2002). "Functional recovery following traumatic spinal cord injury mediated by a unique polymer scaffold seeded with neural stem cells." Proc Natl Acad Sci U S A **99**(5): 3024-9.

Thu, B., P. Bruheim, et al. (1996). "Alginate polycation microcapsules. II. Some functional properties." Biomaterials **17**(11): 1069-79.

Van Raamsdonk, J. M. and P. L. Chang (2001). "Osmotic pressure test: a simple, quantitative method to assess the mechanical stability of alginate microcapsules." J Biomed Mater Res **54**(2): 264-71.

van Raamsdonk, J. M., R. M. Cornelius, et al. (2002). "Deterioration of polyamino acid-coated alginate microcapsules in vivo." J Biomater Sci Polym Ed **13**(8): 863-84.

Wang, M. S., R. F. Childs, et al. (2005). "A novel method to enhance the stability of alginate-poly-L-lysine-alginate microcapsules." J Biomater Sci Polym Ed **16**(1): 91-113.

Wang, X. and H. G. Spencer (1998). "Calcium alginate gels: formation and stability in the presence of an inert electrolyte." Polymer **39**: 2759-2764.

Wikstrom, J., M. Elomaa, et al. (2008). "Alginate-based microencapsulation of retinal pigment epithelial cell line for cell therapy." Biomaterials **29**(7): 869-76.

Wilkins, A. and A. Compston (2005). "Trophic factors attenuate nitric oxide mediated neuronal and axonal injury in vitro: roles and interactions of mitogen-activated protein kinase signalling pathways." J Neurochem **92**(6): 1487-96.

CHAPTER 3
IN VIVO STABILITY AND BIOCOMPATIBILITY OF CALCIUM ALGINATE DISKS

Abstract

Alginate is a commonly used biomedical hydrogel whose *in vivo* degradation behavior is only beginning to be understood. The use of alginate in the central nervous system is gaining popularity as an electrode coating, cell encapsulation matrix, and for duraplasty. However, it is necessary to understand how the hydrogel will behave *in vivo* to aid in the development of alginate for use as a neural interface material. The goal of the current study was to compare the rheological behavior of explanted alginate disks and the inflammatory response to subcutaneously implanted alginate hydrogels over a 3 month period. Specifically, the effects due to (1) *in situ* gelling, (2) diffusion gelling and (3) use of a poly-L-lysine coating were investigated. While all samples' complex moduli decreased 80% in the first day, *in situ* gelled alginate was more stable for the first week of implantation. The poly-L-lysine coating offered some stability increases for diffusion gelled alginate, but the stability in both conditions remained significantly lower than *in situ* gelled alginate. There were no differences in biocompatibility that clearly suggested one gelation method over another. These results indicate that *in situ* gelation is the preferred method in neural interface applications where stability is the primary concern.

Keywords: Hydrogel, Alginate, Degradation, Biocompatibility

Introduction

Recently, there have been several reports utilizing alginate in advanced neural interface technologies. These include microelectrode coatings, cell scaffolds, neural stem cell encapsulation, and development of an artificial dura mater (Becker and Kipke 2003; Vetter, Becker et al. 2003; Kim, Abidian et al. 2004; Kajiwara, Ogata et al. 2005; Purcell and Kipke 2006; Purcell, Seymour et al. 2006; Nunamaker, Otto et al. in submission; Nunamaker, Otto et al. in submission). Alginate shows promise and utility as a material in the development of advanced neural interfaces. Its long-term biocompatibility, mild reaction conditions that allow hydrogel cross-linking while in direct contact with neural tissues, and minimal risk of seizure activity in rats are especially important considering the imminent and prolonged contact of the hydrogel components with neural tissues (Draget, SkjakBraek et al. 1997; Le Tallec, Korwin-Zmijowska et al. 1997; Aydelotte, Thonar et al. 1998; Becker, Kipke et al. 2001; Becker, Kipke et al. 2002; Becker and Kipke 2003; Nguyen, Qian et al. 2003; Becker, Preul et al. 2005). Unfortunately, little is known about the long-term stability of alginate, which may be important to the lifetime of advanced neural prosthetic devices incorporating this material.

Alginate is a naturally occurring polysaccharide copolymer that can be used to create hydrogels with a broad range of material properties. Derived from brown algae, alginate is composed of blocks of both β-D-mannuronic acid (M) and α-L-guluronic acid (G) linked together by 1,4-bonds (Haug 1964; Lahaye 2001). Alginate is water soluble and can be ionically cross-linked by various divalent ions (Haug and Smidsrod 1965). Currently Ca^{2+} is preferred to cross-link alginate for biomedical applications due to the mild reaction conditions compared to the cellular toxicity of both Ba^{2+} and Sr^{2+} (Haug

and Smidsrod 1965; Smidsrod and Haug 1965; Draget, SkjakBraek et al. 1997; Wideroe and Danielsen 2001). In the process of cross-linking, the calcium ions interact with the carboxyl groups of the G blocks of two neighboring alginate chains forming an "egg box" orientation (Grant, Morris et al. 1973). Because of the large variety of alginate sources and G and M block ratios, the properties of the resulting cross-linked gels can be highly variable. Alginate with a higher G content typically results in stronger gels; while alginate with a higher M content yields more flexible gels (Amsden and Turner 1999).

Two methods of gelation have been extensively described and used to create alginate hydrogels: diffusion gelling and *in situ* gelling (Figure 3.1) (Haug and Smidsrod 1965; Smidsrod and Haug 1965; Smidsrod and Haug 1972; Wang, Zhang et al. 1993; Wang, Zhang et al. 1994; Yamagiwa, Kozawa et al. 1995; Ishikawa, Ueyama et al. 1999; Becker, Kipke et al. 2001; Kuo and Ma 2001; Shchipunov, Koneva et al. 2002; Liu, Qian et al. 2003; Mammarella and Rubiolo 2003). $CaCl_2$ is a commonly used calcium source that relies on diffusion to cross-link alginate. Ca^{2+} can readily dissociate from the Cl^- to cross-link the first carboxyl groups with which it comes into contact. This rapid reaction creates a skin around the volume of liquid alginate. Subsequently, the calcium ions diffuse inward (i.e. diffusion gelling), increasing the skin's thickness as the alginate bolus is cross-linked (Blandino, Macias et al. 1999; Bienaime, Barbotin et al. 2003). Although this results in rapid gel formation, the resulting hydrogel structure is highly variable (Aydelotte, Thonar et al. 1998; Bienaime, Barbotin et al. 2003). Despite this, diffusion gelling remains an ideal approach that is widely used for rapidly encapsulating cells in microspheres of alginate (Li, Altreuter et al. 1996; Kulseng, Thu et al. 1997; Strand,

Morch et al. 2000; Kuo and Ma 2001; Rokstad, Holtan et al. 2002; Wang, Shelton et al. 2003).

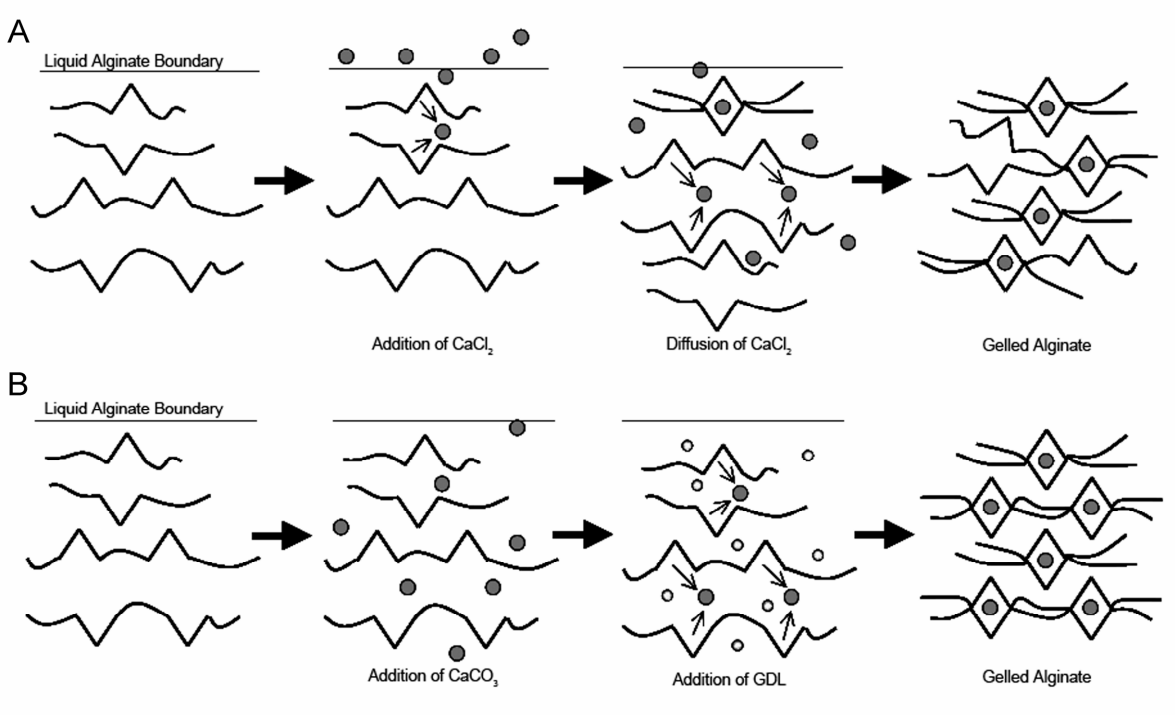

Figure 3.1. Diffusion and *in situ* gelling of liquid alginate. A. Diffusion gelling. Calcium ions diffuse through the liquid alginate boundary, cross-linking alginate strands as the ions move through the volume of alginate. Cross-links are not uniformly distributed throughout the gel. B. *In situ* gelling. $CaCO_3$ is mixed with alginate to create a homogeneous mixture (black circles). D-Glucono-δ-lactone (GDL, grey circles) is added to acidify the solution and release calcium ions, making them available for cross-linking. The resultant hydrogel has a uniform distribution of cross-links.

$CaCO_3$ and $CaSO_4$ are commonly used Ca^{2+} sources that rely on internal gelling through the release of calcium ions *in situ*. In the case of $CaCO_3$, poorly soluble calcium ions in the form of $CaCO_3$ are homogeneously mixed with alginate and then the Ca^{2+} is solubilized by the addition of catalyst, such as D-glucono-δ-lactone (GDL). GDL slowly acidifies the alginate:$CaCO_3$ solution, driving the release of Ca^{2+} (Draget, Ostgaard et al. 1991; Shchipunov, Koneva et al. 2002). Calcium ions bind to the nearest available

carboxyl groups on the alginate molecules, cross-linking the hydrogel in a spatially uniform manner. This method can be time intensive due to the time required for the hydrolysis of GDL and subsequent calcium release; however, the resultant hydrogel has a more uniform and reproducible structure (Draget, Ostgaard et al. 1991; Kuo and Ma 2001; Shchipunov, Koneva et al. 2002).

Diffusion gelled alginate has previously been shown to destabilize both *in vitro* and *in vivo* (LeRoux, Guilak et al. 1999; King, Sandler et al. 2001; Kong, Alsberg et al. 2004). Prolonged exposure to sodium ions decreases both compressive and shear stiffness of alginate, suggesting that physiological conditions will soften the gel over a time period of up to 7 days after gelation (LeRoux, Guilak et al. 1999). Further, LeRoux *et al*. showed that high M alginate hydrogels exhibited a significant decrease in complex modulus but retained solid-like behavior after 7 days of exposure to 0.15M NaCl and 1.8mM $CaCl_2$ (LeRoux, Guilak et al. 1999). Kong *et al.*, however, demonstrated the superior retention of elastic modulus of high G alginate over high M alginate implanted up to 35 days (Kong, Alsberg et al. 2004). This effect is due to calcium's higher affinity for G sites than M sites, resulting in a more dense distribution of cross-links in a high G concentration hydrogels. This dense distribution of cross-links enhances the stability of high G alginate hydrogels after prolonged exposure to the inert electrolytes found *in vivo*, thereby decreasing the effect of ion exchange at the cross-link site (Kong, Alsberg et al. 2004). While these previous studies support our current investigations of high G alginate stability *in vivo*, there are currently no studies that investigate stability differences based on gelation method.

Poly-L-lysine (PLL) coatings are commonly used to stabilize alginate capsules and provide a barrier to immune system components such as IgG in cell encapsulation applications (Kulseng, Thu et al. 1997; Gugerli, Cantana et al. 2002). Unfortunately, there is evidence that the PLL coating itself may be toxic to encapsulated cells and cause an unfavorable foreign body response (King, Sandler et al. 2001; Strand, Ryan et al. 2001; Rokstad, Holtan et al. 2002; King, Lau et al. 2003). Additionally, claims that PLL coatings improve alginate mechanical stability have been based on *in vitro* findings. PLL-coated alginate capsules seeded with proliferative cells remained intact for longer periods of time compared to non-coated capsules in culture (Benson, Papas et al. 1997; Rokstad, Holtan et al. 2002). Given the potential toxicity of PLL on encapsulated cells, these results may be confounded by a slight reduction in cell proliferation, which could in turn result in more stable capsules. While quantitative testing has revealed that increased PLL membrane thickness corresponds with more mechanically stable non-seeded capsules *in vitro*, quantitative *in vivo* mechanical testing has not been reported in the literature (Gugerli, Cantana et al. 2002). Given that polycation coatings remain controversial after 25 years of research due to questionable biocompatibility, and that quantitative *in vivo* material testing data is lacking, there is a clear need to explore the *in vivo* biocompatibility and stability of PLL-coated alginate in comparison to uncoated alginate (Orive, Hernandez et al. 2003).

In the current study, we investigated alginate disks cross-linked with $CaCl_2$ or $CaCO_3$ and measured each of the following parameters over time: (1) weight changes, (2) complex modulus, (3) loss angle, and (4) biological response to the subcutaneously implanted

disks. Additionally, we investigated the effects of PLL coatings on $CaCl_2$ cross-linked alginate disks on these same four parameters. The goal of this paper was to identify stability and biocompatibility differences in diffusion gelled and *in situ* gelled alginate samples and evaluate the necessity of PLL coatings for enhanced stability. Specifically, we wanted to identify any advantages (biocompatibility or stability) of the specific gelation methods and hydrogel coating to guide future development of advanced neural interface technologies.

Materials and Methods

Alginate Hydrogel Preparation

High G content sodium alginate (66% G acid) was acquired from Novamatrix (Pronova UP LVG, Drammen, Norway). Non-coated hydrogels were prepared as previously described but with sterilized chemical components (Nunamaker, Otto et al. in submission; Nunamaker, Otto et al. in submission). Briefly, 1.95 wt% 43 mPas alginate was cross-linked following one of the reaction schemes outlined in Figure 3.1. The gelation method and volume of the resulting hydrogels for each specific experiment is outlined in Table 3.1. Rheology hydrogels were created in a sterile 10 ml beaker: 2 ml alginate was reacted with (1) 100 mM $CaCO_3$ (Sigma, St. Louis, MO) and 80 mM GDL (Sigma, St. Louis, MO) (final concentrations), or (2) 2 ml 200 mM $CaCl_2$ (Sigma, St. Louis, MO) (Table 3.1). Histology hydrogels were created in a single well of a sterile 24 well tissue culture plate: 500 µl of alginate was reacted with (1) 100 mM $CaCO_3$ and 80 mM GDL (final concentrations), or (2) 500 µl 200 mM $CaCl_2$ (Table 3.1). Hydrogels created via *in situ* gelling ($CaCO_3$) were well mixed before addition of GDL to ensure homogeneous distribution of cross-links throughout the gel. Hydrogels created via

diffusion gelling ($CaCl_2$) were cross-linked by slowly pipetting the $CaCl_2$ solution onto the bolus of alginate. All gels were allowed to fully cross-link under sterile conditions for 12 hours prior to implantation.

	Experiment	Alginate Volume (ml)	Cross-linker Volume	GDL (mg)	PLL Coating	*n* per Time Point
$CaCO_3$	Histology	0.5	5 mg	7.1	No	6
	Rheology	2	20 mg	28.4	No	5
$CaCl_2$	Histology	0.5	0.5 mL; 200 mM	0	No	6
	Rheology	2	2 mL; 200 m*M*	0	No	5
$CaCl_2$/PLL	Histology	0.5	0.5 mL; 200 m*M*	0	Yes	6
	Rheology	2	2 mL; 200 m*M*	0	Yes	5

Table 3.1. The gelation conditions for all hydrogels to be implanted subcutaneously and analyzed via rheology or histology.

To test the effect of a PLL coating, $CaCl_2$ hydrogels made for rheology and histology were additionally coated with poly-L-lysine ($CaCl_2$/PLL) as described by Strand *et al*. (Table 3.1)(Strand, Gaserod et al. 2002). Briefly, alginate disks were rinsed in physiological saline and incubated for 10 minutes in 0.1% PLL in saline. PLL-HCl (15,000-30,000 MW) was obtained from Sigma (St. Louis, MO). Disks were rinsed again in saline and incubated for 10 minutes in 0.1% alginate in saline. Disks were rinsed a final time in saline prior to implantation. To maintain similarity to PLL coated hydrogels, $CaCl_2$ gels were also rinsed in saline several times prior to implantation.

Surgery

Alginate hydrogel stability and biocompatibility were tested in 300 g Sprague Dawley rats (Charles River Laboratories, Wilmington, MA). All procedures were approved by the University of Michigan Committee on Use and Care of Animals. Anesthesia was administered using an intra-peritoneal injection of an anesthetic cocktail (comprised of Ketamine, Xylazine, and Acepromazine, each at concentrations of 100 mg/ml and a respective mixing ratio of 5:0.5:1) administered at 0.15 ml/100 g body weight. Rats were indicated for rheology or histology before surgical implantation due to the size difference in the gels. All hydrogels were implanted in separate subcutaneous pouches created on the abdomen and the skin was securely closed with surgical staples.

Forty-eight rats were utilized in the rheology study, each receiving four hydrogels. The hydrogel conditions ($CaCO_3$, $CaCl_2$, or $CaCl_2$/PLL) were chosen at random for each animal, but no animal received more than 2 gels of the same condition. At the time of hydrogel recovery, the rats were deeply anesthetized with anesthetic cocktail (0.3 ml/100 g body weight) and then euthanized with a cardiac injection of 1 ml Fatal-Plus® (Pentobarbital 390 mg/ml, Vortech Pharmaceutical, Dearborn, MI). Five hydrogels per condition were recovered at each time point (1, 3, 5, 7, 14, 21, and 90 days) by removing the hydrogel from the subcutaneous pouch. All hydrogels were weighed and rheological measurements taken immediately following explantation.

Twelve rats were utilized in the histology study. Each rat was implanted with 2 gels per condition for all conditions ($CaCO_3$, $CaCl_2$, and $CaCl_2$/PLL), resulting in a total of 6

implants per animal. At each predetermined time point (7, 14, 21, and 90 days), the hydrogels were recovered from 3 rats per time point to evaluate the biological response to the implants. Rats were euthanized in the same manner as described for the rheology study. The tissue and alginate disk were explanted *en bloc* and treated with Bouin's Fixative for 24 hours.

Disk Weight Change

To determine the swelling/shrinking behavior of the hydrogels, all gels indicated for rheology were weighed prior to implantation. Immediately upon explantation, all gels were weighed again to determine an increase or decrease in disk weight. The average weight difference and standard error were calculated for each hydrogel condition ($CaCO_3$, $CaCl_2$, and $CaCl_2$/PLL) and time point (1, 3, 5, 7, 14, 21, and 90 days).

Rheology: Complex Modulus and Loss Angle

The viscoelastic behavior of the hydrogels was tested with a parallel plate rheometer (AR 550, TA Instruments, New Castle, DE) using a 25 mm plate at 37 ˚C. The alginate samples were compressed to 10% and subjected to a 1% strain across a frequency sweep of 1 to 100 rad/s at each level. Sandpaper (150-grit) was placed on the plate surfaces to minimize the occurrence of slip at the plate/sample interface. The storage (G') and loss moduli (G") were calculated by the rheometer and recorded for further analysis.

The complex modulus (G^*), which represents the frequency-dependent stiffness of the hydrogel, and loss angle, δ, which provides a relative measure of viscous effects to elastic effects in a material, were calculated as previously described (Nunamaker, Otto et al. in

submission). Low values of δ indicate minimal internal damping, a result of energy dissipation and internal friction in deformation cycles due to internal entanglements and cross-link density (δ = 0˚, elastic solid; δ = 90˚, Newtonian viscous fluid) (LeRoux, Guilak et al. 1999). The response of alginate to shear is a good indicator of the fatigue resistance and how it will perform *in vivo*. Brain tissue typically exhibits a complex modulus ranging from 1 to 24 kPa and alginate is expected to remain in this range (Donnelly and Medige 1997). For application in or on the brain, the frequency range of 1 Hz – 5 Hz was chosen, as this represents the heart rate frequency range of humans and rats and therefore the highest oscillation rate the gels would be exposed to *in vivo*. Average G^* and δ and the respective standard errors at 1 Hz and 5 Hz were calculated.

Histology

Tissue samples were dehydrated in a graded series of ethanol washes (10-70 %), embedded in paraffin, and sectioned with a microtome. Two 8 μm-thick sections per implant were each stained with hematoxylin and eosin (H&E) or Masson's trichrome (MT) based on previous reports (Kyriakides, Leach et al. 1999; Kang, Kang et al. 2005). H&E-stained sections were used to detect the presence of inflammatory response cells.

MT-stained sections were used to assess the degree of cell infiltration surrounding the implant on a qualitative scale (0-4), and to quantitatively evaluate the thickness of the encapsulating collagen layer as described (King, Sandler et al. 2001; Bos, Hennink et al. 2005; Kang, Kang et al. 2005). The scoring levels indicated increasing levels of infiltration: (0) no cells present on the surface of the alginate; (1) less than 50% of the surface area of alginate covered by cellular attachment indicating minor infiltration; (2)

greater than 50% of the surface area of alginate covered by cellular attachment indicating moderate infiltration; (3) 100% of the surface area of alginate covered by cellular attachment indicated severe infiltration. Due to the amount of variation seen in both of these measurements, infiltration scores were taken from 10 separate hydrogel fragments in different regions of the same tissue section. Similarly, collagen thickness was measured around 10 separate hydrogel fragments by taking 8 equally spaced measurements around each fragment. The repeated measures for each parameter (cell infiltration and encapsulation thickness) for a given tissue section were averaged, resulting in one infiltration score and one encapsulation thickness per section. For each parameter the results for a condition then were combined to calculate the average and standard error for each condition (7, 14, 21 and 90 days for CaCO3, CaCl2, and CaCl2/PLL).

Statistics

All results were analyzed for normality and subsequently analyzed by the appropriate ANOVA (parametric or non-parametric). When indicated, the appropriate post-hoc test was utilized to determine significant differences in the data. The statistical test used in each situation is reported with the results for each section of the study.

Results

Disk Weight Change

Due to the nature of gelation and coating of the hydrogels, the gels had significantly different initial weights (Dunn's comparison test). $CaCO_3$ reacted alginate was significantly heavier than $CaCl_2$ or $CaCl_2$/PLL reacted alginate ($p < 0.001$, Figure 3.2A).

$CaCl_2$/PLL hydrogels were also significantly heavier than $CaCl_2$ reacted alginate ($p <$ 0.001, Figure 3.2A) due to the PLL coating of the hydrogel.

Hydrogel weights varied with duration of implant (Figure 3.2B). $CaCO_3$ reacted hydrogels trended towards a continual decrease in weight over the entire time course ($p <$ 0.001, Kruskal-Wallis ANOVA). $CaCl_2$ and $CaCl_2$/PLL gels both decreased in weight on day 1, but subsequently demonstrated a significant weight gain up to day 7 before significantly decreasing in weight for the remainder of the implant duration ($p < 0.005$, Kruskal-Wallis ANOVA). Both $CaCO_3$ and $CaCl_2$/PLL hydrogels decreased approximately 30% in weight by day 90, but $CaCl_2$ only decreased 17%.

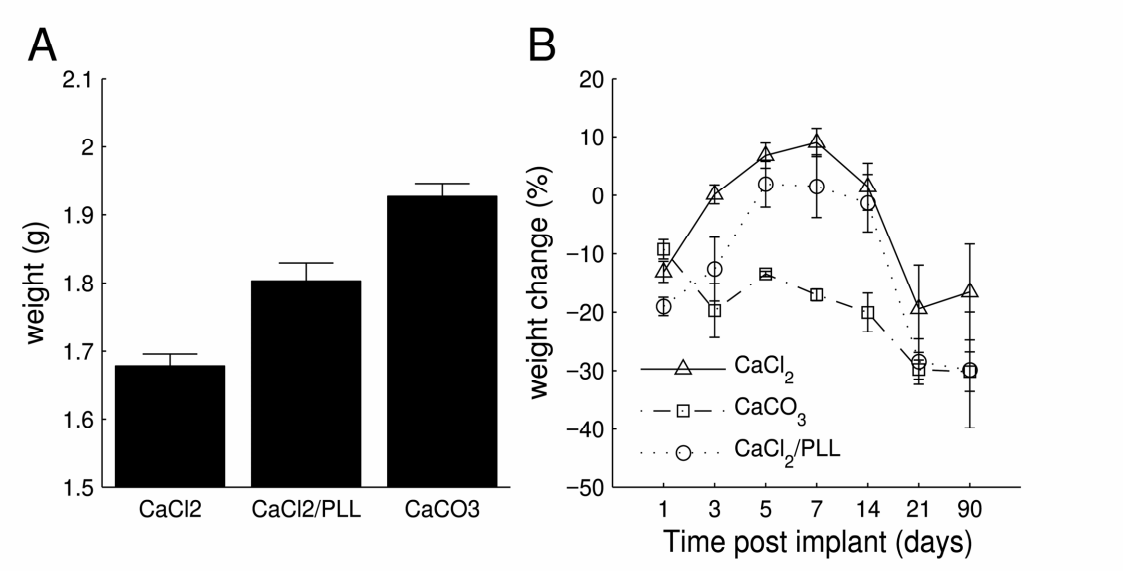

Figure 3.2. Differences in hydrogel weight. A. On day 0, the alginate's weights were significantly different for each condition. $CaCO_3$ reacted gels were the heaviest initially ($p < 0.001$). $CaCl_2$/PLL hydrogel were significantly heavier than $CaCl_2$ reacted gels on day 0 ($p < 0.001$). B. Hydrogel weight changes with time. All of the hydrogels decreased in weight on day 1; however, the weights of the $CaCl_2$ and $CaCl_2$/PLL hydrogels then increased until day 7. After day 7, these gels begin to decrease in weight for the remainder of the time course. $CaCO_3$ hydrogels decreased in weight over the entire time course. n = 5.

Rheology: Complex Modulus and Loss Angle

G^* varied with both experimental condition and time. No significant difference in G^* existed between experimental conditions initially ($p = 0.099$, ANOVA). A large decrease (> 80%) in G^* was determined for all experimental conditions for 1 day post implant ($p < 0.001$, Figure 3.3A). By day 3, G^* was significantly greater for $CaCO_3$ reacted alginate than $CaCl_2$ or $CaCl_2$/PLL. This phenomena continued until day 7 ($p < 0.01$, Figure 3.3A), after which no significant differences in G^* existed between the hydrogels. $CaCl_2$/PLL was significantly greater than $CaCl_2$ on day 7 ($p < 0.01$). When the G^* data for the hydrogels were normalized to their initial (day 0) measurements, G^* for $CaCO_3$ was significantly greater than $CaCl_2$ or $CaCl_2$/PLL for days 1-7 for both 1 Hz and 5 Hz ($p < 0.01$, Figure 3.3B and C) and $CaCl_2$/PLL was significantly greater than $CaCl_2$ on day 7 ($p < 0.01$). At day 14 and above, there was no significant difference in G^* between the 3 different conditions, but G^* increased significantly for all experimental conditions ($p < 0.05$).

δ varied with experimental condition and time. $CaCO_3$ had a significantly lower δ than $CaCl_2$ or $CaCl_2$/PLL on days 0 and 1 ($p < 0.001$, ANOVA, Figure 3.3D). All three conditions varied significantly with time ($p < 0.001$). δ significantly decreased for all conditions up to 3 days post implant ($p < 0.01$) and then slowly increased up to day 90, significantly exceeding initial δ measurements by 2.5 times ($p < 0.001$). When δ was normalized to the initial measurements for each condition, no difference was detected until day 3 (Figure 3.3E and F). On day 3, $CaCO_3$ was significantly greater than $CaCl_2$ (p

< 0.01), and on day 5, $CaCO_3$ was significantly greater than $CaCl_2$ and $CaCl_2$/PLL ($p <$ 0.01) at both 1 and 5 Hz. There was no significant difference at any other time point.

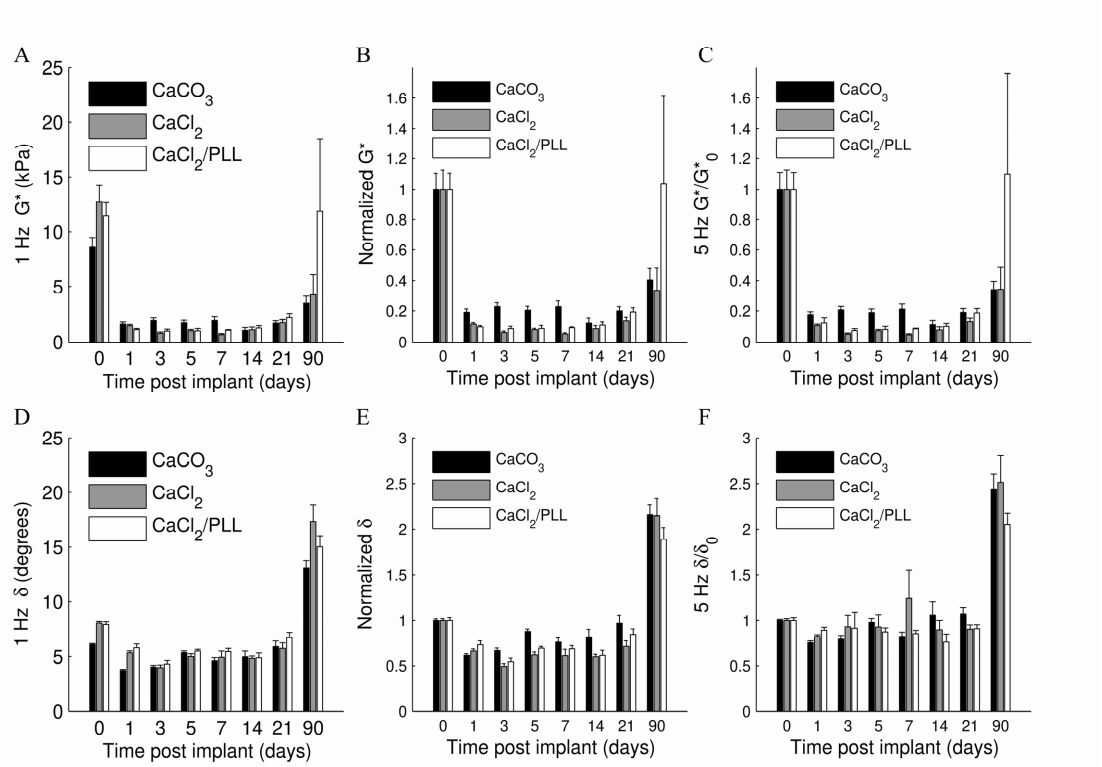

Figure 3.3. G^* and δ changes over time at 10% compression. A-C: G^* changes over time at 1 and 5 Hz. D-F: δ changes over time at 1 and 5 Hz. A. Raw data average G^* for each time point at 1 Hz. Initially, G^* for $CaCO_3$ was smaller than G^* for either $CaCl_2$ or $CaCl_2$/PLL, but increased by day 7 to become significantly greater than both conditions ($p < 0.01$). After day 14, G^* increased for all conditions. B. Normalized G^* averages for each condition over time at 1 Hz. G^* for $CaCO_3$ was greater than $CaCl_2$ and $CaCl_2$/PLL for all time points except day 90. C. Normalized G^* averages for each condition over time at 5 Hz. G^* for $CaCO_3$ remained greater than $CaCl_2$ and $CaCl_2$/PLL for all time points except day 90. D. Raw data average δ for each time point at 1 Hz. δ for $CaCO_3$ was lower than $CaCl_2$ and $CaCl_2$/PLL until day 5. After day 14, δ increased for all conditions ($p < 0.001$). E. Normalized δ averages for each condition over time at 1 Hz. δ for all conditions decreased until day 3 and then increased to day 90. F. Normalized δ averages for each condition over time at 5 Hz. δ changes were smaller at 5 Hz than 1 Hz and no significant increase was detected until day 90 for all conditions. n = 5.

Histology

In general, $CaCO_3$ and PLL-coated implants were more intact than uncoated $CaCl_2$ implants at 7 days. After day 14, all disks displayed increasing levels of hydrogel

fragmentation with collagen around each fragment, increasing the separation of the fragment from the main disk. Macrophages were seen in the tissue around all disks at all of the time points (Figure 3.4). After 21 and 90 days, fibrosis and granulation tissue were present in the surrounding connective tissue and were indicative of normal wound healing (Figure 3.4).

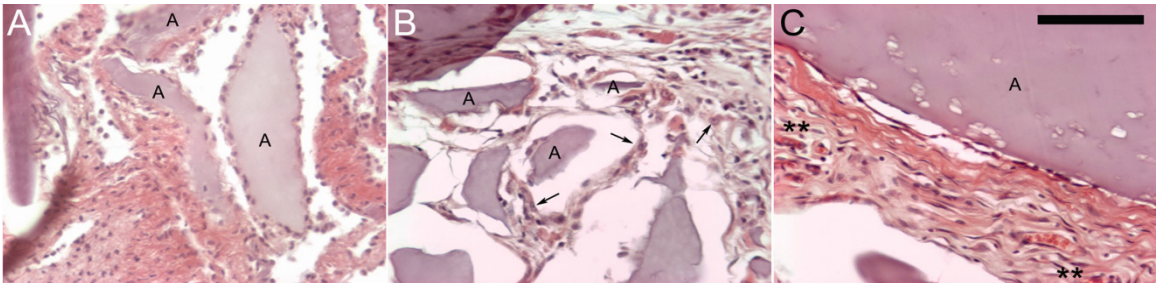

Figure 3.4. Inflammatory response to alginate over time. Micrographs are at 400x magnification of HE stained sections. The scale bar in C represents 50 μm in all micrographs. A. $CaCl_2$/PLL samples 7 days post implantation. Fragmentation of the alginate (A, not all labeled) has already begun and many macrophages and lymphocytes were present in the tissue and around the alginate. B. $CaCl_2$ reacted alginate, 14 days post implantation. Fibroblasts had begun secreting collagen around the alginate fragments (A, not all labeled). Macrophages were still present in the tissue (indicated by arrows). C. $CaCO_3$ reacted alginate, 90 days post implantation. A thick encapsulation layer was detectable around the alginate (A) filled with fibroblasts and new capillaries which comprise granulation tissue (**).

The encapsulation layer thickness varied with time (Figure 3.5). Collagen encapsulation was low initially, then increased significantly at day 14 for $CaCl_2$ and $CaCl_2$/PLL implants and 21 days for $CaCO_3$ hydrogels ($p < 0.05$, ANOVA). Encapsulation thickness was in the range of 15-35 μm for all conditions at 14, 21, and 90 days post-implantation. $CaCO_3$ gels had significantly thicker encapsulation than other conditions on day 21 ($p < 0.05$) but no other significant differences were detected.

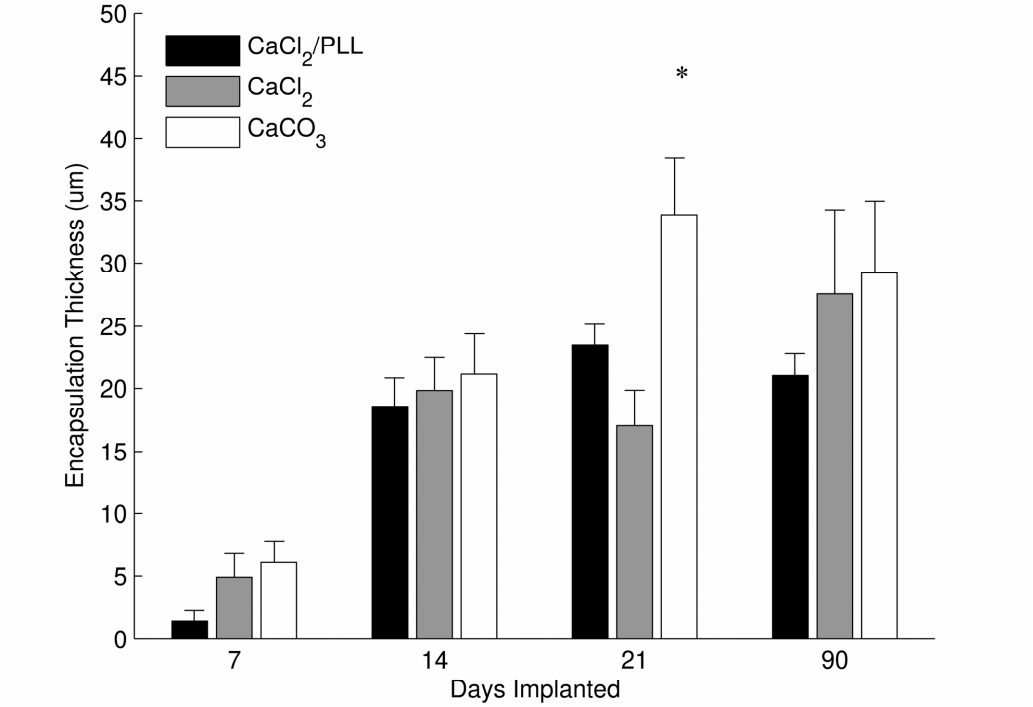

Figure 3.5. Collagen encapsulation thickness around alginate disks over time. Encapsulation thickness increased over time for all conditions ($p < 0.05$). No difference existed between conditions except day 21; $CaCO_3$ reacted alginate had a significantly thicker encapsulation layer than $CaCl_2$/PLL or $CaCl_2$ ($p < 0.05$, *). n = 6.

Cell infiltration of the alginate disks varied with time (Figure 3.6). Cell infiltration was initially high (scores ranged from 0.9 - 1.5 on day 7), and then significantly decreased for all conditions ($p < 0.05$, ANOVA). No significant differences in cell infiltration were detected between the conditions at any time point.

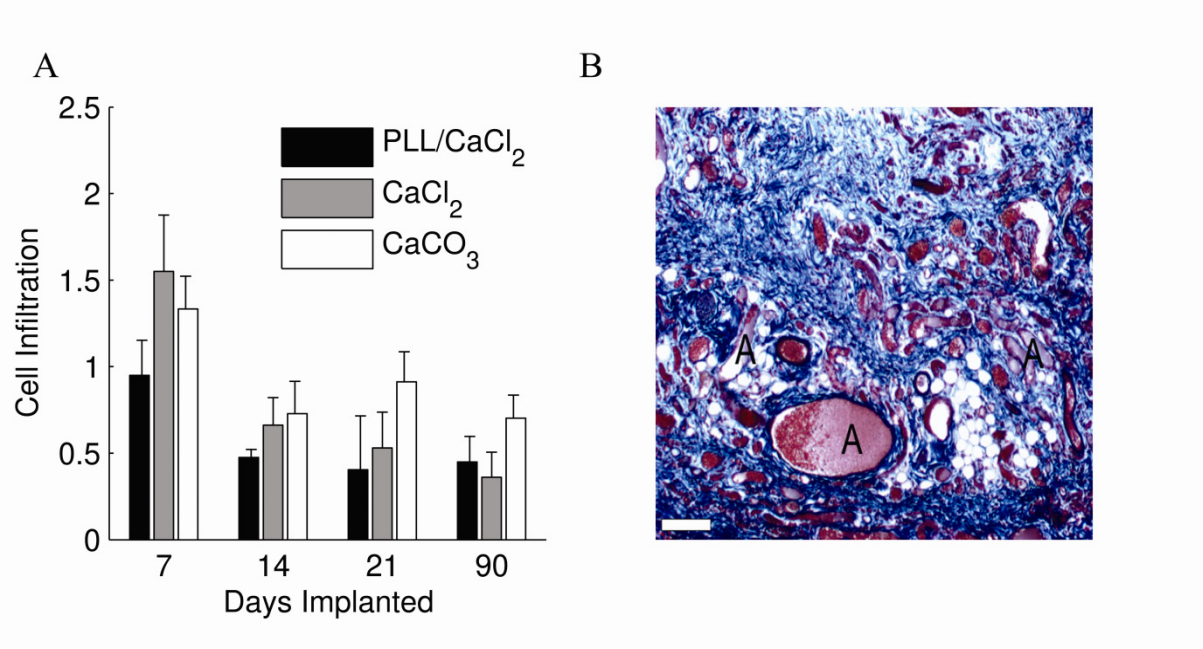

Figure 3.6: Cellular infiltration of alginate disks over time. A. Initially, cell infiltration approached moderate levels for all gel conditions ($1 \leq x \leq 2$), but decreased by day 14 and stabilized at minor infiltration levels ($x \leq 1$). This decrease from day 7 was significant for all conditions ($p < 0.05$) and there was no significant difference between conditions at any time point, $n = 6$. B. A representative micrograph ($CaCl_2$, 7 days post implant) illustrating the varied nature of the infiltration level in a single condition (A indicates alginate fragments). The scale bar represents 200 μm.

Discussion

To gain insight into the destabilization of alginate for the development of advanced neural interface technologies, we investigated the stability and biological response to alginate in the rat subcutaneous implantation model. The responses demonstrated in this experimental paradigm were expected to be representative of alginate degradation in neural interface applications, albeit a more rigorous test environment. The effects due to *in situ* gelling versus diffusion gelling and use of a PLL coating were investigated. While all samples' complex moduli decreased 80% in the first day, the *in situ* gelled alginate was more stable for the first week of implant. More significantly, the *in situ* gelled alginate was the only condition that remained within the biologically relevant G^* range

over the entire 3 month period. This indicates that there is an increased potential of mechanical failure for diffusion gelled alginate during the first week of implant, even in the presence of a PLL coating. However, there were no differences in the histology that would clearly suggest the use of one gelation method over another. Additionally, there appears to be no significant differences between the mechanical stability of the different hydrogels after the first week. Based on these results, the use of *in situ* gelled alginate is more desirable than diffusion gelled alginate in neural interface applications that require high stability during the first week of implantation.

In situ gelled alginate disks exhibited significantly different weight changes compared to diffusion gelled alginate disks. Although all of the hydrogels exhibited a decrease in weight on the first day, indicating an exudation of liquid, $CaCO_3$ continued to decrease in weight over all time points, indicative of hydrogel degradation over time (Bajpai and Sharma 2004). Conversely, $CaCl_2$ and $CaCl_2$/PLL hydrogels increased in weight for the first week indicating swelling but then decreased in weight, exhibiting similar hydrogel degradation behavior as $CaCO_3$ (Bajpai and Sharma 2004). A larger weight change for $CaCl_2$/PLL hydrogels than $CaCl_2$ hydrogels after 3 months was also detected but is likely due to the loss of the PLL coating, which accounted for initial weight differences between the two experimental conditions. The initial exudation of liquid explanation is supported by the measured decrease in δ for all of the conditions on day 1. An exudation of liquid without hydrogel degradation would cause an increase in internal entanglements detected as a decrease in δ (LeRoux, Guilak et al. 1999). This may also be responsible for the significant decrease in G^* seen on day 1. The movement of water out of the

hydrogel could have changed the underlying structure of the hydrogel enough to cause the observed decrease in G^*. Based on these observations, the authors hypothesize that the exudation of liquid from the alginate matrix initially causes the hydrogel to lose stability due to a loss of hydrogen bonding within the matrix and a loss of surface tension on the surfaces of the hydrogel.

Alginate degradation over time was not evident in all of the experimental outcomes. The weight change stabilized for all of the experimental conditions between days 21 and 90. Over these same time points, G^* increased, indicating increasing hydrogel stiffness with time. However, this weight stabilization and increase in G^* was accompanied by a significant increase in δ indicating degradation of the hydrogel structure. The lack of agreement between the data can be explained by the replacement of the degrading alginate with fibroblasts and collagen. The formation of granulation tissue amid the remaining degrading alginate fragments between these two time points contributed to the observed weight stabilization, increased G^*, and decreased δ for all hydrogel conditions.

Alginate disk fragmentation was an unexpected phenomenon demonstrated by all of the experimental conditions. The fractionation of the implants increased with sequential time points, making mechanical testing increasingly more difficult. All of the alginate pieces collected for a given disk sample were used together for these studies. The authors hypothesize that the fragmentation was due to the combination of destabilization of calcium cross-links by phosphates in the extracellular fluid and phagocytosis of alginate fibers by macrophages.

Due to the pulsation of the brain with heart rate and respiratory rate, the alginate will be subject to oscillatory strain *in vivo*. The response of alginate to shear is a good indicator of the fatigue resistance and how it will perform *in vivo*. Brain tissue typically exhibits a complex modulus ranging from 1 to 24 kPa (Donnelly and Medige 1997). It is necessary for alginate to remain in this range to avoid fatigue when used in the central nervous system. $CaCO_3$ reacted alginate disks all remained in this range for all time points, indicating sufficient long-term stability. $CaCl_2$ hydrogels fell below this range on days 3, 5, 7 and $CaCl_2$/PLL hydrogels on days 3 and 5 indicating material fatigue. This is can be attributed to the swelling demonstrated by the hydrogels over this timeframe, which disrupted the hydrogels' underlying chemical interactions and structure (Wang and Spencer 1998; Kong, Alsberg et al. 2004). Previously, Strand et al. determined that PLL coated alginate caused a fibrotic reaction more quickly than alginate alone (Strand, Ryan et al. 2001). Although a similar effect was not detected in the current study, it is possible that low level fibrosis was responsible for the increase in G^* over uncoated $CaCl_2$ gels on day 7. Based on these results, diffusion gelled alginate hydrogels have potential to mechanically fail during the first week of implant when used as a neural interface material.

Cellular infiltration for the alginate disks was due to the large pore size and phagocytosis of the surface alginate fragments. Although alginate is inherently non-sticky and cells are not likely to adhere to the alginate, they are able to treat it as a foreign body. The pore size of gelled, high guluronic acid content alginate is relatively large, 200 – 400 nm (Veluraja and Atkins 1989). This is sufficient to allow phosphate molecules to diffuse

into the matrix, thereby destabilizing the ionic interactions that hold the hydrogel together. Additionally, the individual strands of alginate have been measured at 13-26 nm (Veluraja and Atkins 1989), small enough for macrophages to begin sequestering portions of the destabilized strands. This combination of destabilization and phagocytosis is responsible for the early cellular infiltration detected histologically.

The results indicate that *in situ* gelled alginate is more stable *in vivo* than diffusion gelled alginate during the first week of implantation. Based on initial hydrogel weights alone, diffusion gelled hydrogels would have been hypothesized to have a higher cross-link density and improved stability. The significantly lower weight of $CaCl_2$ reacted hydrogels compared to $CaCO_3$ reacted hydrogels potentially indicated a lower level of water retention in the hydrogel matrix. This was hypothesized to contribute to improved long term stability of the hydrogels but this is not what was found in the current study. $CaCO_3$ reacted alginate hydrogels had a significantly higher G^* and a significantly smaller decrease in G^* over the first 7 days ($p < 0.01$). $CaCO_3$ reacted gels additionally exhibited significantly lower δ measurements initially, indicating a denser distribution of cross-links and entanglements which possibly contributed to the improved stability *in vivo*. Previously, Kong *et al*. indicated that high G alginate was more stable than high M alginate due to the cross-link density of the high G alginate (Kong, Alsberg et al. 2004). The high cross-link density allowed the hydrogel to maintain a small pore size and resist tissue growth and replacement of the alginate scaffold used in that study (Kong, Alsberg et al. 2004). This explanation of cross-link density contributing to stability is applicable to the enhanced stability seen with $CaCO_3$ gels over $CaCl_2$ gels in the current study.

Additionally, *in situ* gelled alginate did not swell like diffusion gelled alginate, thereby minimizing the influx of chemical species that disrupt the ionic interaction of Ca^{2+} with the alginate carboxylic acid residues (Kong, Alsberg et al. 2004). These mechanisms worked together, maintaining the G^* of *in situ* gelled alginate hydrogels within the biologically relevant range for advanced neural interface technologies (1 – 24 kPa).

Acknowledgements

This work was supported by the Michigan Economic Development Corridor. The authors gratefully thank Drs. Timothy Becker and Paul Makidon, and Kaylan Brakora for insightful discussions and Neural Intervention Technologies for the use of their rheometer.

References

Amsden, B. and N. Turner (1999). "Diffusion characteristics of calcium alginate gels." Biotechnol Bioeng **65**(5): 605-610.

Aydelotte, M. B., E. J. M. A. Thonar, et al. (1998). "Culture of chondrocytes in alginate gel: Variations in conditions of gelation influence the structure of the alginate gel, and the arrangement and morphology of proliferating chondrocytes." In Vitro Cellular & Developmental Biology-Animal **34**(2): 123-130.

Bajpai, S. K. and S. Sharma (2004). "Investigation of swelling/degradation behaviour of alginate beads crosslinked with Ca2+ and Ba2+ ions." Reactive & Functional Polymers **59**(2): 129-140.

Becker, T. A. and D. R. Kipke (2003). ALGEL® as a dural sealant: determination of effects on the sensori-motor cortex in rats. 25th Annual International Conference of the IEEE/EMBS, Cancun, Mexico.

Becker, T. A., D. R. Kipke, et al. (2001). "Calcium alginate gel: A biocompatible and mechanically stable polymer for endovascular embolization." Journal of Biomedical Materials Research **54**(1): 76-86.

Becker, T. A., D. R. Kipke, et al. (2002). "In vivo assessment of calcium alginate gel for endovascular embolization of a cerebral arteriovenous malformation model using the swine rete mirabile." Neurosurgery **51**(2): 453-458.

Becker, T. A., M. C. Preul, et al. (2005). "Calcium alginate gel as a biocompatible material for endovascular arteriovenous malformation embolization: six-month results in an animal model." Neurosurgery **56**(4): 793-801.

Benson, J. P., K. K. Papas, et al. (1997). "Towards the development of a bioartificial pancreas: effects of poly-L-lysine on alginate beads with BTC3 cells." Cell Transplant **6**(4): 395-402.

Bienaime, C., J. N. Barbotin, et al. (2003). "How to build an adapted and bioactive cell microenvironment? A chemical interaction study of the structure of Ca-alginate matrices and their repercussion on confined cells." Journal of Biomedical Materials Research Part A **67A**(2): 376-388.

Blandino, A., M. Macias, et al. (1999). "Formation of calcium alginate gel capsules: Influence of sodium alginate and CaCl2 concentration on gelation kinetics." Journal of Bioscience and Bioengineering **88**(6): 686-689.

Bos, G. W., W. E. Hennink, et al. (2005). "Tissue reactions of in situ formed dextran hydrogels crosslinked by stereocomplex formation after subcutaneous implantation in rats." Biomaterials **26**(18): 3901-3909.

Donnelly, B. R. and J. Medige (1997). "Shear properties of human brain tissue." Journal of Biomechanical Engineering-Transactions of the Asme **119**(4): 423-432.

Draget, K. I., K. Ostgaard, et al. (1991). "Homogeneous Alginat Gels: A Technical Approach." Carbohydrate Polymers.

Draget, K. I., G. SkjakBraek, et al. (1997). "Alginate based new materials." International Journal of Biological Macromolecules **21**(1-2): 47-55.

Grant, G. T., E. R. Morris, et al. (1973). "Biological Interactions between Polysaccharides and Divalent Cations - Egg-Box Model." Febs Letters **32**(1): 195-198.

Gugerli, R., E. Cantana, et al. (2002). "Quantitative study of the production and properties of alginate/poly-L-lysine microcapsules." J Microencapsul **19**(5): 571-90.

Gugerli, R., E. Cantana, et al. (2002). "Quantitative study of the production and properties of alginate/poly-L-lysine microcapsules." Journal of Microencapsulation **19**(5): 571-590.

Haug, A. (1964). Composition and properties of alginates. Norwegian Institute of Seaweed Research**:** 1-123.

Haug, A. and O. Smidsrod (1965). "Effect of Divalent Metals on Properties of Alginate Solutions .2. Comparison of Different Metal Ions." Acta Chemica Scandinavica **19**(2): 341-351.

Ishikawa, K., Y. Ueyama, et al. (1999). "Self-setting barrier membrane for guided tissue regeneration method: initial evaluation of alginate membrane made with sodium alginate and calcium chloride aqueous solutions." J Biomed Mater Res **47**(2): 111-115.

Kajiwara, K., S. Ogata, et al. (2005). "Promotion of neurite outgrowth from fetal hippocampal cells by TNF-alpha receptor 1-derived peptide." Cell Transplant **14**(9): 665-672.

Kang, B. C., K. S. Kang, et al. (2005). "Biocompatibility and long-term toxicity of InnoPol implant, a biodegradable polymer scaffold." Exp Anim **54**(1): 37-52.

Kim, D. H., M. Abidian, et al. (2004). "Conducting polymers grown in hydrogel scaffolds coated on neural prosthetic devices." J Biomed Mater Res A **71**(4): 577-585.

King, A., J. Lau, et al. (2003). "The effect of capsule composition in the reversal of hyperglycemia in diabetic mice transplanted with microencapsulated allogeneic islets." Diabetes Technol Ther **5**(4): 653-63.

King, A., S. Sandler, et al. (2001). "The effect of host factors and capsule composition on the cellular overgrowth on implanted alginate capsules." J Biomed Mater Res **57**(3): 374-83.

King, A., S. Sandler, et al. (2001). "The effect of host factors and capsule composition on the cellular overgrowth on implanted alginate capsules." J Biomed Mater Res **57**(3): 374-383.

Kong, H. J., E. Alsberg, et al. (2004). "Controlling degradation of hydrogels via the size of cross-linked junctions." Advanced Materials **16**(21): 1917-1921.

Kulseng, B., B. Thu, et al. (1997). "Alginate polylysine microcapsules as immune barrier: permeability of cytokines and immunoglobulins over the capsule membrane." Cell Transplant **6**(4): 387-94.

Kulseng, B., B. Thu, et al. (1997). "Alginate polylysine microcapsules as immune barrier: Permeability of cytokines and immunoglobulins over the capsule membrane." Cell Transplantation **6**(4): 387-394.

Kuo, C. K. and P. X. Ma (2001). "Ionically crosslinked alginate hydrogels as scaffolds for tissue engineering: part 1. Structure, gelation rate and mechanical properties." Biomaterials **22**(6): 511-521.

Kyriakides, T. R., K. J. Leach, et al. (1999). "Mice that lack the angiogenesis inhibitor, thrombospondin 2, mount an altered foreign body reaction characterized by increased vascularity." Proc Natl Acad Sci U S A **96**(8): 4449-4454.

Lahaye, M. (2001). "Chemistry and physico-chemistry of phycocolloids." Cahiers De Biologie Marine **42**(1-2): 137-157.

Le Tallec, L. P., C. Korwin-Zmijowska, et al. (1997). "Limitations of alginate gels as a culture model for the study of the effects of UVA radiation on human dermal fibroblasts." Cell Biol Toxicol **13**(2): 95-102.

LeRoux, M. A., F. Guilak, et al. (1999). "Compressive and shear properties of alginate gel: effects of sodium ions and alginate concentration." Journal of Biomedical Materials Research **47**(1): 46-53.

Li, R. H., D. H. Altreuter, et al. (1996). "Transport characterization of hydrogel matrices for cell encapsulation." Biotechnology and Bioengineering **50**(4): 365-373.

Liu, X. X., L. Y. Qian, et al. (2003). "Rheology characterization of sol-gel transition in aqueous alginate solutions induced by calcium cations through in situ release." Polymer **44**(2): 407-412.

Mammarella, E. J. and A. C. Rubiolo (2003). "Crosslinking kinetics of cation-hydrocolloid gels." Chemical Engineering Journal **94**(1): 73-77.

Nguyen, H., J. J. Qian, et al. (2003). "Enhanced cell attachment and osteoblastic activity by P-15 peptide-coated matrix in hydrogels." Biochem Biophys Res Commun **311**(1): 179-186.

Nunamaker, E. A., K. J. Otto, et al. (in submission). "Diffusion Based Gelling of Alginate: Development of a Dural Sealant." Journal of Biomedical Materials Research Part B: Applied Biomaterials.

Nunamaker, E. A., K. J. Otto, et al. (in submission). "In Situ Based Gelling of Alginate: Development of a Dural Replacement Patch." Journal of Biomedical Materials Research Part B: Applied Biomaterials.

Orive, G., R. M. Hernandez, et al. (2003). "Cell encapsulation: promise and progress." Nat Med **9**(1): 104-107.

Purcell, E. K. and D. R. Kipke (2006). In Vitro Development and Characterization of a Cortical Neural Stem Cell-Seeded Alginate Scaffold. Society For Biomaterials Annual Meeting and Exposition: New Applications and Technologies Pittsburgh, Pennsylvania, USA.

Purcell, E. K., J. Seymour, et al. (2006). A Neural Stem Cell-Seeded Open Channel Probe. 2006 MRS Spring Meeting, San Francisco, CA, USA.

Rokstad, A. M., S. Holtan, et al. (2002). "Microencapsulation of cells producing therapeutic proteins: Optimizing cell growth and secretion." Cell Transplantation **11**(4): 313-324.

Rokstad, A. M., S. Holtan, et al. (2002). "Microencapsulation of cells producing therapeutic proteins: optimizing cell growth and secretion." Cell Transplant **11**(4): 313-24.

Shchipunov, Y. A., E. L. Koneva, et al. (2002). "Homogeneous alginate gels: Phase behavior and rheological properties." Polymer Science Series A **44**(7): 758-766.

Smidsrod, O. and A. Haug (1965). "Effect of Divalent Metals on Properties of Alginate Solutions .I. Calcium Ions." Acta Chemica Scandinavica **19**(2): 329.

Smidsrod, O. and A. Haug (1972). "Dependence Upon Gel-Sol State of Ion-Exchange Properties of Alginates." Acta Chemica Scandinavica **26**(5): 2063.

Strand, B. L., O. Gaserod, et al. (2002). "Alginate-polylysine-alginate microcapsules: effect of size reduction on capsule properties." J Microencapsul **19**(5): 615-630.

Strand, B. L., Y. A. Morch, et al. (2000). "Alginate as immobilization matrix for cells." Minerva Biotecnologica **12**(4): 223-233.

Strand, B. L., T. L. Ryan, et al. (2001). "Poly-L-Lysine induces fibrosis on alginate microcapsules via the induction of cytokines." Cell Transplant **10**(3): 263-75.

Strand, B. L., T. L. Ryan, et al. (2001). "Poly-L-Lysine induces fibrosis on alginate microcapsules via the induction of cytokines." Cell Transplant **10**(3): 263-275.

Veluraja, K. and E. D. T. Atkins (1989). "Electron-Microscopic Study of Guluronate-Rich Alginate." Carbohydrate Research **187**(2): 313-316.

Vetter, R. J., T. A. Becker, et al. (2003). The use of ALGEL as an artificial dura for chronic cortical implant neuroprosthetics. First International IEEE EMBS Conference on Neural Engineering, Capri Island, Italy.

Wang, L., R. M. Shelton, et al. (2003). "Evaluation of sodium alginate for bone marrow cell tissue engineering." Biomaterials **24**(20): 3475-3481.

Wang, X. W. and H. G. Spencer (1998). "Calcium alginate gels: Formation and stability in the presence of an inert electrolyte." Polymer **39**(13): 2759-2764.

Wang, Z. Y., Q. Z. Zhang, et al. (1993). "Sol-Gel Transition of Alginate Solution by Addition of Calcium-Ions - Alginate Concentration-Dependence of Gel Point." Journal De Physique Ii **3**(1): 1-7.

Wang, Z. Y., Q. Z. Zhang, et al. (1994). "Sol-Gel Transition of Alginate Solution by the Addition of Various Divalent-Cations - a Rheological Study." Biopolymers **34**(6): 737-746.

Wideroe, H. and S. Danielsen (2001). "Evaluation of the use of Sr2+ in alginate immobilization of cells." Naturwissenschaften **88**(5): 224-228.

Yamagiwa, K., T. Kozawa, et al. (1995). "Effects of Alginate Composition and Gelling Conditions on Diffusional and Mechanical-Properties of Calcium-Alginate Gel Beads." Journal of Chemical Engineering of Japan **28**(4): 462-467.

CHAPTER 4
NEURAL STEM CELL-SEEDING MITIGATES THE EARLY TISSUE RESPONSE TO NEURAL PROSTHESES

Abstract

Neural prosthetics capable of recording or stimulating neuronal activity may restore function for patients with motor and sensory deficits resulting from injury or degenerative disease. However, inconsistent recording quality and stability in chronic applications remains a significant challenge. A likely reason for this is the reactive tissue response to the devices following implantation into the brain, which is characterized by neuronal loss and glial encapsulation. We have developed a neural stem cell-seeded probe to facilitate integration of a synthetic prosthesis with the surrounding brain tissue. We fabricated parylene devices that include an open well seeded with neural stem cells encapsulated in an alginate hydrogel scaffold. Quantitative and qualitative data showing the distribution of neuronal, glial, and progenitor cells surrounding seeded and control devices is reported over four time points spanning three months. Neuronal loss and glial encapsulation were mitigated by cell seeding during the initial week of implantation, and exacerbated after six weeks post-insertion. We hypothesize that graft cells secrete neuroprotective and neurotrophic factors that effect the desired healing response early in the study, with subsequent cell death and scaffold degradation accounting for a reversal of these results later. Applications of this biohybrid technology include neural recording and sensing studies in research settings, and relevance in a clinical setting is a future possibility.

Introduction

Neuroprosthetic devices have the capacity to record signals from a patient's uninjured cortex. These signals may then be used to place an exterior assistive device under the patient's control, thus restoring function while circumventing nervous tissue that has been damaged by injury or disease (Schwartz, Cui et al. 2006; Donoghue, Nurmikko et al. 2007; Fitzsimmons, Drake et al. 2007). In the last decade, monkeys were shown to be able to successfully control a cursor on a computer screen or a robotic arm using voluntary cortical signals (Taylor, Tillery et al. 2002; Carmena, Lebedev et al. 2003). Recent work has demonstrated these feats by tetraplegic humans implanted years after injury (Hochberg, Serruya et al. 2006; Donoghue, Nurmikko et al. 2007). Further, a recent study has demonstrated cortical control of a complex, multi-jointed robotic arm with a "hand" gripper by monkeys during a self-feeding task (Velliste, Perel et al. 2008). Thus, neuroprostheses have the potential to restore some level of function to the 200,000 patients currently suffering from full or partial paralysis in the U.S. (Polikov, Tresco et al. 2005).

While such results are encouraging, these devices are currently plagued by inconsistent performance in terms of recording longevity and stability (Rousche and Normann 1998; Liu, McCreery et al. 1999; Williams, Rennaker et al. 1999; Nicolelis, Dimitrov et al. 2003; Polikov, Tresco et al. 2005; Liu, McCreery et al. 2006; Schwartz, Cui et al. 2006). In order for neuroprostheses to be useful in research and clinical settings, stable, long-term recordings from large populations of neurons in multiple brain areas must be reliably and reproducibly achieved (Lebedev and Nicolelis 2006). Following

implantation into the brain, a reactive tissue response occurs to the prostheses, which is believed to be a major contributing factor to their inconsistent performance. An encapsulation layer composed of microglia and astrocytes isolates the device from the surrounding tissue, and neuronal density within the effective recording radius of the probe is reduced (Edell, Toi et al. 1992; Turner, Shain et al. 1999; Szarowski, Andersen et al. 2003; Kim, Hitchcock et al. 2004; Biran, Martin et al. 2005; Polikov, Tresco et al. 2005). The glial sheath creates a diffusion barrier to the transmission of ions through the extracellular space which may affect recording quality (Roitbak and Sykova 1999). Additionally, impedance magnitude at 1 kHz (the fundamental frequency of the neuronal action potential) increases at recording sites with "extensive" glial reactivity (Williams, Hippensteel et al. 2007). While the relationship between recording quality and neuronal density has yet to be defined, it is reasonable to believe that neuronal loss would result in a reduction of signal quality. The reported 40% loss of neuronal density within 100 microns of the device surface in the first month after implantation is particularly concerning, given that this region produces the large amplitude, reliably separated spikes useful for neural prostheses (Henze, Borhegyi et al. 2000; Biran, Martin et al. 2005).

The tissue response to implanted prostheses is a characteristic reaction to central nervous system (CNS) damage (Silver and Miller 2004). Stem and progenitor cell therapy have shown promise as one approach to repair CNS injury, where mechanisms may include cell replacement and reinnervation, or a bystander effect, where the transplanted cells support host tissue by secreting therapeutic factors, correcting a biochemical deficit or inhibiting cytotoxic injury processes (Teng, Lavik et al. 2002; Lindvall, Kokaia et al.

2004; Pluchino, Zanotti et al. 2005; Gaillard, Prestoz et al. 2007). In support of the "bystander" or "chaperone" effect, several studies suggest that undifferentiated neural stem cells have an innate ability to promote healing and axonal regeneration of host neurons as well as a reduction in glial scar formation (Ourednik, Ourednik et al. 2002; Teng, Lavik et al. 2002; Lu, Jones et al. 2003; Heine, Conant et al. 2004; Llado, Haenggeli et al. 2004; Pluchino, Zanotti et al. 2005). This is believed to be due to constitutive secretion of multiple neurotrophic factors (Ourednik, Ourednik et al. 2002; Teng, Lavik et al. 2002; Lu, Jones et al. 2003; Llado, Haenggeli et al. 2004), as well as the degrading of molecules which are inhibitory to axonal growth (Heine, Conant et al. 2004). Additionally, the ability of undifferentiated neural precursor cells to protect injured CNS tissue by displaying neuroprotective immune functions has been reported (Pluchino, Zanotti et al. 2005).

We have developed a neural stem cell (NSC)-seeded biohybrid probe hypothesized to improve device integration with brain tissue, and the tissue response to the probes *in vivo* in rats was evaluated over a three month time period. The parylene devices contain a hollow well containing an NSC-seeded alginate hydrogel scaffold. Alginate is a biocompatible polysaccharide polymer which forms a hydrogel following cross-linking with divalent cations such as calcium. This material is commonly used to encapsulate secretory cells, localize them to an implant site, and provide an immuno-isolating barrier between the engrafted cells and the host tissue (Orive, Hernandez et al. 2003). We have previously demonstrated the release of neurotrophic and neuroprotective factors from NSCs encapsulated in alginate (Purcell, Singh et al. 2008). Here, we show that

combining a cortical prosthesis with this scaffold diminishes the early tissue response and facilitates initial integration of the device with the surrounding brain tissue. Cell-seeding increases neuronal loss and glial encapsulation after six weeks, presumably due to a loss of graft cell viability and scaffold integrity.

Materials and Methods

Probe Manufacture

The probes were microfabricated in the Lurie Nanofabrication Facility using methods previously described, and the process is illustrated in Figure 4.1 (Seymour and Kipke 2007). Briefly, a sacrificial release layer of SiO_2 was grown on a Si wafer. Parylene-C (Specialty Coating, Indianapolis, IN) was deposited (5-microns thick) via chemical vapor deposition. SU-8 2025 (Microchem, Newton, MA) was spincoated and patterned to create the core of each tine. Parylene was etched using oxygen plasma RIE. Probes were released using hydrofluoric acid and then thoroughly rinsed in acetone, ethanol and DI water. Final dimensions of the probe were 2.6 mm long, 200 microns wide and 40 microns thick. An opening through the thickness of the device measuring 100 microns across and 2.1 mm in length was designed to carry scaffold material (Figures 4.1, 4.3a). Support arms to this feature had square cross-sections measuring 40 microns on each side.

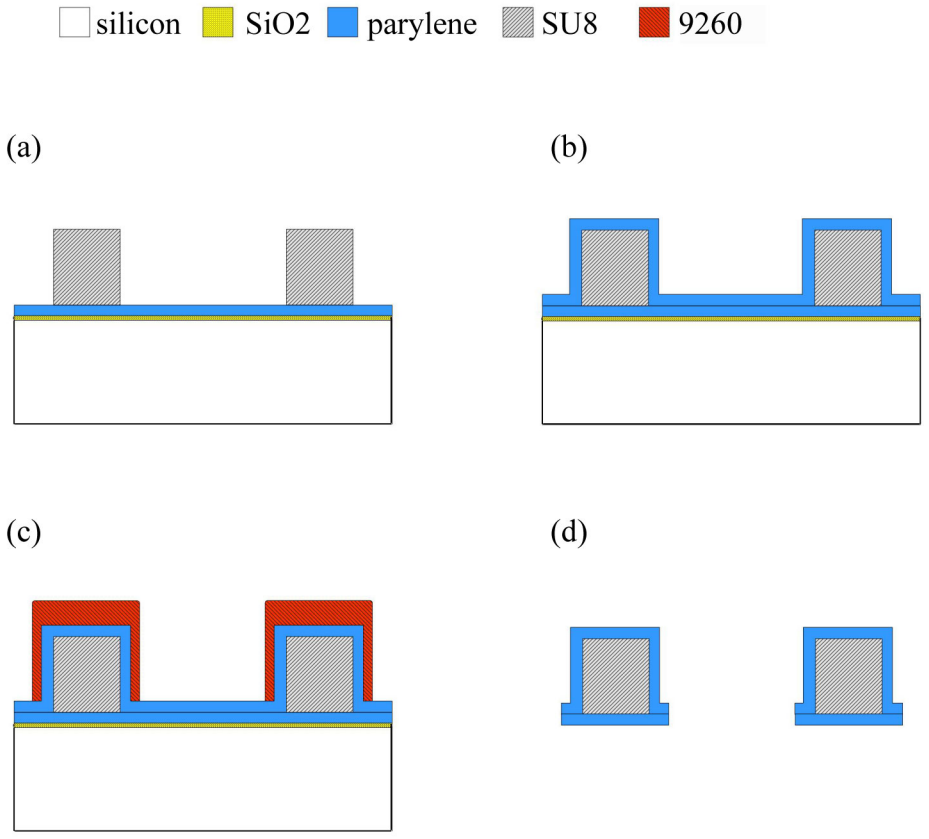

Figure 4.1. Cross-sectional view of wafer level fabrication. (a) Parylene deposited on SiO_2 sacrificial layer. SU-8 patterned shank. (b) Parylene encapsulated SU-8 structure. (c) 9260 resist patterned to form thick mask over shank. (d) Etched and released final structure. Photolithography masks used steps in (a, c).

Cell Culture and Probe Scaffolding

E14 murine cortical neural stem cells (NSCs) were obtained from StemCell Technologies (Vancouver, BC), cultured as neurospheres and expanded with 20 ng/mL epidermal growth factor (EGF) according to the supplier's protocol. The culture and stem cell characteristics of these cells have been described (Reynolds and Weiss 1992; Reynolds and Weiss 1996). The cells are a heterogeneous mixture of stem and progenitor cells (Reynolds and Weiss 1996). Probe scaffolding was achieved by mixing a cell slurry with

alginate 50:50, rapidly dip-coating the probe in the mixture, and cross-linking with a 0.1 M calcium chloride solution. The alginate was highly purified with 68% guluronic acid content and MW = 219,0000 g/mol from NovaMatrix (Drammen, Norway). This composition was chosen based on a previous study (Purcell, Singh et al. 2008). Probes had a final concentration of 10,000,000 cells/mL in 1% w/v alginate, resulting in approximately 100 cells in the microscale probe well. Non-seeded probes were treated identically to NSC-seeded probes, with the exceptions that cells and/or alginate were omitted from the coating procedure.

Probe Implantation

Sixteen male Sprague Dawley rats (300–350 g) were each implanted with four untethered probes (two containing NSC-seeded alginate, one with alginate only, and one untreated probe) using a surgical procedure similar to those previously reported (Vetter, Williams et al. 2004; Seymour and Kipke 2007). Anesthesia was achieved via a ketamine cocktail. A 3x3 mm craniotomy was centered over the somatosensory cortex (-2.0 mm AP, +/- 4.0 mm ML from Bregma) in each hemisphere. Dura was resected and two probes (one seeded, one unseeded) were manually inserted in each craniotomy with an approximate 2 mm span between them. Calcium alginate was used for duraplasty followed by surgical closure with silicone and dental acrylic. No immunosuppressive treatments were used. All procedures strictly complied with the United States Department of Agriculture guidelines for the care and use of laboratory animals and were approved by the University of Michigan Animal Care and Use Committee.

Histology and Quantitative Analysis

After implantation, animals were deeply anesthetized and transcardially perfused with 4% paraformaldehyde at the appropriate time point (1 day, 1 week, 6 weeks, or 3 months, n=4 animals per time point). Brain tissue was explanted, postfixed overnight in 4% paraformaldehyde, and cryoembedded following sucrose protection. Probes were left *in situ* for histology. Serial 12 micron thick sections along the shank of the probes were collected, and eight tissue sections between cortical layers II and V were randomly selected and immunostained for NeuN (1:100, Millipore Corporation, Billerica, MA) and Neurofilament (1:1000, Novus Biologicals, Littleton,CO) and counterstained with Hoechst (1 μg/mL, Invitrogen Corporation, Carlsbad, CA) for quantitative analysis of tissue response. Six sections were stained with Ox-42 (1:100, Serotec, Oxford, UK), glial fibrillary acidic protein (GFAP, 1:100), and Hoechst (1 μg/mL) to assess glial encapsulation qualitatively. Six sections per probe were stained for nestin (1:100, StemCell Technologies, Vancouver, BC), GFAP (1:100, Sigma, St. Louis, MO), and M2 (1:10, Iowa Hybridoma Bank, Iowa City, Iowa) for identification of murine-derived NSCs and possible differentiation status. Six additional sections were stained with neuronal class III β-tubulin (TUJ-1) antibody (1:500, StemCell Technologies, Vancouver, BC), NG-2 (1:500, Millipore Corporation, Billerica, MA) and M2 (1:10, Iowa Hybridoma Bank, Iowa City, Iowa) to identify neuronal and oligodendrocyte precursors respectively. Six sections per probe were stained for doublecortin (1:1000, Abcam, Cambridge, UK) and M2, and counterstained with Hoechst. Where positive M2 staining was observed, a total of twelve sections were stained with nestin and GFAP and analyzed

for a quantification of the expression of these markers as an indication of differentiation status; approximately 60 cells in each of two animals were counted.

The immunohistochemistry procedure has been described (Cowell, Plane et al. 2003). Briefly, sections were hydrated in buffer (PBS or TBS), blocked with 10% normal goat serum, and incubated overnight with primary antibodies at 4˚C. Sections were then rinsed, incubated in the appropriate secondary antibodies (1:200 Alexa-350, 488, and/or 568, Invitrogen), counterstained with Hoechst, and coverslipped with ProLong Gold (Invitrogen). Antibody solutions included 0.3% triton X-100 and 5% normal goat serum. Buffer was used in place of primary antibody for controls. Confocal images were collected with an Olympus FV500 microscope with a 20X or 40X objective.

A MatLAB graphical user interface was developed in-house to facilitate cell counting, and this method has been described previously (Seymour and Kipke 2007). An outline of the exterior edge of the probe cross-section was delineated using a differential interference contrast (DIC) and UV fluorescence image. A blinded technician selected all nuclei as either neuronal (NeuN+, Hoechst+) or nonneuronal (Hoechst+ only) within a software-defined 175 micron radius of the probe surface. A representative image after cell counting and the resulting histograms are illustrated in Figure 4.2. Four optical images (3 mm step size) in each of eight physical sections per probe were analyzed. The software algorithm used the coordinates of the user-selected nuclei to calculate the shortest distance to the probe surface, bin the counts by distance, and calculate the

sampling area of each bin to result in neuronal and non-neuronal densities as a function of distance from the probe.

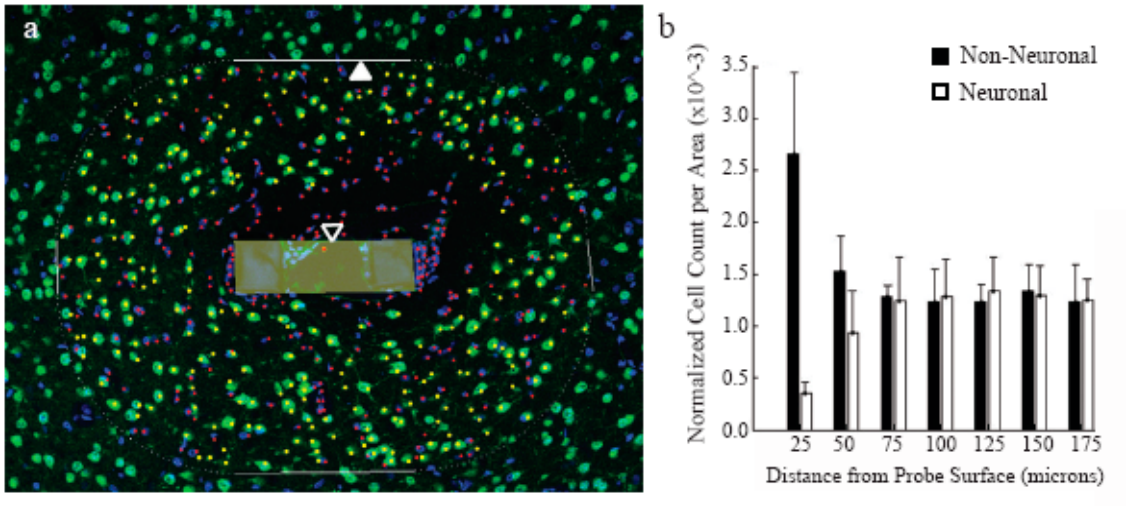

Figure 4.2. Neuronal (NeuN+ in green, Hoechst+ in blue) and non-neuronal (NeuN-, Hoechst+) nuclei counted by a blinded observer (a), and the resulting output (b). A MatLAB interface calculated the counting boundary (closed arrow) based on the user-defined probe surface boundary (open arrow, shaded area), and a blinded observer manually selected neuronal and non-neuronal nuclei within this region (shown in yellow and red, respectively). The algorithm stored the location of each nucleus relative to the probe surface, binned counts in 25 micron increments, and normalized counts to cells per pixel in each bin (b). This number was converted to cells per square millimeter for data analysis.

Statistics

For neuronal and non-neuronal density, eight sections were analyzed for each of four probes per animal, with four animals evaluated for each of four time points. Data was binned into seven 25-micron distance bins from the probe surface; a total of 2,688 individual data points for both neuronal and non-neuronal densities were used to generate the statistical models.

A linear mixed effects model was used to evaluate the responses of neuronal density and nonneuronal density due the clustering of multiple probe evaluations within each animal.

The fixed effects were the probe condition, distance, and time. The random effect was the animal subject. Analysis was performed using the statistical package SPSS (Chicago, IL). Results were assessed by Fisher's Least Significant Difference method and termed statistically significant at the p=0.05 level.

A univariate general linear model was used to assess the correlative relationship between neuronal density and non-neuronal density. Common correlation methods (such as Pearson's correlation) were not used as these techniques do not take in to account the fixed and random effects of the data, and may yield an inflated correlation coefficient. The fixed effects were the probe condition, distance, and time. The random effect was the animal subject. Non-neuronal density was defined as a covariate in order to assess it as a predictor of neuronal density.

Results and Discussion

Probe Design and In Vivo NSC Detection

Parylene devices were successfully designed and fabricated containing a hollow well for scaffold retention (Arrow, Figure 4.3a-b). Immunohistochemistry for the murine-specific marker M2 allowed for the *in vivo* detection of cortical neural stem cells derived from embryonic mice based on a previous report (Teng, Lavik et al. 2002). Alginate and parylene autofluoresced in green and blue respectively, enabling visualization of these structures (Figure 4.3c-e). Neural stem cells were detected at the 1 day time point *in vivo*, and mainly expressed a combination of nestin and GFAP, with limited doublecortin (DCX, typically indicative of neuronal precursors) expression also observed (Figure 4.3c-

e). Approximately 44% of M2-positive cells were associated with nestin, 5.5% expressed GFAP, and 36% displayed both of these markers, indicating undifferentiated cells, astrocytes, and glial progenitors (or, reactive astrocytes) respectively (Messam, Hou et al. 2000). There was no evidence of TUJ-1 or NG-2 positivity. The markers observed were similar to those reported in the literature, where the majority of neural stem and progenitor cells express nestin and GFAP, and neuronal and oligodendrocyte markers are observed far less frequently (Reynolds and Weiss 1996; Ourednik, Ourednik et al. 2002; Teng, Lavik et al. 2002). The somewhat limited detection of NSCs and identification of

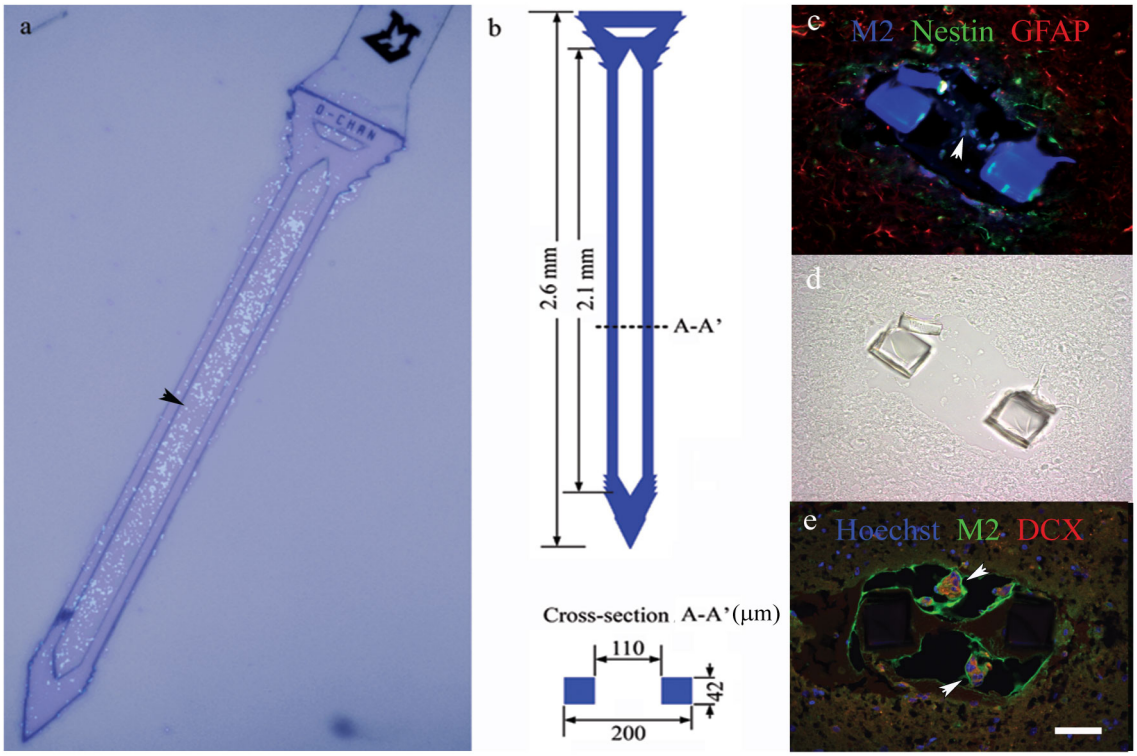

Figure 4.3. A neural stem cell-seeded probe (a) and associated dimensions (b). Cells are Hoechst-stained and nuclei appear fluorescent blue (a). Cross-section views of neural stem cell-seeded probes 1 day following implantation from two animals (c-e). The companion brightfield DIC image for (c) is shown in (d) for reference due to autofluorescence of the parylene probe. Graft cells (M2-labeled) were associated with nestin (c), GFAP (c), and doublecortin (DCX, e) expression. Alginate also autofluoresces green. Scale = 50 microns for (c)-(e).

their differentiation status *in vivo* is likely due to the relatively small number of cells initially present in the microscale device and the reportedly large loss (>90%) in progenitor graft cell viability within the initial days following implantation (Sortwell, Pitzer et al. 2000; Bakshi, Keck et al. 2005).

Scaffold Condition Effects on Neuronal and Non-Neuronal Densities

Quantitative and qualitative analysis of neuronal and non-neuronal densities within the first 175 microns of the probes revealed the degree of injury around the implants as a function of scaffold condition, time, and distance from the probe surface (Figures 4.4-6). Neural stem cell-seeded probes had a higher surrounding neuronal density compared to untreated probes at one day post-implantation (Figure 4.4a, $p=0.023$; mean NSC ND=585, mean probe ND=555 cells/mm^2). Neuronal density was increased around NSC probes compared to both control conditions at the one week time point (Figure 4.4a, $p\leq0.002$; mean NSC ND=911, mean alginate ND=813, mean probe ND=819 cells/mm^2). The experimental probes had reduced non-neuronal encapsulation compared to alginate-only probes at one day and untreated probes at one week after insertion (Figure 4.4b, $p\leq0.001$; 1 day means: NSC NND=925, alginate NND=1047; 1 week means: NSC NND=1612, probe NND=1778 cells/mm^2). The mitigation of the early tissue response is likely due to an initial bystander effect of the NSCs. The increased neuronal density surrounding seeded probes may result from the secretion of multiple neuroprotective factors by the grafted cells, both known and yet to be elucidated. We have previously demonstrated the release of brain derived neurotrophic factor (BDNF), glial derived

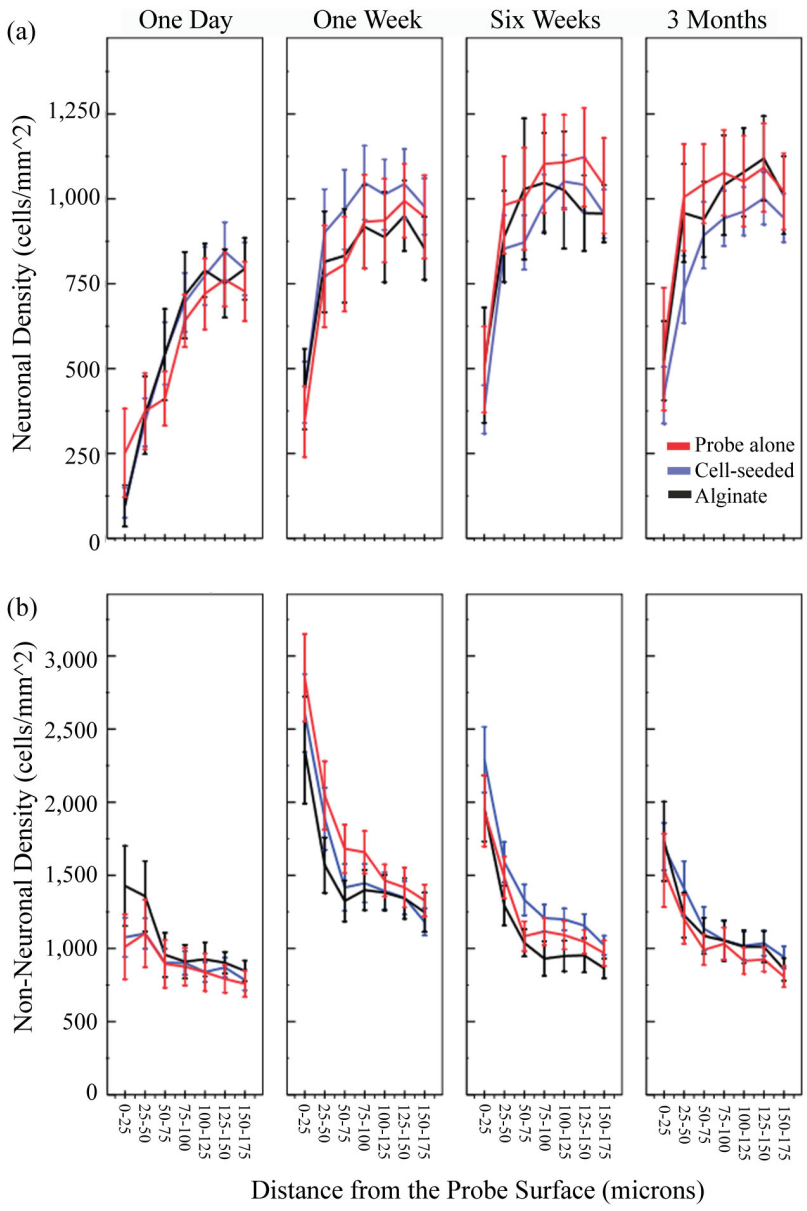

Figure 4.4. Mean neuronal density (a) and non-neuronal density (b) surrounding implants over time as a function of distance from the probe surface (± s.e.m). Neural stem cell-seeded probes had a higher neuronal density surrounding them compared to untreated probes at one day and both control conditions at one week post-implant (a, $p<0.05$). Cell-seeding reduced non-neuronal encapsulation compared to alginate-only probes at one day and untreated probes at one week post implant ($p\leq0.001$). At six weeks and three months post implantation, the neural stem cell-seeded probes had reduced neuronal density and increased non-neuronal density surrounding them in comparison to both control conditions ($p<0.05$).

neurotrophic factor (GDNF) and nerve growth factor (NGF) from alginate-encapsulated NSCs over a three week time period *in vitro* (Purcell, Singh et al. 2008). These neurotrophic factors are known to support neuronal survival and plasticity in various models of axonopathy and neuropathy (Kolb, Gorny et al. 1997; Han and Holtzman 2000; Nicole, Ali et al. 2001; Lu, Jones et al. 2003; Wilkins and Compston 2005). The neuroprotective effect of medium conditioned by NSC-seeded alginate beads was further verified using a serum-withdrawal mediated cell death model in PC-12 cells (Purcell, Singh et al. 2008). Alternatively, the increase in neuronal density could be due, in part, to the neuronal differentiation and integration of graft cells into the surrounding brain tissue. However, no direct evidence of this phenomenon was seen in the immunohistochemistry results, and the degree of neuronal density increase is unlikely to be largely explained by the number of cells seeded onto the microscale implant. The production of new neurons by endogenous stem cells originating in the host is an additional, and unexplored, possibility. This also seems improbable as a primary cause of results, as neural stem cells originating in the subventricular zone have been shown to contribute primarily to astrogliosis, with neuronal differentiation rarely observed following migration to the site of cortical trauma (Salman, Ghosh et al. 2004). However, it is worth noting that evidence of doublecortin positivity was observed in one graft (Figure 4.3e), as well as in host tissue one week after implantation (Supplementary Figure 4.1). Doublecortin (DCX) is a microtubule-associated protein expressed primarily in migrating neuronal precursors, and reportedly may also be associated with mature astrocytes according to Verwer *et al.* (Francis, Koulakoff et al. 1999; Verwer, Sluiter et al. 2007). Expression of DCX around neural implants has not been previously reported

in the literature, and may represent an additional target for future strategies to improve device-tissue integration if its presence indicates a regenerative capacity of the injured brain, the grafted cells, or a combination of both.

At six weeks and three months post implantation, the neural stem cell-seeded probes had reduced neuronal density and increased non-neuronal encapsulation surrounding them in comparison to both control conditions (Figure 4.4, $p \leq 0.049$ for neuronal density at six weeks, $p \leq 0.001$ at three months, $p < 0.001$ for non-neuronal density at both time points; 6 week means (cells/mm^2): NSC ND=877, alginate ND=916, probe ND=978, NSC NND=1400, alginate NND=1141, probe NND=1247; 3 month means (cells/mm^2): NSC ND=843, alginate ND=953, probe ND=978, NSC NND=1185, alginate NND=1140, probe NND=1058). This effect may be due to reduced NSC viability over time, which has been reported previously and may be aggravated by degradation of the alginate scaffold (Sortwell, Pitzer et al. 2000; Bakshi, Keck et al. 2005). Alginate stability drops markedly during the first 24 hours *in vivo*, and is prone to fragmentation over the following three months (Nunamaker, Purcell et al. 2007). This may leave the grafted cells vulnerable to an immune reaction, and such a response may account for the exacerbation of the tissue response after six weeks.

Alginate coating (without cell seeding) had no effect on neuronal density surrounding probes over the course of the study (Figure 4.4a). However, alginate coating yielded mixed effects on non-neuronal density (Figure 4.4b). One day after implantation, alginate coated probes had a significantly higher non-neuronal density than NSC-seeded and control probes (Figure 4.4b, $p \leq 0.001$). This effect was especially pronounced within

the first fifty microns of the probe surface. Interestingly, microglia appeared to have a ramified, or "surveilling", morphology surrounding a neural stem cell-alginate probe initially, whereas activated cells with an amoeboid structure were found near an alginate probe in the same hemisphere of one animal (Figure 4.5). An initial loss of calcium ions to the surrounding tissue, resulting in a potentially injurious hypertonic environment and activation of glia, could explain this. Alginate with varying compositions has been shown to experience a dramatic loss in mechanical stability after one day of implantation, indicating a loss of calcium cross-links (Nunamaker, Purcell et al. 2007). Interestingly, cell-seeded alginate does not exhibit this initial glial activation; the encapsulated cells may buffer the surrounding tissue from this effect (Figure 4.5). Additionally, the total volume of alginate contained on the probe may be less in the cell-seeded condition. One week after implantation, alginate probes reduce non-neuronal density in comparison to untreated probes, likely due to the non-adhesive nature of the gel ($p<0.001$) (Rowley, Madlambayan et al. 1999). Alternatively, alginate may buffer the mechanical mismatch between the probe and surrounding brain tissue, and reduce glial encapsulation as a consequence. By six weeks post-implantation, alginate and untreated probes have equivalent non-neuronal densities surrounding them. The alginate scaffold is likely to have significantly degraded by this time point.

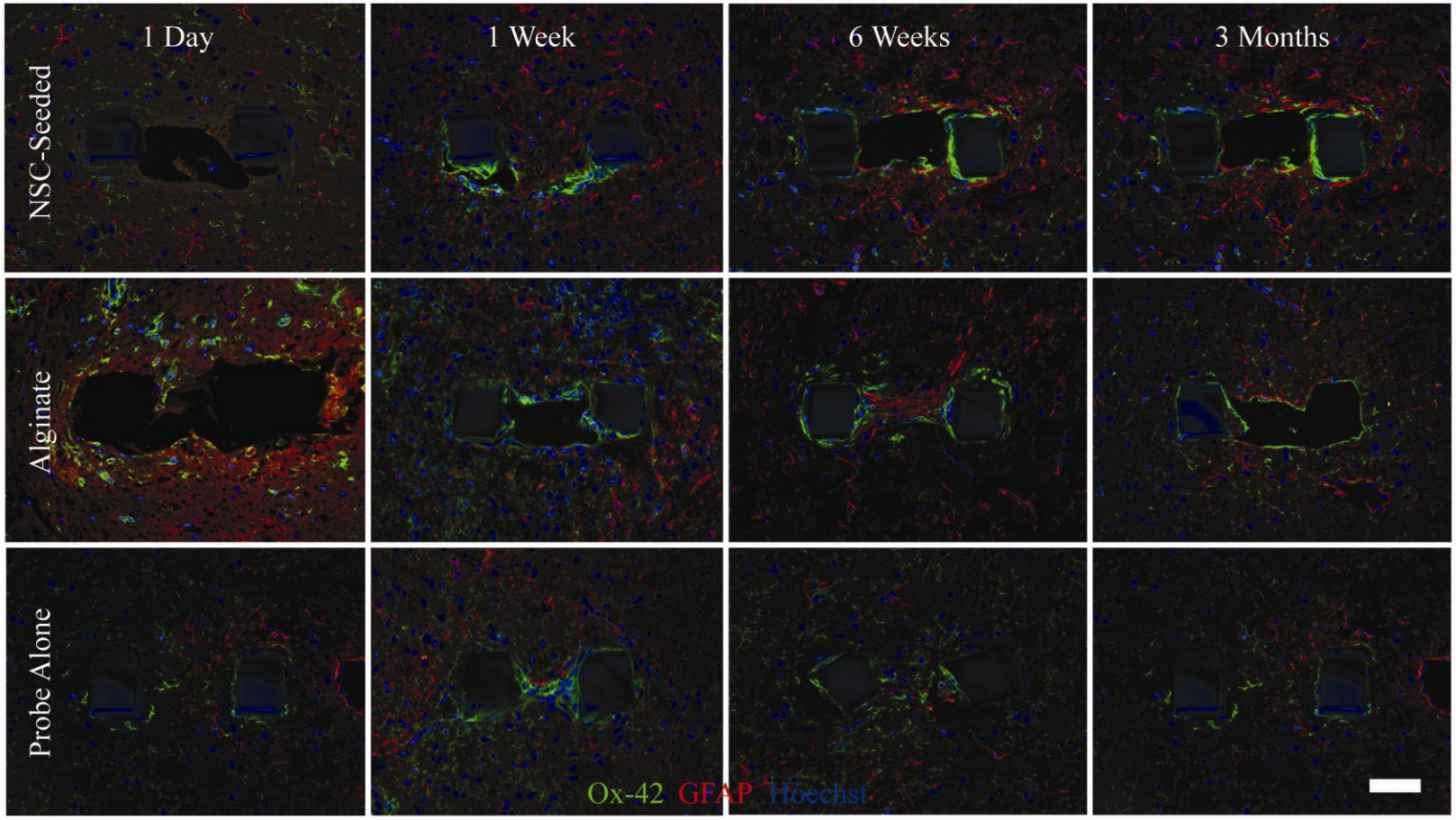

Figure 4.5. Glial encapsulation of each probe condition over the three month time course. Ox-42 labeled microglia (green) and GFAP labeled astrocytes (red) are shown. Images are taken from probes implanted in the same animal at each time point. Appendix C contains additional views of selected images.

Neuronal and Non-Neuronal Densities as a Function of Distance

Neuronal density increased as a function of distance from the probe, and non-neuronal density decreased reciprocally. Neuronal density was minimal in the first 25 microns of the probe, with significant incremental increases in the 25-50, 50-75, and 75-100 micron bins (Figure 4.4a, $p<0.001$). Neuronal density stabilized thereafter, with similar neurofilament staining patterns across conditions. The loss of neuronal soma within the first 100 microns of the probe is particularly concerning, considering that reliably sorted, large amplitude spikes are recorded when neurons are within 50 microns of recording sites, and no discernable signals are detected from cells greater than 140 microns from probes (Henze, Borhegyi et al. 2000). There was a significant decrease in non-neuronal density as a function of distance from the probe surface (Figure 4.4b). Non-neuronal density was highest in the 0-25 micron bin, and significantly decreased in the 25-50 micron bin, followed by a further decrease in the 50-75 micron bin ($p<0.001$). Non-neuronal density stabilized thereafter. Again, the greatest glial encapsulation of the device occurred in the region yielding the highest quality signals. The observation that the tissue response is the most severe in the recordable region surrounding the probe indicates that this phenomenon may result in recording instability, and corroborates previous reports (Szarowski, Andersen et al. 2003; Kim, Hitchcock et al. 2004; Biran, Martin et al. 2005).

The Correlation between Neuronal and Non-Neuronal Densities

There was a significant negative correlation between neuronal and non-neuronal densities (Figure 4.4a-b, $p<0.001$). This result expands upon previous work, which has

demonstrated an inverse relationship between microglial and neurofilament staining as a function of distance from implanted probes (Biran, Martin et al. 2005). The most likely reason for this is the deleterious effects on neuronal viability and axonal outgrowth by the glial scar. Reactive microglia involved in the injury response to probes are known to elute potentially neurotoxic inflammatory cytokines, and reactive astrocytes may produce proteoglycans inhibitory to axonal regeneration (Silver and Miller 2004; Biran, Martin et al. 2005). Simple displacement of the neurons is unlikely to be the reason for the negative correlation between neuronal and non-neuronal densities, as neuronal density increased and then reached a plateau as a function of distance from the probe surface. If there had been displacement, we would have expected a clustering of neurons (indicated by an increase in neuronal density) in the region adjacent to the glial sheath.

Neuronal and Non-Neuronal Densities as a Function of Time

There are general trends in the distribution of neurons and glial elements surrounding the devices as a function of time. Neurofilament disruption indicative of axonal damage was evident immediately after implantation for all conditions and accompanied the dramatic loss of neuronal density within the first 100 microns of the probe surface (Figure 4.6; Figure 4.4a, $p \leq 0.036$) (Chen, Meaney et al. 1999). This injury response appeared considerably improved one week after surgery, and neuronal density was significantly increased at this time (Figure 4.6; Figure 4.4a, $p < 0.01$). Values stabilized thereafter. Non-neuronal density is lowest one day after transplantation, followed by a peak value of this metric one week after implantation (Figure 4.5; Figure 4.4b, $p < 0.05$). By six weeks, a thin glial sheath surrounded all probes, with non-neuronal densities progressively

decreasing through the three month time point (Figure 4.5; Figure 4.4b, $p<0.001$). These results corroborate a qualitative study of the glial encapsulation of silicon probes (Szarowski, Andersen et al. 2003). Sustained glial activation and neuronal density loss within the first 100 microns surrounding the insertion site of silicon probes was reported in a study which quantified these responses after two and four weeks *in vivo* (Biran, Martin et al. 2005). In these studies, the use of silicon probes necessitated the removal of the devices prior to tissue processing, potentially disrupting the interface. Our results are in general agreement with these reports in the literature, and expand upon them as a quantitative data set studying an intact device-tissue interface over multiple time points spanning three months.

Changes in neuronal density surrounding neural prostheses as a function of time have not been demonstrated previously in the literature. The initially severe injury seen following insertion, followed by a return of neuronal soma near the probe at one week, corresponds well with the variation in recording quality observed with silicon probes; there is typically a loss and recovery of unit recordings generally corresponding to this time course (Ludwig, Uram et al. 2005). However, recording quality often diminishes over subsequent weeks and months, which is not predicted by the general improvements in six week and three month neuronal and non-neuronal density data. It may be that slight increases in neuronal density are negated by the compact glial sheath formed at later time points, which may impede ionic transfer to recording sites (Roitbak and Sykova 1999) Alternatively, the data raises the possibility of neuronal plasticity and the formation of

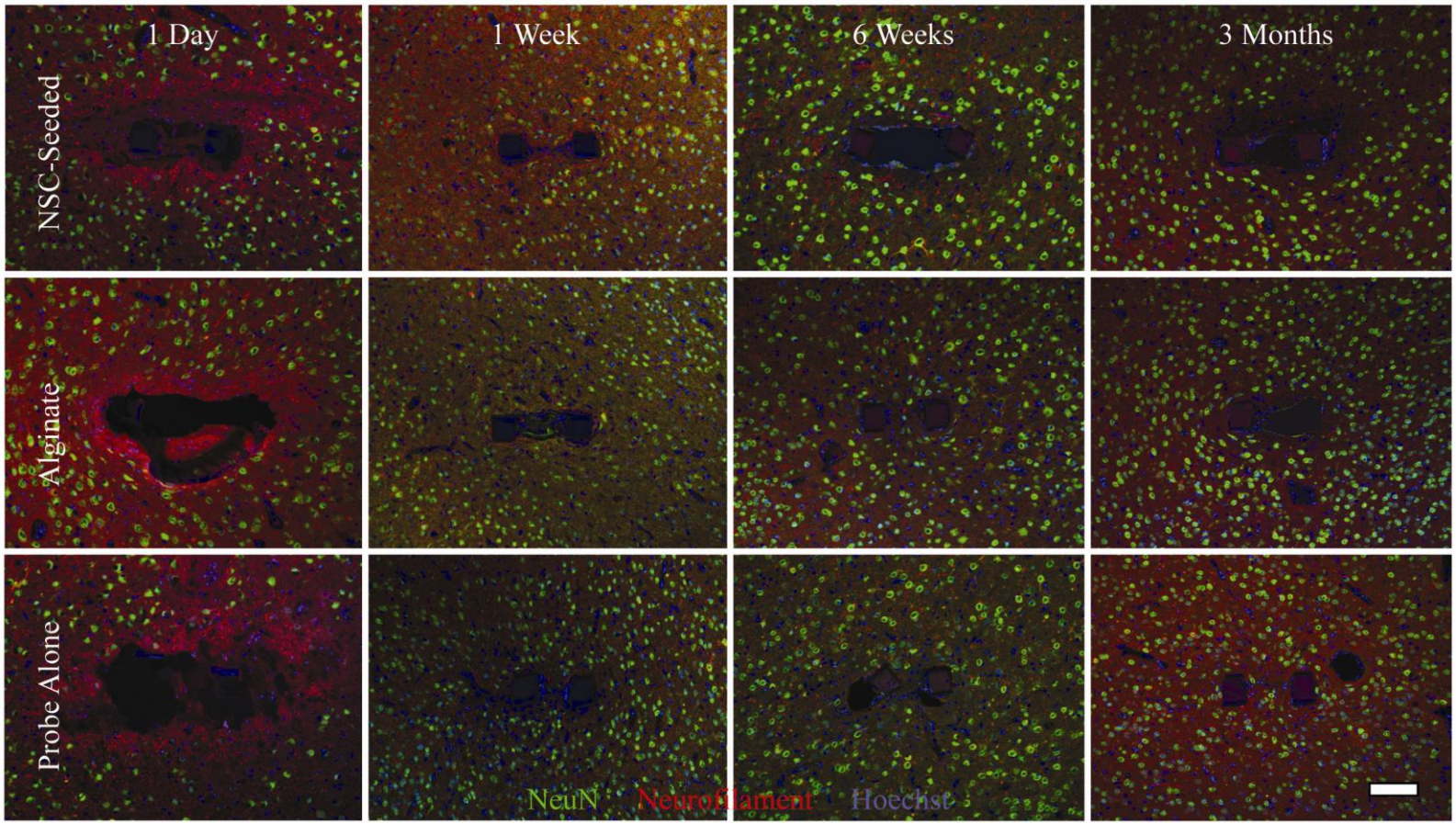

Figure 4.6. Immunohistochemistry for neuronal markers (NeuN, green; neurofilament, red) around probes reveals an initial injury response characterized by decreased neuronal density and neurofilament disruption indicative of damaged axons. A marked improvement occurs within the first week, with a significant increase in neuronal density ($p \leq 0.006$) and improved neurofilament distribution. Appendix C contains additional views of selected images.

silent synapses as additional explanations for recording instability. Henze *et al.* have reported detecting approximately six units per tetrode, despite estimations that 60-100 neurons should have sufficient amplitude to be discernible above noise (Henze, Borhegyi et al. 2000). Whether or not the neurons located within a recordable distance from electrodes are functionally normal or not is unknown. Understanding not only changes in the structure, but also the function, of tissue surrounding the probes may enable additional intervention strategies to improve recording stability.

Conclusions

Our data show that neural stem cell-seeding attenuates the initial tissue response associated with the introduction of a foreign body into the brain. Given the physical isolation of the graft cells from the surrounding tissue, *in vitro* data demonstrating the secretion of neuroprotective factors by the scaffold (Purcell, Singh et al. 2008), and evidence that the majority of cells express nestin initially *in vivo*, a bystander effect is the likely mechanism. Doublecortin-positive immature neurons were associated primarily with seeded probes one week after implantation, possibly indicating a regenerative capacity of the injured brain, graft cells, or both (Supplementary Figure 4.1). Reduced graft cell viability and function over time, followed by a secondary inflammatory reaction to cellular debris, may explain the deleterious effect of cell-seeding at later time points. Degradation of the alginate scaffold may leave transplanted cells vulnerable to immune rejection. It is also possible that an early reduction of glial activation by neural stem cells intensifies neuronal injury later (Hanisch and Kettenmann 2007). Future studies of this biohybrid device will include investigating these mechanisms further, improving cell

viability and scaffold integrity, and functionalizing recording sites for neurophysiology studies.

Acknowledgements

The authors gratefully thank Aparna Singh for surgical assistance, and Joe Kazemi from the Center for Statistical Consultation and Research at the University of Michigan for guidance with the mixed model development. The M2 antibody was obtained from the Developmental Studies Hybridoma Bank, where it was developed under the auspices of the NICHD and maintained by The University of Iowa, Department of Biological Sciences, Iowa City, IA 52242. This work was supported by the Center for Neural Communication Technology (NIBIB, P41-EB002030).

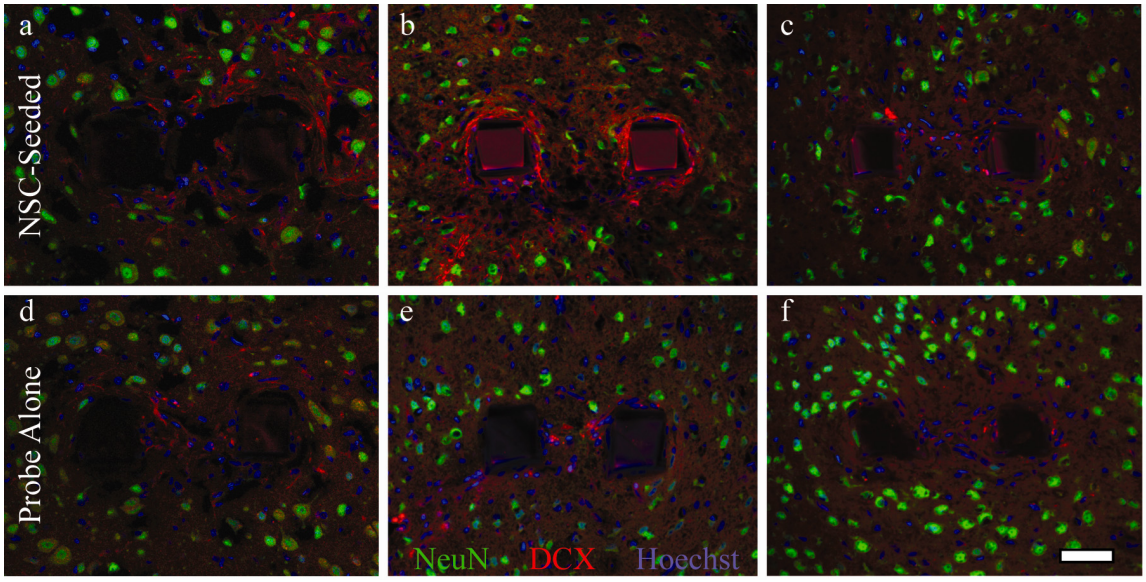

Supplementary Figure 4.1. Doublecortin staining (DCX, red) was detected in three of four animals one week post-implantation (a-c, d-f). Doublecortin (DCX) is a microtubule-associated protein expressed in migrating neuronal precursors, but may also be associated with mature astrocytes. DCX has been observed during glial scar formation following traumatic brain injury, with peak expression occurring at 1 week post-injury (Francis, Koulakoff et al. 1999; Itoh, Satou et al. 2007). Tissue was also labeled with NeuN (mature neuronal nuclei, green) and Hoechst (nuclear counterstain, blue). Expression appeared enhanced in NSC-seeded (a-c) probes compared to controls from the same animal (probe only, d-f). No staining was observed in the remaining animals. The origin and function of DCX-expressing cells are yet to be elucidated, could possibly indicate a regenerative capacity of the injured brain, the grafted cells, or a combination of both. Scale = 50 microns. Appendix C contains additional views of selected images.

References

Bakshi, A., C. A. Keck, et al. (2005). "Caspase-mediated cell death predominates following engraftment of neural progenitor cells into traumatically injured rat brain." Brain Res 1065(1-2): 8-19.

Biran, R., D. C. Martin, et al. (2005). "Neuronal cell loss accompanies the brain tissue response to chronically implanted silicon microelectrode arrays." Exp Neurol 195(1): 115-26.

Carmena, J. M., M. A. Lebedev, et al. (2003). "Learning to control a brain-machine interface for reaching and grasping by primates." PLoS Biol 1(2): E42.

Chen, X. H., D. F. Meaney, et al. (1999). "Evolution of neurofilament subtype accumulation in axons following diffuse brain injury in the pig." J Neuropathol Exp Neurol 58(6): 588-96.

Cowell, R. M., J. M. Plane, et al. (2003). "Complement activation contributes to hypoxic-ischemic brain injury in neonatal rats." J Neurosci 23(28): 9459-68.

Donoghue, J. P., A. Nurmikko, et al. (2007). "Assistive technology and robotic control using motor cortex ensemble-based neural interface systems in humans with tetraplegia." J Physiol 579(Pt 3): 603-11.

Edell, D. J., V. V. Toi, et al. (1992). "Factors influencing the biocompatibility of insertable silicon microshafts in cerebral cortex." IEEE Trans Biomed Eng 39(6): 635-43.

Fitzsimmons, N. A., W. Drake, et al. (2007). "Primate reaching cued by multichannel spatiotemporal cortical microstimulation." J Neurosci 27(21): 5593-602.

Francis, F., A. Koulakoff, et al. (1999). "Doublecortin is a developmentally regulated, microtubule-associated protein expressed in migrating and differentiating neurons." Neuron 23(2): 247-56.

Gaillard, A., L. Prestoz, et al. (2007). "Reestablishment of damaged adult motor pathways by grafted embryonic cortical neurons." Nat Neurosci 10(10): 1294-9.

Han, B. H. and D. M. Holtzman (2000). "BDNF protects the neonatal brain from hypoxic-ischemic injury in vivo via the ERK pathway." J Neurosci 20(15): 5775-81.

Hanisch, U. K. and H. Kettenmann (2007). "Microglia: active sensor and versatile effector cells in the normal and pathologic brain." Nat Neurosci 10(11): 1387-94.

Heine, W., K. Conant, et al. (2004). "Transplanted neural stem cells promote axonal regeneration through chronically denervated peripheral nerves." Exp Neurol 189(2): 231-40.

Henze, D. A., Z. Borhegyi, et al. (2000). "Intracellular features predicted by extracellular recordings in the hippocampus in vivo." J Neurophysiol 84(1): 390-400.

Hochberg, L. R., M. D. Serruya, et al. (2006). "Neuronal ensemble control of prosthetic devices by a human with tetraplegia." Nature 442(7099): 164-71.

Itoh, T., T. Satou, et al. (2007). "Immature and mature neurons coexist among glial scars after rat traumatic brain injury." Neurol Res 29(7): 734-42.

Kim, Y. T., R. W. Hitchcock, et al. (2004). "Chronic response of adult rat brain tissue to implants anchored to the skull." Biomaterials 25(12): 2229-37.

Kolb, B., G. Gorny, et al. (1997). "Nerve growth factor stimulates growth of cortical pyramidal neurons in young adult rats." Brain Res 751(2): 289-94.

Lebedev, M. A. and M. A. Nicolelis (2006). "Brain-machine interfaces: past, present and future." Trends Neurosci 29(9): 536-46.

Lindvall, O., Z. Kokaia, et al. (2004). "Stem cell therapy for human neurodegenerative disorders-how to make it work." Nat Med 10 Suppl: S42-50.

Liu, X., D. B. McCreery, et al. (2006). "Evaluation of the stability of intracortical microelectrode arrays." IEEE Trans Neural Syst Rehabil Eng 14(1): 91-100.

Liu, X., D. B. McCreery, et al. (1999). "Stability of the interface between neural tissue and chronically implanted intracortical microelectrodes." IEEE Trans Rehabil Eng 7(3): 315-26.

Llado, J., C. Haenggeli, et al. (2004). "Neural stem cells protect against glutamate-induced excitotoxicity and promote survival of injured motor neurons through the secretion of neurotrophic factors." Mol Cell Neurosci 27(3): 322-31.

Lu, P., L. L. Jones, et al. (2003). "Neural stem cells constitutively secrete neurotrophic factors and promote extensive host axonal growth after spinal cord injury." Exp Neurol 181(2): 115-29.

Ludwig, K. A., J. Uram, et al. (2005). "Chronic neural recordings using silicon microelectrode arrays electrochemically deposited with a poly(3,4-ethylenedioxythiphene) (PEDOT) film."

Messam, C. A., J. Hou, et al. (2000). "Coexpression of nestin in neural and glial cells in the developing human CNS defined by a human-specific anti-nestin antibody." Exp Neurol 161(2): 585-96.

Nicole, O., C. Ali, et al. (2001). "Neuroprotection mediated by glial cell line-derived neurotrophic factor: involvement of a reduction of NMDA-induced calcium influx by the mitogen-activated protein kinase pathway." J Neurosci 21(9): 3024-33.

Nicolelis, M. A., D. Dimitrov, et al. (2003). "Chronic, multisite, multielectrode recordings in macaque monkeys." Proc Natl Acad Sci U S A 100(19): 11041-6.

Nunamaker, E. A., E. K. Purcell, et al. (2007). "In vivo stability and biocompatibility of implanted calcium alginate disks." J Biomed Mater Res A 83(4): 1128-37.

Orive, G., R. M. Hernandez, et al. (2003). "Cell encapsulation: promise and progress." Nat Med 9(1): 104-7.

Ourednik, J., V. Ourednik, et al. (2002). "Neural stem cells display an inherent mechanism for rescuing dysfunctional neurons." Nat Biotechnol 20(11): 1103-10.

Pluchino, S., L. Zanotti, et al. (2005). "Neurosphere-derived multipotent precursors promote neuroprotection by an immunomodulatory mechanism." Nature 436(7048): 266-71.

Polikov, V. S., P. A. Tresco, et al. (2005). "Response of brain tissue to chronically implanted neural electrodes." J Neurosci Methods 148(1): 1-18.

Purcell, E. K., A. Singh, et al. (2008). In Vitro Development and Characterization of a Cortical Neural Stem Cell-Seeded Alginate Scaffold Tissue Engineering (in submission).

Reynolds, B. A. and S. Weiss (1992). "Generation of neurons and astrocytes from isolated cells of the adult mammalian central nervous system." Science 255(5052): 1707-10.

Reynolds, B. A. and S. Weiss (1996). "Clonal and population analyses demonstrate that an EGF-responsive mammalian embryonic CNS precursor is a stem cell." Dev Biol 175(1): 1-13.

Roitbak, T. and E. Sykova (1999). "Diffusion barriers evoked in the rat cortex by reactive astrogliosis." Glia 28(1): 40-8.

Rousche, P. J. and R. A. Normann (1998). "Chronic recording capability of the Utah Intracortical Electrode Array in cat sensory cortex." J Neurosci Methods 82(1): 1-15.

Rowley, J. A., G. Madlambayan, et al. (1999). "Alginate hydrogels as synthetic extracellular matrix materials." Biomaterials 20(1): 45-53.

Salman, H., P. Ghosh, et al. (2004). "Subventricular zone neural stem cells remodel the brain following traumatic injury in adult mice." J Neurotrauma 21(3): 283-92.

Schwartz, A. B., X. T. Cui, et al. (2006). "Brain-controlled interfaces: movement restoration with neural prosthetics." Neuron 52(1): 205-20.

Seymour, J. P. and D. R. Kipke (2007). "Neural probe design for reduced tissue encapsulation in CNS." Biomaterials 28(25): 3594-607.

Silver, J. and J. H. Miller (2004). "Regeneration beyond the glial scar." Nat Rev Neurosci 5(2): 146-56.

Sortwell, C. E., M. R. Pitzer, et al. (2000). "Time course of apoptotic cell death within mesencephalic cell suspension grafts: implications for improving grafted dopamine neuron survival." Exp Neurol 165(2): 268-77.

Szarowski, D. H., M. D. Andersen, et al. (2003). "Brain responses to micro-machined silicon devices." Brain Res 983(1-2): 23-35.

Taylor, D. M., S. I. Tillery, et al. (2002). "Direct cortical control of 3D neuroprosthetic devices." Science 296(5574): 1829-32.

Teng, Y. D., E. B. Lavik, et al. (2002). "Functional recovery following traumatic spinal cord injury mediated by a unique polymer scaffold seeded with neural stem cells." Proc Natl Acad Sci U S A 99(5): 3024-9.

Turner, J. N., W. Shain, et al. (1999). "Cerebral astrocyte response to micromachined silicon implants." Exp Neurol 156(1): 33-49.

Velliste, M., S. Perel, et al. (2008). "Cortical control of a prosthetic arm for self-feeding." Nature.

Verwer, R. W., A. A. Sluiter, et al. (2007). "Mature astrocytes in the adult human neocortex express the early neuronal marker doublecortin." Brain 130(Pt 12): 3321-35.

Vetter, R. J., J. C. Williams, et al. (2004). "Chronic neural recording using silicon-substrate microelectrode arrays implanted in cerebral cortex." IEEE Trans Biomed Eng 51(6): 896-904.

Wilkins, A. and A. Compston (2005). "Trophic factors attenuate nitric oxide mediated neuronal and axonal injury in vitro: roles and interactions of mitogen-activated protein kinase signalling pathways." J Neurochem 92(6): 1487-96.

Williams, J. C., J. A. Hippensteel, et al. (2007). "Complex impedance spectroscopy for monitoring tissue responses to inserted neural implants." J Neural Eng 4(4): 410-23.

Williams, J. C., R. L. Rennaker, et al. (1999). "Long-term neural recording characteristics of wire microelectrode arrays implanted in cerebral cortex." Brain Res Brain Res Protoc 4(3): 303-13.

CHAPTER 5
CELL-CYCLE INHIBITION EFFECTS ON THE RECORDING QUALITY AND TISSUE RESPONSE OF CHRONIC NEURAL PROBES

Abstract

Neural prostheses are currently plagued by recording instability, which limits their utility in research and clinical settings. The tissue response which occurs to these devices *in vivo* is likely a key contributing factor to this issue. After implantation, probes are encapsulated by glia and neuronal density in the surrounding tissue is reduced. We hypothesized that re-entry into the cell cycle may be associated with the reactive gliosis surrounding probes, and that administration of a cell cycle inhibitor (flavopiridol) at the time of surgery would reduce this effect. We investigated the effects of flavopiridol on recording quality and impedance over a 28 day time period, and conducted histology at 3 and 28 days post-implantation. Flavopiridol reduced the expression of a cell cycle protein (cyclin D1) in microglia surrounding probes at the 3 day time point. Impedance at 1 kHz was reduced by drug administration across the study period compared to vehicle controls. Correlations between recording (SNR, units) and impedance metrics revealed a significant, but small, inverse relationship between these variables. However, the relationship between impedance and recording quality was not strong enough for flavopiridol to result in an improvement in SNR or the number of units. Additionally, the effects of the drug were not reflected in the variable endpoint histology data collected from tissue in which the interface with the device was damaged upon probe

explantation. Our data indicate that flavopiridol is an effective treatment for reducing impedance *in vivo*, likely through inhibiting microglial encapsulation of recording devices. However, this did not translate to improvements in recording quality, and combination of flavopiridol with a second strategy which enhances neuronal signal may further improve results. Finally, the correlation between endpoint histology and electrophysiology metrics across all animals provides quantitative evidence for a direct relationship between recording quality and the tissue response to neural prostheses.

Introduction

Neural prostheses record action potentials from a patient's cortex which may then be used to control external assistive devices (Taylor, Tillery et al. 2002; Carmena, Lebedev et al. 2003; Hochberg, Serruya et al. 2006; Schwartz, Cui et al. 2006; Donoghue, Nurmikko et al. 2007; Fitzsimmons, Drake et al. 2007; Velliste, Perel et al. 2008). Therefore, these systems have the potential to restore some level of function to the 200,000 individuals currently suffering from full or partial paralysis in the U.S., as well as patients immobilized by neurodegenerative disease (Polikov, Tresco et al. 2005) For neural prostheses to be useful in clinical and research settings, stable recordings from large populations of neurons in multiple brain areas should be reliably and reproducibly achieved over a period of several years (Lebedev and Nicolelis 2006). However, recording longevity and stability is highly variable according to numerous reports, and the reactive tissue response that occurs to devices following implantation into the brain is likely to be a key contributing factor (Rousche and Normann 1998; Liu, McCreery et al. 1999; Williams, Rennaker et al. 1999; Nicolelis, Dimitrov et al. 2003; Polikov, Tresco et

al. 2005; Liu, McCreery et al. 2006; Schwartz, Cui et al. 2006). Neuronal density is reduced surrounding probes following insertion, and an encapsulating sheath of microglia and astrocytes further isolates the devices from their neuronal signal sources (Edell, Toi et al. 1992; Turner, Shain et al. 1999; Szarowski, Andersen et al. 2003; Kim, Hitchcock et al. 2004; Biran, Martin et al. 2005; Polikov, Tresco et al. 2005). However, evidence of a direct cause-effect relationship between recording quality and histology metrics remains limited. Williams *et al.* report recording sites with extensive glial reactivity to have increased impedance magnitude at 1 kHz (the fundamental frequency of the neuronal action potential), as well as a non-linear relationship between the real and imaginary components of impedance (Williams, Hippensteel et al. 2007). Additionally, neuronal density within the first 100 microns of the device surface is reduced, and this region produces the large amplitude, reliably separated spikes useful for neural prostheses (Henze, Borhegyi et al. 2000; Biran, Martin et al. 2005; Purcell, Seymour et al. 2008).

While neuronal loss and glial encapsulation surrounding neural prostheses are well documented phenomena, the mechanisms underlying these changes in the device-tissue interface remain largely unexplored. Certainly, inflammation plays a role; the release of inflammatory cytokines from cells attached to explanted probes has been demonstrated, and anti-inflammatory drugs such as dexamethasone have reduced impedance and astrogliosis associated with probes *in vivo* (Shain, Spataro et al. 2003; Spataro, Dilgen et al. 2005; Bjornsson, Oh et al. 2006; Kim and Martin 2006; Zhong and Bellamkonda 2007). Another contributing factor is the rupture of vasculature during insertion, which has been observed up to 300 microns from the probe surface (Bjornsson, Oh et al. 2006).

If neuronal density surrounding probes is reduced due to cell death, then understanding the underlying mechanisms (i.e. apoptosis, necrosis, excitoxicity, inflammation, etc.), and their relative contributions, would allow for the development of appropriately targeted pharmacological intervention strategies. The functionality of the remaining neurons also needs to be explored. Likewise, understanding the signals resulting in the activation or quiescence of glia surrounding probes could enable improved methods of promoting device-tissue integration.

In recent years, a contribution of cell-cycle re-entry to the activation of glia, as well as neuronal apoptosis, has been demonstrated in models of central nervous system (CNS) injury (Verdaguer, Jimenez et al. 2004; Di Giovanni, Movsesyan et al. 2005; Appert-Collin, Hugel et al. 2006; Alvira, Tajes et al. 2007; Byrnes, Stoica et al. 2007). The cell cycle is a complex process through which cells progress from a quiescent to a proliferative state, and cellular advancement through this cycle is controlled by cyclin dependent kinases (CDKs) and associated cyclins (Schafer 1998). Following CNS injury and an associated upregulation of these cell-cycle proteins, mitotic cells (namely, microglia and astrocytes) proliferate, while non-mitotic cells (differentiated neurons) undergo caspase-mediated apoptosis (Cernak, Stoica et al. 2005). Flavopiridol is a flavonoid drug which is a broad CDK inhibitor and arrests progression through the cell cycle (Swanton 2004). Di Giovanni *et al.* showed a single injection of flavopiridol intracerebroventricularly reduced expression of the cell cycle protein cyclin D1, decreased neuronal cell death, reduced glial activation, and improved motor and cognitive recovery following traumatic brain injury in rats (Di Giovanni, Movsesyan et

al. 2005). Flavopiridol has resulted in improved functional and histological outcomes in *in vitro* and *in vivo* models of spinal cord injury, Parkinson's disease, motorneuron apoptosis, and excitotoxic injury (Verdaguer, Jimenez et al. 2004; Appert-Collin, Hugel et al. 2006; Alvira, Tajes et al. 2007; Byrnes, Stoica et al. 2007).

We hypothesized that the implantation of neural prostheses may result in an upregulation of cell cycle proteins in the adjacent tissue, which is associated with neuronal apoptosis and the activation and proliferation of glia. Therefore, cell cycle re-entry could be involved in the prototypic glial encapsulation and neuronal density loss surrounding these devices. Furthermore, cell cycle inhibitors may reduce these effects, and cause an improvement in recording quality and impedance data as a result. We collected histology, impedance, and electrophysiology data over a 28 day time period in rats that were injected intracerebroventricularly (ICV) with either flavopiridol or vehicle alone at the time of probe insertion. We report reduced impedance and reduced expression of cell cycle proteins in drug-treated animals. There was no relationship between drug treatment and quantitative histology. No effect on recording quality was observed; however, a general association between these data and the time course of the tissue response was noted. Finally, significant correlations between histology, impedance, and recording metrics are shown.

Methods

Probe Implantation and Intracerebroventricular (ICV) Injection

Sixteen channel chronic silicon probes with 1250 μm^2 iridium recording sites and a 2.1 mm long single shank were provided by the University of Michigan Center for Neural Communications Technology (CNCT) (See Appendix B for a diagram). The design and fabrication of these probes has been described (Drake, Wise et al. 1988). Sixteen male Sprague Dawley rats (300–350 g) were implanted with the devices using a surgical procedure similar to those previously reported (Ludwig, Uram et al. 2006). Anesthesia was achieved via a ketamine cocktail. A 3x2 mm craniotomy was centered over the motor cortex, dura was resected and the probe was manually inserted into the brain (+3.0 mm AP, 2.5 mm ML, -1.4 mm DV from Bregma). The electrode connector was grounded to a bone-screw over parietal cortex using a stainless steel ground wire. Prior to probe insertion, "flavopiridol"/"drug" and "control" rats were injected ICV with 5 µL of 250 µM flavopiridol (Sigma, St. Louis, MO) dissolved in artificial cerebrospinal fluid (ACSF) or ACSF alone respectively. The solution was administered over the course of one minute through a cannula (Plastics One, Roanoke, VA) attached to a stereotaxic frame and inserted into the left lateral ventricle (-0.8 mm AP, 1.5 mm ML, -4.3 mm DV from Bregma). The cannula was immediately withdrawn following the injection. Surgical closure was achieved with a combination of GelFoam (Henry Schein, Inc., Miami, FL), silicone (World Precision Instruments, Sarasota, FL), and dental acrylic (Co-Oral-Ite, Dental Mfg. Co., Santa Monica, CA). All procedures strictly complied with the United States Department of Agriculture guidelines for the care and use of laboratory

animals and were approved by the University of Michigan Animal Care and Use Committee.

Neural Recordings

Neural recordings were taken from ten animals (five control, five flavopiridol) immediately following surgery, and every three to four days thereafter over a 28 day time course. The remaining animals were processed for histology at the 3 day time point. Animals were placed in a Faraday cage and thirty second segments of high speed data were collected using a TDT multi-channel acquisition system (Tucker-Davis Technologies, Gainesville, FL) as previously described (Ludwig, Uram et al. 2006). Single and multi-unit recordings were sampled at 24414 Hz and bandpass filtered from 450-5000 Hz. Local field potentials (LFPs) were sampled at 1 Hz and bandpass filtered from 3 to 90 Hz.

Offline analysis using custom automated MatLAB (Mathworks Inc., MA) software was performed as reported previously (Ludwig, Uram et al. 2006). Briefly, candidate waveforms were identified when peaks exceeded an amplitude threshold window 3.5 standard deviations above and below the mean of the sample distribution. A 2.4 ms candidate waveform snippet centered on the absolute minimum of the waveform was then removed from the recorded segment and stored. After all candidate waveforms had been removed, the peak-to-peak amplitude (rather than RMS) of the noise voltage was calculated as six times the standard deviation of the recording, thus including approximately 99.7 percent of the noise data (Ludwig, Miriani et al. 2008). Waveforms

with a cluster membership index of greater than 0.8 were used to determine a mean waveform for a cluster after initial principal component analysis and fuzzy C-means clustering. The signal-to-noise ratio (SNR) for a given cluster was defined as the peak-to-peak amplitude of the mean waveform for each cluster divided by the peak-to-peak amplitude of the noise floor. Units were defined as clusters with a mean SNR of 1.1 or greater; the discrepancy between this and previous SNR values reported for units of moderate to high quality is accounted for by the difference between calculating SNR using the peak-to-peak amplitude of the noise floor instead of RMS (Ludwig, Miriani et al. 2008). Common average referencing, in which the average of all the recordings on every functional electrode site is taken and used as a reference, was used to remove noise sources common to every electrode site (such as motion artifact, 60 Hz noise, instrumentation noise, thermal noise, and biological sources of noise) as previously described (Ludwig, Miriani et al. 2008).

Impedance Spectroscopy

Impedance spectroscopy measurements were taken for animals on the same days as neural recordings using an Autolab potentiostat PGSTAT12 (Eco Chemie, Utrecht, The Netherlands) and associated frequency response analyzer (Brinkmann, Westbury, NY). A 25 mV RMS sine wave was applied with frequencies varying logarithmically from 10 Hz to 10 kHz using a stainless steel bone screw as the reference electrode.

Immunohistochemistry and Analysis

Animals were deeply anesthetized and transcardially perfused with 4% paraformaldehyde at the appropriate time point following probe implantation (3 days, n=3 animals per

group; 28 days, n=5 animals per group). A single drug-treated rat brain in the 3 day histology group was not analyzed due to poor fixation and tissue processing. Brain tissue was explanted, postfixed overnight in 4% paraformaldehyde, and cryoembedded following sucrose protection. Probes were removed from the tissue prior to processing. Serial 12 micron thick sections along the tract of the probes were collected, and eight tissue sections spanning the shank of the probe were randomly selected and immunostained for NeuN (1:100, Millipore Corporation, Billerica, MA) and counterstained with Hoechst (1 μg/mL, Invitrogen Corporation, Carlsbad, CA) for quantitative analysis of tissue response. Four of these sections were also stained with cyclin D1 (CD-1, 1:100, Abcam, Cambridge, MA) to investigate possible re-entry into the cell cycle. An additional four sections were stained with Ox-42 (1:100, Serotec, Oxford, UK), CD-1 (1:100, Abcam, Cambridge, MA), and Hoechst (1 μg/mL). A final four sections were stained for glial fibrillary acidic protein (GFAP, 1:100, Sigma, St. Louis, MO), CD-1 (1:100, Millipore Corporation, Billerica, MA), and Hoechst (1 μg/mL). These sections were used to qualitatively assess the role of cell cycle protein expression in glial activation and probe encapsulation. Sections were hydrated in buffer (PBS), blocked with 10% normal goat serum, and incubated overnight with primary antibodies at 4˚C. Sections were then rinsed, incubated in the appropriate secondary antibodies (1:200 Alexa-488, and 568, Invitrogen), counterstained with Hoechst, and coverslipped with ProLong Gold (Invitrogen). Antibody solutions included 0.3% triton X-100 and 5% normal goat serum. Buffer was used in place of primary antibody for controls. Confocal images were collected with an Olympus FV500 microscope with the 20X objective.

Neuronal and non-neuronal densities were analyzed using a MatLAB graphical user interface as described previously (Seymour and Kipke 2007; Purcell, Seymour et al. 2008). An outline of the exterior edge of the tract cross-section for each image was delineated using a differential interference contrast (DIC) and UV fluorescence image. A blinded technician selected all nuclei as either neuronal (NeuN+, Hoechst+) or non-neuronal (Hoechst+ only) within a software-defined 100 micron radius of the probe surface. The software algorithm used the coordinates of the user-selected nuclei to calculate the shortest distance to the tract edge, bin the counts by distance, and calculate the sampling area of each bin to result in neuronal and non-neuronal densities as a function of distance from the probe tract.

Statistical Analysis

A linear mixed model ANOVA was used to assess the effect of time and condition on impedance and recording metrics. The random effect was the individual animal, and multiple electrode sites were included as a repeated measure. Time and condition were included as fixed factors. A linear mixed model was similarly used to assess the effects of distance and condition on neuronal and non-neuronal densities, although the data was averaged across multiple sections per animal and site-by-site analysis was not possible.

Correlation between impedance and recording metrics over the course of the study were achieved by using a linear mixed model in which these values were standardized, and one variable was defined as a predictor (covariate). The individual animal was included as a random effect to control for correlated observations within the same rat. A Spearman's

ranked coefficient followed by a two-tailed *t* test for significance was calculated to assess the strength of correlation between endpoint tissue response, recording, and impedance data across all study animals. Significance was defined at the 0.05 level for all tests.

Results

Impedance Spectroscopy

The impedance of electrode recording sites at 1 kHz (the fundamental frequency of the neuronal action potential) and 10 Hz (in frequency range of LFPs) is shown in Figure 5.1. Impedance was decreased by flavopiridol administration at both frequencies ($p<0.001$, mixed model ANOVA). Analysis of the time course of impedance changes for the combined group of animals revealed general trends which may be explained by the tissue response to the devices. Impedance at 1 kHz increased from initially low values in the 0-3 day time period at 7 days post-implantation (Figure 5.1a, $p<0.001$). Values stabilized thereafter until a final significant increase at 28 days ($p<0.05$). Similarly, a significant increase in impedance values at 10 Hz three days after the day of surgery was observed (Figure 5.1b, $p<0.01$). Values stabilized until a significant increase at 28 days ($p<0.001$). Initially low impedance in the 3 day time period after device implantation, followed by increased, and more variable, values in the two weeks thereafter, has been previously reported (Ludwig, Uram et al. 2005). Swelling and reduced cell density surrounding probes associated with initial insertion trauma is likely the reason for the initially low values. The increased impedance beginning one week after insertion corresponds with the return of cells to the surface of the probe and progressive glial encapsulation (Szarowski, Andersen et al. 2003; Ludwig, Uram et al. 2005; Purcell, Seymour et al.

2008). The final increase in impedance values at the 28 day time point was driven by control animals.

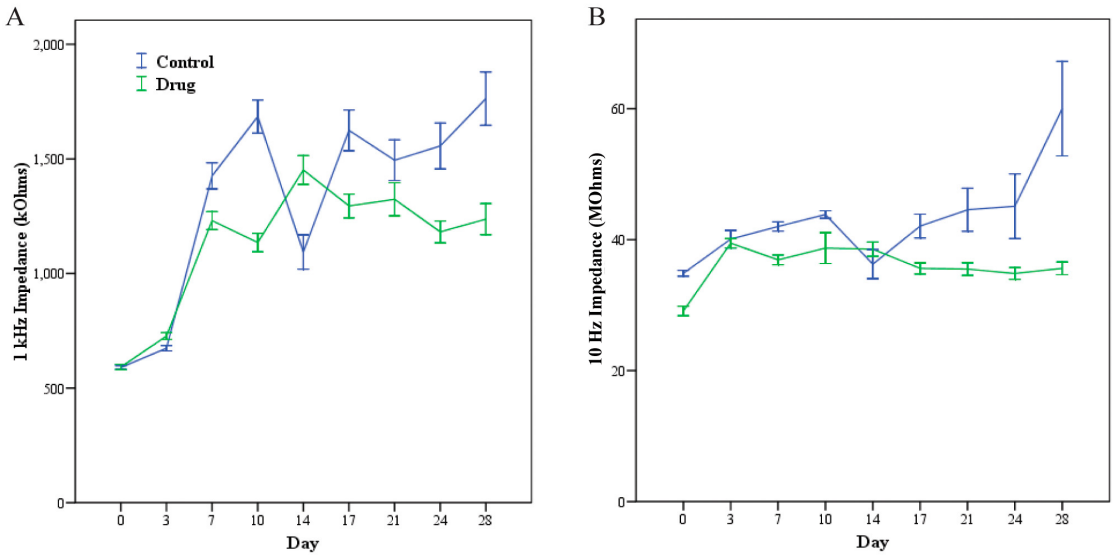

Figure 5.1. Administration of the cell-cycle inhibiting drug flavopiridol immediately prior to neural prosthetic device insertion reduced impedance at 1 kHz and 10 Hz (mixed model ANOVA, $p<0.001$). Impedance increased following implantation in the 3 to 7 day timeframe, coinciding with a reported period of increased cellular density surrounding probes (Purcell, Seymour et al. 2008) ($p<0.01$). Mean ± s.e.m. is shown.

Neural Recording Data

Flavopiridol had no effect on any of the recording metrics studied (mixed model ANOVA) (Figure 5.2a-e). The time course of recording quality metrics generally followed the sequence of tissue response events reported in the literature: initial insertion injury, followed by swelling/edema, a subsequent return of neurons and glia near the probe surface, and, finally, a combination of neuronal density loss and the formation of a compact glial encapsulation layer around the device (Szarowski, Andersen et al. 2003; Biran, Martin et al. 2005; Purcell, Seymour et al. 2008). The number of units, SNR, and LFP amplitude follow a similar time course in which peak values on the day of surgery

significantly dropped three days later ($p<0.001$), followed by an increase at the 10 day time point ($p<0.05$) (Figure 5a-c). In the initial days following surgery, there is significant damage and swelling due to insertion trauma, and few neuronal soma are found within 100 microns of the implanted device (Purcell, Seymour et al. 2008), which may account for the reduction of recording quality at the 3 day time point (Figure 5a-c). These metrics are significantly increased one week later, during a period of dramatic tissue recovery, a return of neuronal sources, and maximal glial activation (Szarowski, Andersen et al. 2003; Ludwig, Uram et al. 2005; Purcell, Seymour et al. 2008). During this time, signal and noise increase as cells return to the region surrounding the probes ($p<0.05$, Figure 5d-e). After the 10-14 day time period, decreases in the number of units, SNR, signal amplitude, and noise occur corresponding to the formation of an encapsulating, compact glial sheath as reported in the literature (Figure 5.2, a-b, d-e) (Szarowski, Andersen et al. 2003; Purcell, Seymour et al. 2008). LFPs, which are low frequency signals derived from aggregates of neurons rather than single cells, are likely less sensitive to the nuanced changes in the device-tissue interface after the period of insertion trauma and initial recovery, and do not decrease in amplitude in this timeframe (Schwartz, Cui et al. 2006). Although neuronal density surrounding probes is known to be decreased in comparison to control tissue in this time period, decreasing density with time has not been shown and is unlikely to provide a simple explanation for the loss in recording quality (Biran, Martin et al. 2005; Purcell, Seymour et al. 2008).

A

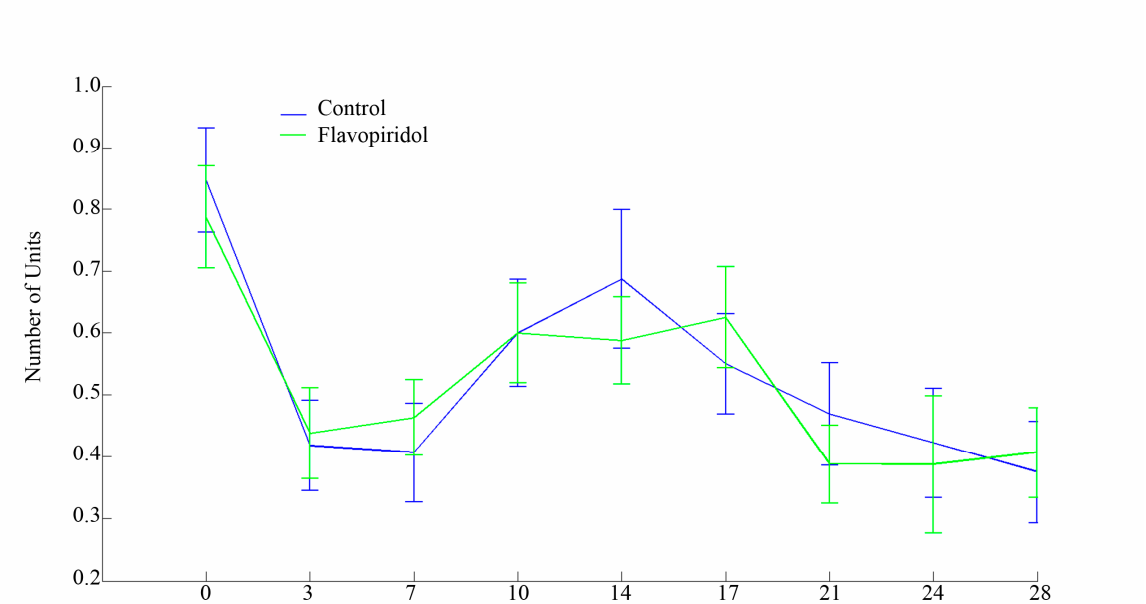
Control
Flavopiridol
Number of Units
1.0
0.9
0.8
0.7
0.6
0.5
0.4
0.3
0.2
0
3
7
10
14
17
21
24
28

B

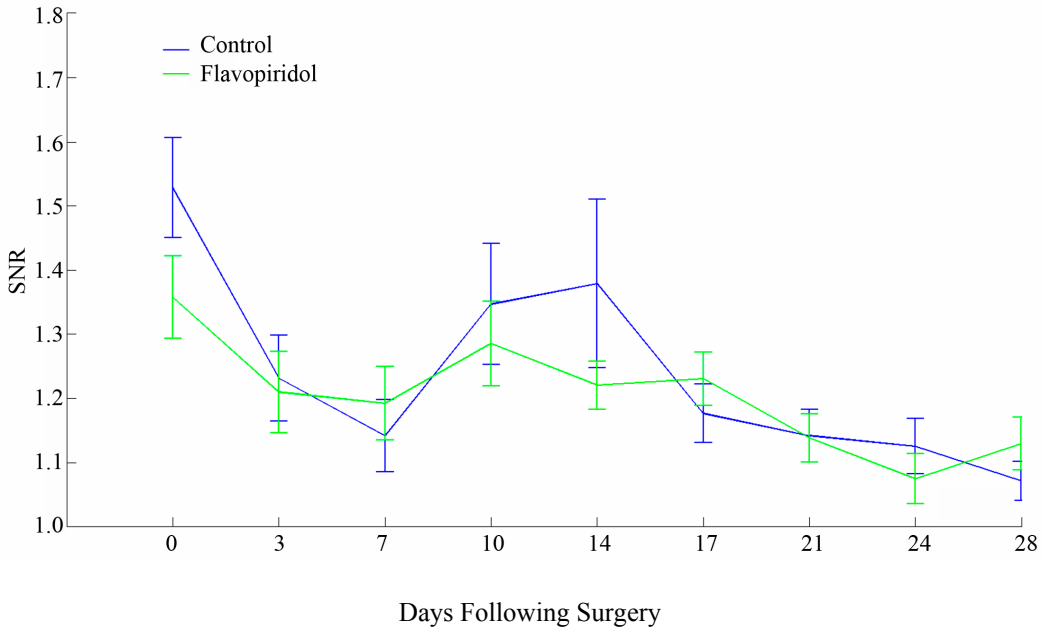
Control
Flavopiridol
SNR
1.8
1.7
1.6
1.5
1.4
1.3
1.2
1.1
1.0
0
3
7
10
14
17
21
24
28
Days Following Surgery

C

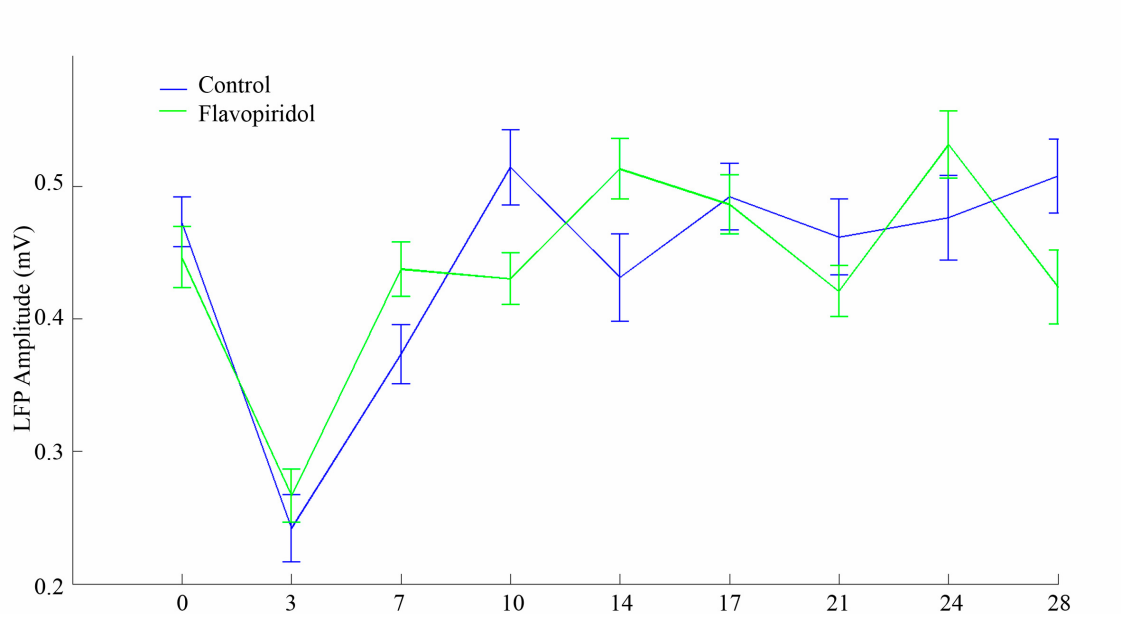
Control
Flavopiridol
LFP Amplitude (mV)
0.2
0.3
0.4
0.5
0
3
7
10
14
17
21
24
28

D

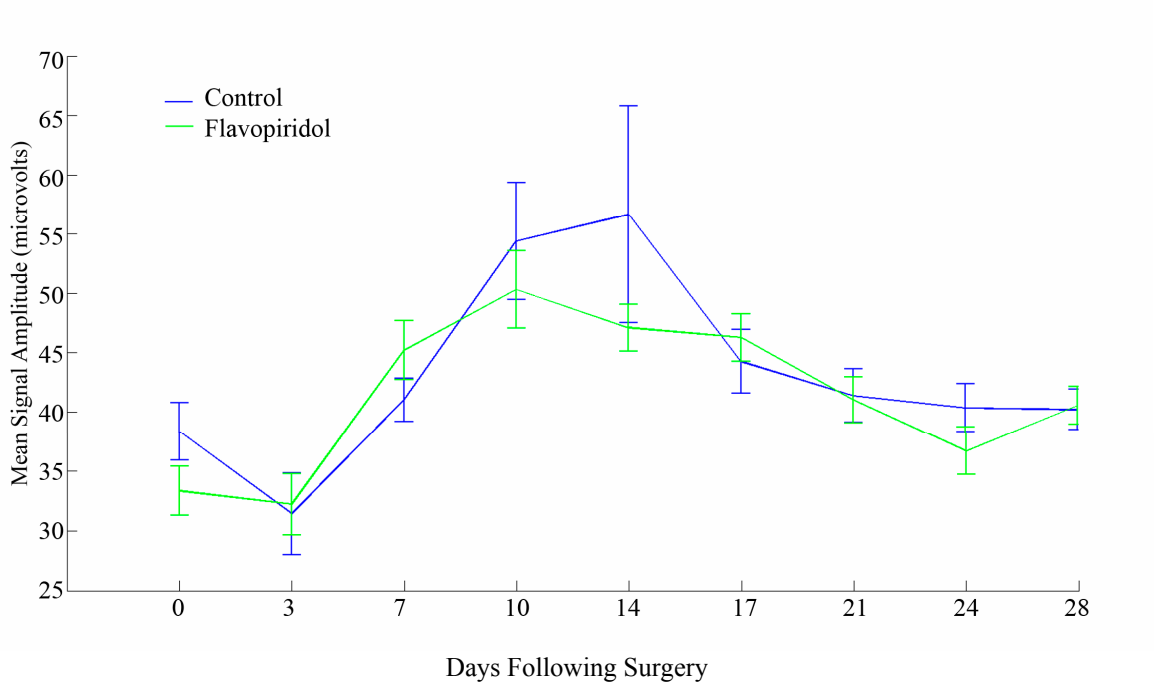
Control
Flavopiridol
Mean Signal Amplitude (microvolts)
25
30
35
40
45
50
55
60
65
70
0
3
7
10
14
17
21
24
28
Days Following Surgery

E

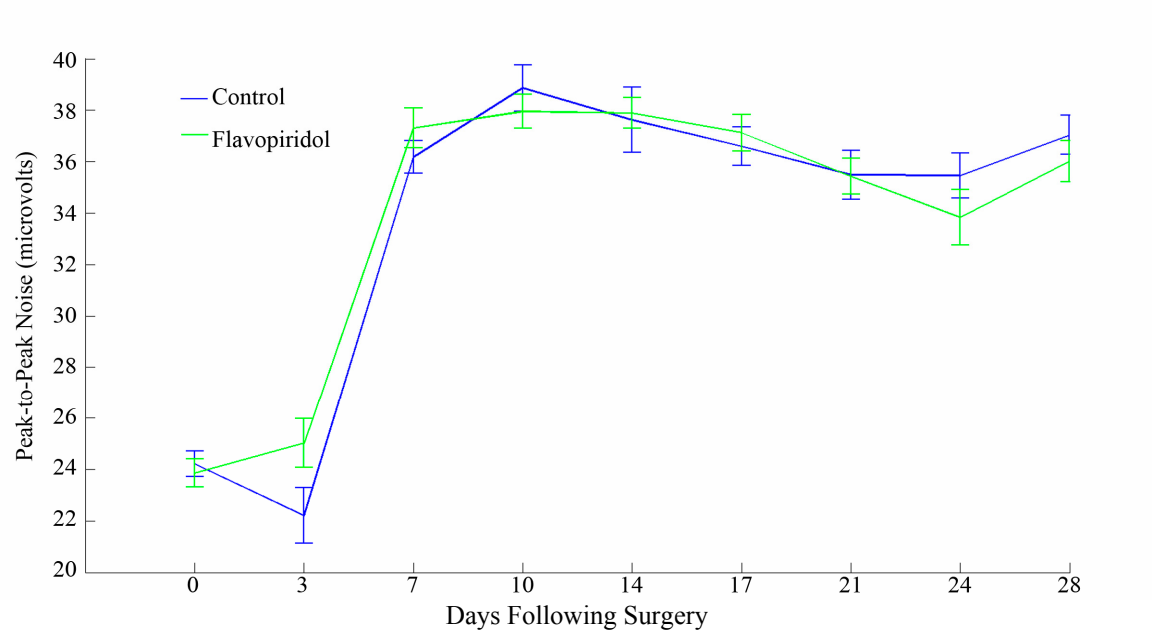

Figure 5.2. Analysis of recording quality over the 28 day study period showed no effect of flavopiridol administration. The progression of these values over the duration of the study may be explained by the tissue response to the probes. Recording quality decreases in the 0-3 day time period, coinciding with initial insertion trauma (a-c). Recovery of these metrics occurs approximately one week later, when signal and noise are increased as cells return to the device during healing (a-e). Reductions in all metrics except LFP amplitude three to four weeks after surgery occurred during glial encapsulation. "Units" are given per recording site.

Cell Cycle Protein Expression Surrounding Prostheses

Histology at 3 days revealed expression of the cell cycle protein CD-1, primarily in Ox-42 labeled microglia, surrounding probe tracts following implantation (Figure 5.3). The microglia had an activated, amoeboid morphology surrounding probe tracts. Di Giovanni *et al.* reported over 80% of Ox-42-labeled microglia and GFAP-positive astrocytes, as well as approximately 10% of NeuN-stained neurons, coexpressed CD1 surrounding the site of traumatic brain injury in rats at the same time point (Di Giovanni, Movsesyan et al. 2005). Qualitatively, there appeared to be a lesser extent of CD-1 expression in drug treated animals (n=2 drug-treated and 3 controls).

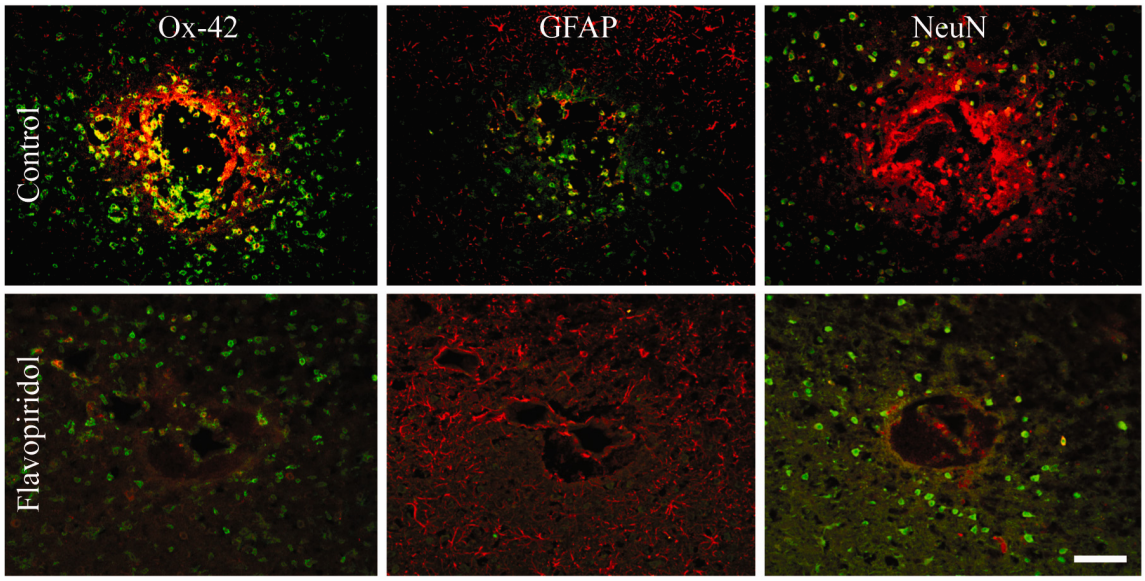

Figure 5.3. Neuroprostheses are associated with an increase in the expression of a cell-cycle protein (CD-1) in neighboring microglia three days after insertion, which appears reduced by flavopiridol administration at the time of surgery. Analysis was qualitative on a sample size of 2-3 animals per group. Images for each marker are from the same control and flavopiridol-treated animals. Ox-42 (green), GFAP (red), and NeuN (green) are shown, and CD-1 is red, green, and red respectively. Coexpressing cells are yellow. Scale = 100 microns. Appendix C contains additional views of selected images.

Neuronal and Non-Neuronal Densities Surrounding Probes

Drug treatment had no statistically significant effects on neuronal or non-neuronal cell densities surrounding the probes. Significant effects of these measurements as a function of distance from the probe surface were noted which indicated improvements in the tissue response further away from the device. ND and ND/NND generally increase and NND generally decreases when comparing these metrics measured from the area nearest the probe tract boundary (within 20 microns) to the region furthest from the boundary (greater than 70 microns away from the tract boundary) at the 28 day time point ($p<0.05$, mixed model ANOVA).

Silicon probes necessitate removal prior to histology, disrupting the tissue-device interface. In particular, the encapsulation layer immediately adjacent to the probe surface, which is predominantly composed of microglia, is likely to be damaged or removed with the prosthesis (Biran, Martin et al. 2005). The microglial sheath was absent from images taken at the 28 day time point, although the distribution of neurons and astrocytes could be observed (Figure 5.5). A steep decline of NND, and incline of ND, immediately near the probe surface is absent, which has been shown for *in situ* analysis of non-functional parylene probes (Figure 5.4) (Purcell, Seymour et al. 2008). This is a further indication that the glial sheath was disturbed upon probe explantation. Additionally, site-by-site analysis would not be accurate in the absence of the device, allowing only for average values for these metrics to be calculated along the probe tract as shown. A larger sample size, or *in situ* probe histology, could reveal significant effects in future studies.

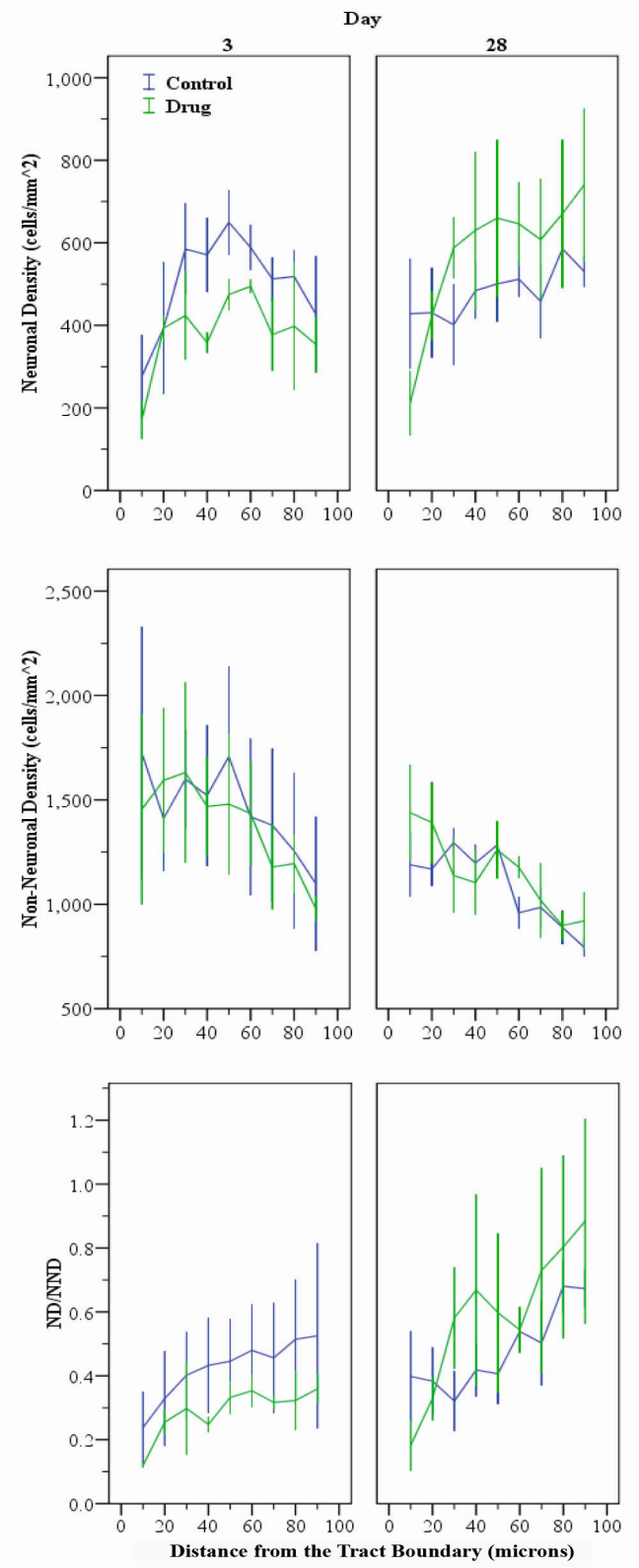

Figure 5.4. Neuronal density (ND), non-neuronal density (NND), and the ratio (ND/NND) between them as a function of distance from the probe tract boundary three and 28 days after probe implantation.

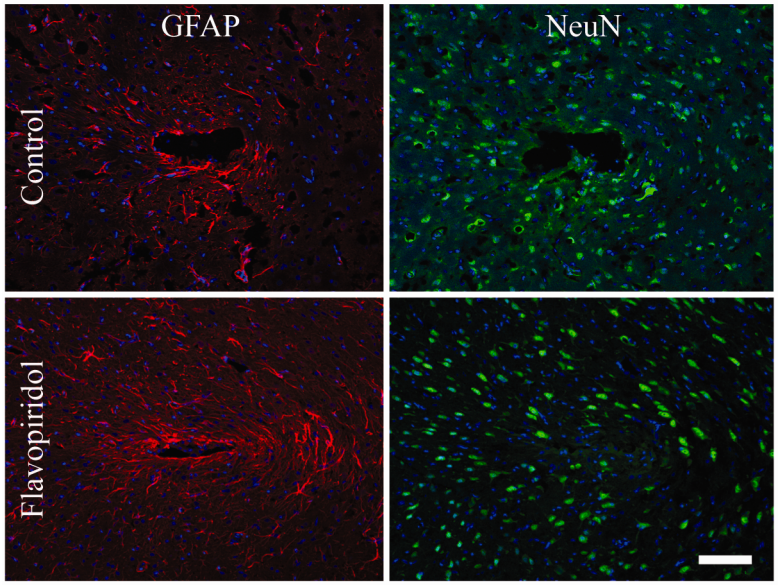

Figure 5.5. Representative images of the distribution of neuronal (NeuN, green) and non-neuronal (Hoechst, blue) nuclei 28 days after implantation (right panels). Glial encapsulation is shown by GFAP-labeled astrocytes (red), but the microglial sheath was absent at this time, likely due to remaining attached to explanted probes (left panels). Images are from the same control and flavopiridol-treated animals. Scale = 100 microns.

Correlations between Impedance, Recording Quality, and Quantitative Histology

Correlations revealed several significant relationships between endpoint histology and electrophysiology metrics at the 28 day time point across all animals (Table 5.1, $p \leq 0.05$, Spearman's rank coefficient test). When interpreting the results, it is important to note that Spearman's test assigns ranks for each data value, and assesses correlations between the ranks, so the variability of the original data is not necessarily reflected. Neuronal and non-neuronal cell densities within 50 microns of the tract surface (the region known to yield reliably sorted units (Henze, Borhegyi et al. 2000)), as well as the ratio between the two, were tested for correlations with SNR, signal, noise, units, LFP amplitude and impedance at 10 Hz and 1 kHz. Increasing 1 kHz impedance was positively correlated with NND and 10 Hz impedance (not shown), and negatively correlated with recording

quality (SNR and Units) and ND/NND. NND was negatively correlated with SNR, signal amplitude (not shown), and units. Thus, increased NND near the probe tract (which likely indicates astrocyte density, Figure 5.5) was related to increased impedance and reduced recording quality. Increased ND/NND correlated positively with improved SNR. Several correlations trended ($p<0.1$) toward significance (not shown), notably: a negative correlation between ND and NND, a positive correlation between impedance and noise, a negative correlation between ND and 1 kHz impedance, and a positive correlation between units and ND/NND. The results corroborate the theory that glial encapsulation decreases recording quality and increases impedance, which has not been quantitatively shown previously.

	1 kHz	**SNR**	**Units**	**NND**	**ND/NND**
1 kHz	1.0	-0.821*	-0.821*	0.829*	-0.829*
SNR	-0.821*	1.0	0.994**	-1.00**	0.829*
Units	-0.821*	0.994**	1.0	-0.986**	0.783
NND	0.829*	-1.00**	-0.986**	1.0	-0.857*
ND/NND	-0.829*	0.829*	0.783	-0.857*	1.0

Table 5.1. Correlation coefficients between histology and electrophysiology measurements at the 28 day time point reveal several significant relationships between these metrics. "NND" is the density of non-neuronal cells within 50 microns of the probe tract boundary. "ND/NND" is the ratio of neuronal to non-neuronal densities within the same region. * = significant at the 0.05 level, ** = significant at the 0.01 level.

Correlations between impedance and recording metrics across all days in the study period also indicated a significant inverse relationship between impedance and recording

quality. Here, the data set was much larger, and could be analyzed on a site-by-site basis while controlling for correlated observations within the same rat using a linear mixed effects model. The analysis demonstrated a significant, but small, inverse relationship between SNR and 1 kHz impedance (-0.24 correlation coefficient, $p<0.001$). A similar effect between units and 1 kHz impedance was observed (-0.26 correlation coefficient, $p<0.001$). There was a stronger, positive relationship between impedance and noise (0.51 correlation coefficient, $p<0.001$).

Discussion

Following implantation into the brain, neural prostheses incite characteristic changes in the surrounding tissue which are hypothesized to reduce recording quality over time. Neuronal density is dramatically reduced surrounding the probe immediately following insertion trauma; this improves over subsequent weeks, but remains at approximately 60% of control levels four weeks later (Biran, Martin et al. 2005; Purcell, Seymour et al. 2008). One day after insertion, the probe is surrounded by activated microglia, which form a thin sheath encapsulating the device during the following week (Szarowski, Andersen et al. 2003; Purcell, Seymour et al. 2008). Astrocytes are maximally activated one week after device implantation, and form a compact sheath approximately three weeks later (Szarowski, Andersen et al. 2003; Biran, Martin et al. 2005). A prevailing hypothesis in the neural engineering field is that these phenomena result in recording instability over time. In fact, numerous intervention strategies, including the use of protein-based coatings (Buchko, Kozloff et al. 2001; Cui, Lee et al. 2001; Cui, Wiler et al. 2003; He and Bellamkonda 2005; He, McConnell et al. 2006) , anti-inflammatory

drugs (Shain, Spataro et al. 2003; Spataro, Dilgen et al. 2005; Kim and Martin 2006; Zhong and Bellamkonda 2007), and hydrogels (Kim, Abidian et al. 2004), have been pursued to mitigate tissue response, and theoretically, improve chronic recording quality. However, the mechanisms underlying the tissue response are still largely unknown, and a direct relationship between *in vivo* recording quality and tissue response metrics has not been defined.

Several studies have demonstrated the role of cell cycle re-entry in gliosis and neuronal death following CNS injury (Verdaguer, Jimenez et al. 2004; Cernak, Stoica et al. 2005; Di Giovanni, Movsesyan et al. 2005; Appert-Collin, Hugel et al. 2006; Alvira, Tajes et al. 2007; Byrnes, Stoica et al. 2007). Di Giovanni *et al.* demonstrated more than 80% of activated microglia and astrocytes, as well as over 10% of neurons, expressed cyclin D1 (CD-1) around the site of traumatic brain injury in rats, indicating re-entry into the cell cycle (Di Giovanni, Movsesyan et al. 2005). A single ICV injection of flavopiridol following injury reduced CD-1 expression in all cells by over 50% and reduced glial proliferation three days after injury. After 28 days, flavopiridol-treated rats had reduced lesion volume and reactive gliosis, as well as improved functional recovery compared to control animals.

We hypothesized that the upregulation of cell cycle proteins may be associated with the tissue response to probes, and that inhibiting cell cycle re-entry with flavopiridol may reduce surrounding glial activation, and, to a lesser extent, neuronal loss. We administered the drug as a single ICV injection, which is easily implemented in research

settings. Our results demonstrate a reduction in microglial activation surrounding probes three days after implantation, with lesser evidence of an effect on astrocyte activation. Additionally, a significant reduction in impedance occurred over the time course of the study, and the two results are likely related. Increased 1 kHz impedance at recording sites associated with GFAP reactivity was demonstrated beginning four days after implantation (Williams, Hippensteel et al. 2007). In the current study, the decreased impedance is more likely due to decreased microglial encapsulation, based on evidence that activation of these cells appears most strongly inhibited by the drug. This sheath likely remains attached to the probe during explantation, which has been shown previously (Biran, Martin et al. 2005). Non-neuronal densities likely reflect astrocyte counts at some distance from the actual probe surface. These values were averaged along the probe tract, tended to be highly variable, and were not significantly affected by drug treatment. Neuronal density, and the ratio between neuronal and non-neuronal density, tended to be higher for drug treated animals four weeks after implantation, but again, the data was too variable to demonstrate significance. The data variability and loss of an intact device-tissue interface illustrate the need for *in situ* probe histology, which leaves the interface intact and allows site-by-site analysis, but requires advanced methods such as multi-photon microscopy for quantitative analysis (Bragin, Hetke et al. 2000; Holecko, Williams et al. 2005; Seymour, Purcell et al. 2008).

A significant, but small, correlation between recording quality (SNR, Units) and 1 kHz impedance was demonstrated over the course of the study, but the relationship was not large enough for the impedance reduction by flavopiridol to result in improved recording

quality over time. Endpoint data for these metrics at 28 days further reinforced the existence of a relationship between these quantities. Suner *et al.* showed an overall lack of correlation between SNR and impedance in a study of two monkeys over a 1.5 year time course. However, in one of the subjects, a significant, but small, correlation between the metrics was shown (r=0.2) (Suner, Fellows et al. 2005). Signal quality was correlated with impedance for both monkeys (r=0.18). The authors suggest a "loose" association between recording quality and impedance. Theoretically, decreased impedance should improve recording quality through a reduction of noise and signal loss through shunt pathways (Shoham and Nagarajan 2003; Ludwig, Uram et al. 2005). Thermal noise is directly proportional to the square root of impedance, but the background activity of distant neurons is a noise source of typically equal importance *in vivo* (Shoham and Nagarajan 2003). This biological noise may, therefore, offset improvements in recording quality derived from reductions in thermal noise. Because the correlation between impedance and recording quality is weak, a large reduction in impedance may be required to result in improved recordings.

There were several significant correlations between 28 day end-point histology and recording metrics at that time point which reinforce prevailing hypotheses in neural engineering, but have not previously been demonstrated quantitatively in the literature. Non-neuronal density within the first 50 microns of the probe tract was positively correlated with impedance, and negatively correlated with SNR, signal amplitude (not shown), and units. Again, NND appears to be predominated by astroglial cells in the current study. Astrogliosis is known to be a diffusion barrier to ionic transmission through nervous tissue, which may result in increased impedance and a loss of signal

through shunt pathways (Roitbak and Sykova 1999). A relationship between increased impedance and GFAP-positive astrocytes has been shown previously (Williams, Hippensteel et al. 2007). Increased NND may also reduce the ability of units to be identified using common sorting methods, resulting in additional biological noise. Increased ND/NND correlated positively with improved SNR and negatively with impedance, and it is intuitive that increasing the signal source (neurons) in proportion to the signal barrier (glia) would have these effects.

Neuronal density trended toward an inverse relationship with non-neuronal density and impedance, although these results were not statistically significant ($p<0.1$). Notably, increased neuronal density alone was not sufficient to improve recording quality; the increase must be normalized for increases in non-neuronal density to have an effect. The trend towards decreased impedance by increased neuronal density may be related simply to the tendency for ND to be inversely related to NND. However, the possibility exists that there is a direct effect of ND on reducing electrode impedance. Anecdotal evidence suggests that plating electrodes with neural cells *in vitro* decreases impedance, while fibroblasts and epithelial cells have the opposite effect (Sarah Richardson-Burns, personal communication). Perhaps neural cells have unique effects on impedance due to their ionically conductive membranes and reduced surface contact with the electrode; these potential mechanisms warrant further investigation (Sarah Richardson-Burns, personal communication). In general, the correlation results indicate that glial encapsulation decreases recording quality and increases impedance, while increased neuronal density/non-neuronal density has the opposite effect.

Flavopiridol likely reduces glial (and particularly, microglial) encapsulation of the device, which resulted in reduced impedance across the study time course. This was not demonstrated by the non-neuronal counts, as the interface was damaged upon explantation. This illustrates the need for *in situ* probe histology, which will leave the interface intact and allow site-by-site analysis, but requires advanced methods (i.e. multiphoton imaging, see Conclusions and Future Directions). A significant, but small, correlation between SNR/Units and 1 kHz impedance was demonstrated over the course of the study, but the relationship was not large enough for the impedance reduction by flavopiridol to result in improved recording quality over time. This indicates that an intervention strategy which combines a glial activation inhibitor such as flavopiridol with a method aimed at protecting neurons, or improving their function/communication with the device, may be the optimal approach for improving recording quality over time. Additionally, prolonged administration of flavopiridol may further improve results. The lack of correlation between neuronal density and recording metrics at the 28 day time point may indicate the importance of the neuronal function (not just density) surrounding the probe (see Conclusions and Future Directions). Finally, endpoint histology and electrophysiology metrics significantly correlated at the 28 day time point, reinforcing the need for improvements in the device-tissue interface to enable long-term recording quality.

Acknowledgements

Many thanks to Kip Ludwig for the use of his recording analysis programs and numerous helpful discussions. Rachel Miriani and Mike Joseph were very helpful with impedance

analysis and training with collecting impedance and recording data. Soumya Yandamuri performed blinded cell counts. Dave Thompson, who is a co-author on this work, assisted with surgeries, data collection, and MatLAB coding. Emily Jutkiewicz provided ICV injection training, which was greatly appreciated. Finally, Kathy Welch from CSCAR consulted on all statistical methods.

References

Alvira, D., M. Tajes, et al. (2007). "Inhibition of cyclin-dependent kinases is neuroprotective in 1-methyl-4-phenylpyridinium-induced apoptosis in neurons." Neuroscience **146**(1): 350-65.

Appert-Collin, A., B. Hugel, et al. (2006). "Cyclin dependent kinase inhibitors prevent apoptosis of postmitotic mouse motoneurons." Life Sci **79**(5): 484-90.

Biran, R., D. C. Martin, et al. (2005). "Neuronal cell loss accompanies the brain tissue response to chronically implanted silicon microelectrode arrays." Exp Neurol **195**(1): 115-26.

Bjornsson, C. S., S. J. Oh, et al. (2006). "Effects of insertion conditions on tissue strain and vascular damage during neuroprosthetic device insertion." J Neural Eng **3**(3): 196-207.

Bragin, A., J. Hetke, et al. (2000). "Multiple site silicon-based probes for chronic recordings in freely moving rats: implantation, recording and histological verification." J Neurosci Methods **98**(1): 77-82.

Buchko, C. J., K. M. Kozloff, et al. (2001). "Surface characterization of porous, biocompatible protein polymer thin films." Biomaterials **22**(11): 1289-300.

Byrnes, K. R., B. A. Stoica, et al. (2007). "Cell cycle activation contributes to post-mitotic cell death and secondary damage after spinal cord injury." Brain **130**(Pt 11): 2977-92.

Carmena, J. M., M. A. Lebedev, et al. (2003). "Learning to control a brain-machine interface for reaching and grasping by primates." PLoS Biol **1**(2): E42.

Cernak, I., B. Stoica, et al. (2005). "Role of the cell cycle in the pathobiology of central nervous system trauma." Cell Cycle **4**(9): 1286-93.

Cui, X., V. A. Lee, et al. (2001). "Surface modification of neural recording electrodes with conducting polymer/biomolecule blends." J Biomed Mater Res **56**(2): 261-72.

Cui, X., J. Wiler, et al. (2003). "In vivo studies of polypyrrole/peptide coated neural probes." Biomaterials **24**(5): 777-87.

Di Giovanni, S., V. Movsesyan, et al. (2005). "Cell cycle inhibition provides neuroprotection and reduces glial proliferation and scar formation after traumatic brain injury." Proc Natl Acad Sci U S A **102**(23): 8333-8.

Donoghue, J. P., A. Nurmikko, et al. (2007). "Assistive technology and robotic control using motor cortex ensemble-based neural interface systems in humans with tetraplegia." J Physiol **579**(Pt 3): 603-11.

Drake, K. L., K. D. Wise, et al. (1988). "Performance of Planar Multisite Microprobes in Recording Extracellular Single-Unit Intracortical Activity." Ieee Transactions on Biomedical Engineering **35**(9): 719-732.

Edell, D. J., V. V. Toi, et al. (1992). "Factors influencing the biocompatibility of insertable silicon microshafts in cerebral cortex." IEEE Trans Biomed Eng **39**(6): 635-43.

Fitzsimmons, N. A., W. Drake, et al. (2007). "Primate reaching cued by multichannel spatiotemporal cortical microstimulation." J Neurosci **27**(21): 5593-602.

He, W. and R. V. Bellamkonda (2005). "Nanoscale neuro-integrative coatings for neural implants." Biomaterials **26**(16): 2983-90.

He, W., G. C. McConnell, et al. (2006). "Nanoscale laminin coating modulates cortical scarring response around implanted silicon microelectrode arrays." J Neural Eng **3**(4): 316-26.

Henze, D. A., Z. Borhegyi, et al. (2000). "Intracellular features predicted by extracellular recordings in the hippocampus in vivo." J Neurophysiol **84**(1): 390-400.

Hochberg, L. R., M. D. Serruya, et al. (2006). "Neuronal ensemble control of prosthetic devices by a human with tetraplegia." Nature **442**(7099): 164-71.

Holecko, M. M., 2nd, J. C. Williams, et al. (2005). "Visualization of the intact interface between neural tissue and implanted microelectrode arrays." J Neural Eng **2**(4): 97-102.

Kim, D. H., M. Abidian, et al. (2004). "Conducting polymers grown in hydrogel scaffolds coated on neural prosthetic devices." J Biomed Mater Res A **71**(4): 577-85.

Kim, D. H. and D. C. Martin (2006). "Sustained release of dexamethasone from hydrophilic matrices using PLGA nanoparticles for neural drug delivery." Biomaterials **27**(15): 3031-7.

Kim, Y. T., R. W. Hitchcock, et al. (2004). "Chronic response of adult rat brain tissue to implants anchored to the skull." Biomaterials **25**(12): 2229-37.

Lebedev, M. A. and M. A. Nicolelis (2006). "Brain-machine interfaces: past, present and future." Trends Neurosci **29**(9): 536-46.

Liu, X., D. B. McCreery, et al. (2006). "Evaluation of the stability of intracortical microelectrode arrays." IEEE Trans Neural Syst Rehabil Eng **14**(1): 91-100.

Liu, X., D. B. McCreery, et al. (1999). "Stability of the interface between neural tissue and chronically implanted intracortical microelectrodes." IEEE Trans Rehabil Eng **7**(3): 315-26.

Ludwig, K. A., R. Miriani, et al. (2008). "Employing a Common Average Reference to Improve Cortical Neuron Recordings from Microelectrode Arrays."

Ludwig, K. A., J. D. Uram, et al. (2006). "Chronic neural recordings using silicon microelectrode arrays electrochemically deposited with a poly(3,4-ethylenedioxythiophene) (PEDOT) film." Journal of Neural Engineering **3**: 59.

Ludwig, K. A., J. D. Uram, et al. (2006). "Chronic neural recordings using silicon microelectrode arrays electrochemically deposited with a poly(3,4-ethylenedioxythiophene) (PEDOT) film." Journal of Neural Engineering **3**(1): 59-70.

Nicolelis, M. A., D. Dimitrov, et al. (2003). "Chronic, multisite, multielectrode recordings in macaque monkeys." Proc Natl Acad Sci U S A **100**(19): 11041-6.

Polikov, V. S., P. A. Tresco, et al. (2005). "Response of brain tissue to chronically implanted neural electrodes." J Neurosci Methods **148**(1): 1-18.

Purcell, E. K., J. P. Seymour, et al. (2008). "Neural Stem Cell-Seeding Mitigates the Early Tissue Response to Chronic Neural Probes." Exp Neurol.

Roitbak, T. and E. Sykova (1999). "Diffusion barriers evoked in the rat cortex by reactive astrogliosis." Glia **28**(1): 40-8.

Rousche, P. J. and R. A. Normann (1998). "Chronic recording capability of the Utah Intracortical Electrode Array in cat sensory cortex." J Neurosci Methods **82**(1): 1-15.

Schafer, K. A. (1998). "The cell cycle: a review." Vet Pathol **35**(6): 461-78.

Schwartz, A. B., X. T. Cui, et al. (2006). "Brain-controlled interfaces: movement restoration with neural prosthetics." Neuron **52**(1): 205-20.

Seymour, J. P. and D. R. Kipke (2007). "Neural probe design for reduced tissue encapsulation in CNS." Biomaterials **28**(25): 3594-607.

Seymour, J. P., E. K. Purcell, et al. (2008). A Method for In Situ Evaluation of Silicon Microelectrode Arrays. Neural Interfaces Conference, Cleveland, OH.

Shain, W., L. Spataro, et al. (2003). "Controlling cellular reactive responses around neural prosthetic devices using peripheral and local intervention strategies." IEEE Trans Neural Syst Rehabil Eng **11**(2): 186-8.

Shoham, S. and S. Nagarajan (2003). The theory of central nervous system recording Neuroprosthetics: Theory and Practice. K. H. a. G. S. Dhillon, Singapore: World Scientific**:** pp 448–65.

Spataro, L., J. Dilgen, et al. (2005). "Dexamethasone treatment reduces astroglia responses to inserted neuroprosthetic devices in rat neocortex." Exp Neurol **194**(2): 289-300.

Suner, S., M. R. Fellows, et al. (2005). "Reliability of signals from a chronically implanted, silicon-based electrode array in non-human primate primary motor cortex." IEEE Trans Neural Syst Rehabil Eng **13**(4): 524-41.

Swanton, C. (2004). "Cell-cycle targeted therapies." Lancet Oncol **5**(1): 27-36.

Szarowski, D. H., M. D. Andersen, et al. (2003). "Brain responses to micro-machined silicon devices." Brain Res **983**(1-2): 23-35.

Taylor, D. M., S. I. Tillery, et al. (2002). "Direct cortical control of 3D neuroprosthetic devices." Science **296**(5574): 1829-32.

Turner, J. N., W. Shain, et al. (1999). "Cerebral astrocyte response to micromachined silicon implants." Exp Neurol **156**(1): 33-49.

Velliste, M., S. Perel, et al. (2008). "Cortical control of a prosthetic arm for self-feeding." Nature.

Verdaguer, E., A. Jimenez, et al. (2004). "Inhibition of cell cycle pathway by flavopiridol promotes survival of cerebellar granule cells after an excitotoxic treatment." J Pharmacol Exp Ther **308**(2): 609-16.

Williams, J. C., J. A. Hippensteel, et al. (2007). "Complex impedance spectroscopy for monitoring tissue responses to inserted neural implants." J Neural Eng **4**(4): 410-23.

Williams, J. C., R. L. Rennaker, et al. (1999). "Long-term neural recording characteristics of wire microelectrode arrays implanted in cerebral cortex." Brain Res Brain Res Protoc **4**(3): 303-13.

Zhong, Y. and R. V. Bellamkonda (2007). "Dexamethasone-coated neural probes elicit attenuated inflammatory response and neuronal loss compared to uncoated neural probes." Brain Res **1148**: 15-27.

CHAPTER 6
CONCLUSIONS AND FUTURE DIRECTIONS

Conclusions

This dissertation describes the *in vitro* and *in vivo* evaluations of cell- and drug-based interventions on the chronic tissue response to implanted neural probes. These studies used a wide variety of techniques in several fields of study, principally: tissue engineering, material science, neuroscience, and neural engineering. The data demonstrate significant effects of the intervention strategies on tissue response and electrophysiology measurements, characterize alginate stability and its use as a neural stem cell scaffold, and add insight into the relationship between the tissue-device interface and recording quality.

Chapter 2 described the evaluation of the effects of alginate composition on the neurotrophic factor release, viability, and proliferation of encapsulated NSCs, as well as on the mechanical stability of the scaffold itself. The results demonstrated that a high G, non-PLL coated alginate composition yielded superior support of neurotrophic factor release from encapsulated NSCs as well as resistance to an osmotic challenge. This scaffold was shown to be potentially useful in the repair of damaged CNS tissue, as evidenced by the neuroprotective effects of medium conditioned by NSC-seeded alginate beads on the serum-withdrawal mediated death of PC-12 cells.

While Chapter 2 reported *in vitro* mechanical stability results, it was of interest to study the *in vivo* degradation behavior of alginate and its relationship to PLL coating. Chapter 3 reported a study in which uncoated and PLL-coated high G alginate disks were washed identically in saline, implanted subcutaneously in rats, and monitored over a three month time period for mechanical stability, weight changes related to swelling behavior, and biocompatibility. All alginate samples experienced an 80% decrease in their complex moduli after 24 hours *in vivo*, followed by stabilization of this metric, progressive fragmentation, cellular infiltration and collagen encapsulation. PLL-coating resulted in a slight but significant increase in the complex modulus seven days after implantation in comparison to non-coated gels; no other significant differences in stability between the two conditions were noted. No differences in biocompatibility were seen. PLL and non-coated gels initially dropped in weight following implantation, followed by similar trends in increasing weight (interpreted as swelling) for a period of two weeks; weight increases were greater for uncoated than coated samples. The data demonstrate little evidence for PLL enhancement of mechanical stability *in vivo*. Combined with the detrimental effect of PLL on neurotrophic factor detection from encapsulated cells and resistance to an osmotic challenge reported in the second chapter, a non-PLL coated scaffold was pursued for probe modification.

Chapter 4 contains the results of an *in vivo* histological assessment of probes scaffolded with neural stem cell-seeded alginate in a hollow well. This study reports a detailed, quantitative histological evaluation of a novel biohybrid device, and is the first such investigation of neural stem cell-seeding as a means to improve integration of a synthetic

neural prosthesis with surrounding brain tissue. Additionally, the study assesses the degree of injury as a function of scaffold condition and distance from the probe surface over the course of four time points spanning three months, making it the most comprehensive quantitative data set evaluating tissue response to neural prostheses reported in the field of neural engineering to date. The data are particularly compelling as they derive from analysis of intact tissue-probe surfaces instead of tissue where the interface has been disrupted by probe removal. Neural stem cell seeding was shown to increase neuronal density surrounding the probe during the first week of implantation, along with reductions in non-neuronal density. At later time points, these effects were reversed and cell-seeding exacerbated the tissue response metrics. The results indicate that NSC-seeding may improve the early injury response through a bystander mechanism, and future studies may extend the effects to a chronic setting by improving alginate stability and graft cell viability.

Chapter 5 describes the effects of a cell cycle inhibiting drug (flavopiridol) on the impedance, recording quality, and tissue response associated with neural prostheses. The drug was administered as a single injection at the time of probe implantation, which could be easily implemented in a research setting, and could be translated into clinical studies. The drug reduced impedance, likely due to a reduction in microglial encapsulation of the device. Although recording quality and impedance were significantly inversely correlated, this effect was not large enough for the impedance reduction by flavopiridol to result in a significant improvement in SNR or the number of units detected. Additionally, endpoint quantitative histology was too variable to

demonstrate an effect of the drug, and this result highlighted the importance of *in situ* probe histology. Finally, endpoint non-neuronal density correlated positively with impedance and negatively with SNR and units, providing the first *in vivo* quantitative evidence supporting the hypothesis that recording quality and tissue response are related. Interestingly, neuronal density did not significantly correlate with recording quality unless normalized to non-neuronal density, which may indicate the importance of neuronal function and the glial barrier to signal transmission.

Future Directions and Preliminary Results

Establishing the Relationship Between Recording Quality and Tissue Response

Despite numerous reports of instability in recordings over time, histological changes associated with the tissue response to neural prostheses, and a body of probe modification literature based on the working hypothesis that the two phenomena are related (see Chapter 1 for references and discussion), the relationship between electrophysiology, impedance, and histology metrics has not been explicitly defined. Williams *et al.* reported increased impedance at 1 kHz at recording sites experiencing gliosis (Williams, Hippensteel et al. 2007). The authors also reported a shift to a more non-linear relationship between real and imaginary impedance components over time, indicating a capacitive contribution of increasing cellular density (Figure 6.1). A similar trend was noted between sites having minimal (linear relationship) and extensive (non-linear relationship) glial reactivity. Suner *et al.* reported a small correlation between signal and impedance, but no overall correlation between SNR and impedance (Suner, Fellows et al. 2005). The results reported in Chapter 5, which show significant correlations between

endpoint non-neuronal density, neuronal density normalized for non-neuronal density, impedance, SNR, and the number of units detected, are an important step in defining the relationship between electrophysiology and the tissue response to neural prostheses. However, refinement and further investigation into these results is required, particularly because explantation of probes prior to histology disrupts the tissue-device interface, resulting in the loss of important data.

(a) Immediately Post-Implant **(b) 7 Days Post-Implant**

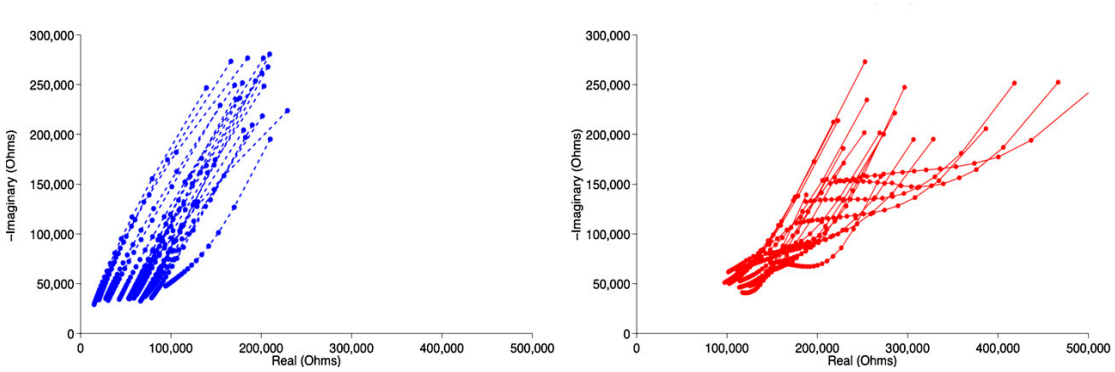

Figure 6.1. Nyquist plots for 20 electrodes immediately after implantation (a) and after 7 days (b), illustrating an increasingly non-linear relationship between real and imaginary components over time (Williams, Hippensteel et al. 2007).

A deeper understanding of the cause-and-effect relationship between recording quality and the tissue response to devices will require improved quantitative histology techniques. Silicon devices are prone to shatter and tear tissue when left *in situ* during conventional sectioning, and are therefore explanted prior to this step. This process damages the probe-tissue interface, resulting in the loss of valuable data in what is potentially the most interesting region to analyze. Additionally, it is extremely difficult, if not impossible, to accurately assess where the electrode sites were located when evaluating samples prepared in this way. The result is a gross, and likely inaccurate,

understanding of the tissue-device interface. Electrode site-specific data is far more desirable; it would allow the investigator to assess the relationship between recordings and tissue response metrics on a site-by-site basis, thus increasing sample size and accuracy.

Recent work in our laboratory has used a combination of cryo-sectioning parallel to the face of the probe, immunohistochemistry of the resulting thick (100-200 microns) sections containing the intact probe, and multiphoton microscopy to enable quantitative site-by-site analysis of cellular density. Previous studies have reported similar sectioning techniques (Bragin, Hetke et al. 2000; Holecko, Williams et al. 2005). Holecko *et al.* further demonstrated the feasibility of GFAP immunohistochemistry on their samples using confocal microscopy for visualization. No attempt at quantitative evaluation of the tissue was made in either of these studies. Our work has demonstrated the ability to count individual cellular nuclei deep into tissue sections on an electrode site-by-site basis (Figure 6.2, preliminary counting data not shown) (Seymour, Purcell et al. 2008). Multiphoton imaging results in improved resolution at greater depths in the section and reduces photobleaching in comparison to confocal imaging. However, there are limitations to this technique as well: algorithms may be required to resolve fluorescence signals when multiple stains are used, access to multiphoton microscopy is limited and expensive, and *in situ* sectioning and staining carries significant risks associated with having a single sample to process as opposed to numerous cross-sections. Further improvements to our methods, as well as exploring new techniques (such as cross-sectioning the probe *in situ* with a diamond knife, immunogold labeling and imaging with

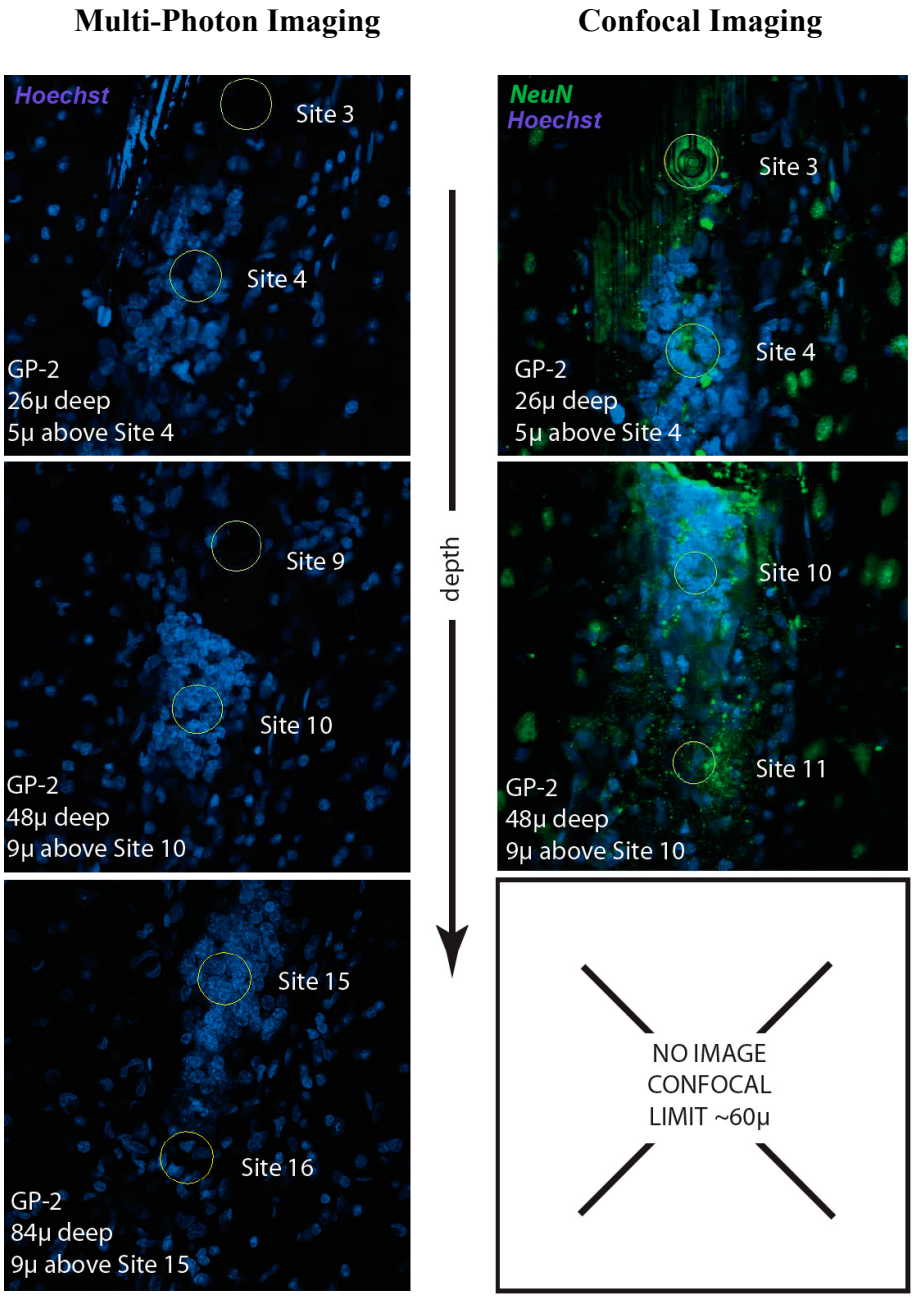

Figure 6.2. Comparison of multi-photon and confocal images of the same electrode sites implanted in guinea pig tissue. Multi-photon imaging provides higher resolution at deeper focal planes (left panels), enabling cell counting near electrode sites not accessible with confocal imaging (right panels). Neuronal and all cellular nuclei are counterstained with NeuN (green) and Hoechst (blue) respectively, and electrode sites are demarcated and labeled (Seymour, Purcell et al. 2008). Also, note the site-by-site variability in cellular densities.

transmission electron microscopy) may enable a comprehensive recording/histology study in the future. Alternatively, this may be possible by using functional polymer probes which may be left in place during conventional sectioning. The development of these devices is on-going. Importantly, a combined histology/recording study may identify the specific mechanisms which most severely impact recording stability and quality. This, in turn, will result in more defined targets for probe modification and tissue response intervention strategies to improve recording stability.

Neuronal Dysfunction and Plasticity after Probe Implantation

Typically, neuronal density surrounding the probe is quantified as a measure of tissue response to the device, and the same is true in the studies reported in Chapters 4 and 5 (Edell, Toi et al. 1992; Biran, Martin et al. 2005; Seymour and Kipke 2007). The implicit assumption is that having more neurons nearer recording sites will result in improved signal. However, this is not necessarily the case. Anecdotal evidence from our lab suggests that neuronal soma may be located in close proximity to recording sites which do not detect units. The lack of correlation between neuronal density and recording quality reported in Chapter 5 may indicate the importance of neuronal function. Additionally, Henze *et al.* have reported detecting approximately six units per tetrode, despite estimations that 60-100 neurons of the 1,000 within a recordable distance from device should have sufficient amplitude to be discernible above noise (Henze, Borhegyi et al. 2000). The authors hypothesize that the majority of the cells may be silent during the recording period, or at least have an insufficient firing rate to be identified by clustering methods. This raises interesting questions: are the majority of cells near the probe functionally silent? If so, is this an unavoidable characteristic of the brain tissue

itself, or in part due to the injury response to the probe? If the latter is true, are there ways to "wake up" these cells?

In recent years, several studies have explored the mechanisms underlying silent synapses. Christopherson *et al.* reported thrombospondin (TSP, an angiostatic extracellular matrix molecule) expression by immature astrocytes promoted synaptogenesis in development. The synapses were ultrastructurally normal but silent during patch clamp recording (Christopherson, Ullian et al. 2005). The authors suggest that while TSP levels are low in the adult brain, their expression in reactive astrocytes may "explain the tendency of axotomized axons to…fail to regenerate when they contact reactive astrocytes," and further state that "drugs that agonize or antagonize TSPs may help promote synaptic plasticity and repair in many CNS diseases." Alterations in AMPA and NMDA receptor expression offer an additional possible explanation for silent synapses (Isaac 2003). During early postnatal development, silent synapses have NMDA, but not AMPA, glutamate receptors; the latter are progressively acquired (Petralia, Esteban et al. 1999; Isaac 2003; Voigt, Opitz et al. 2005). These synapses are functionally silent, although spontaneous synchronous network activity may convert silent synapses to active synapses by the incorporation of AMPA receptors (Voigt, Opitz et al. 2005). Reductions in AMPA receptors have been demonstrated in the vicinity of spinal cord injury sites as early as twenty-four hours after trauma in rats (Grossman, Wolfe et al. 1999). If a similar change in receptor profile or TSP expression were to occur respectively in neurons and astrocytes located near recording electrodes during injury remodeling, strategies to improve recording quality via receptor or TSP agonists/antagonists could be feasible.

The broader issue of neuronal function/dysfunction surrounding probes has not been addressed, and several areas of research may shed light on this issue. The central question to be answered is whether or not the neurons located within a recordable distance from electrodes are functionally normal or not. Neuronal dysfunction was evident on the border of small (~ 1mm diameter), focal lesions in the cat visual cortex in the days immediately following injury (Eysel and Schmidt-Kastner 1991). Cells within the first 0.5 mm of the lesion displayed a depression in extracellular potentials. Increased activity above control values was noted 1 mm away from the lesion border; this metric normalized with further distance from the injury site and may have been due to inhibitory interneuron damage. Studying silent synapse formation around neural prostheses may also shed light on the neuronal dysfunction issue. Additionally, what role does plasticity play in recording quality over time? Brain injury has been shown to induce extensive rewiring of cortical connections, and whether this occurs following device implantation should also be researched (Dancause, Barbay et al. 2005). Finally, what is the mechanism behind neuronal density reduction around probes: are they merely physically displaced, or is cellular death the cause? The data reported in Chapter 4 indicates the latter. If neurons around these devices are dying, what is the mechanism (excitotoxicity, apoptosis, necrosis, etc.) and time course of these events? Knowing the answers to these questions may result in new intervention strategies.

Chronic Recordings with Functionalized Neural Stem Cell-Seeded Probes

The development of a neural stem cell-seeded functional recording device will open the door for numerous future studies investigating the effects of these cells and their released

factors on surrounding neuronal activity. Neurotrophins (specifically, NGF and BDNF) have been shown to enhance or depress neural activity in studies with varying methods and cell populations (Prakash, Cohen-Cory et al. 1996; Zhang, Chi et al. 2008). The neural stem cells may secrete these and other factors *in vivo* which could potentially impact cell viability, plasticity, and electrophysiology metrics, and this device may enable studies to investigate the relationships between these effects. These studies may also add insight into the mechanisms responsible for the *in vivo* results reported in Chapter 4. This research will be enhanced further by the ability to conduct histology with the interface between the parylene probe, graft cells, and surrounding tissue intact. Improved *in vivo* detection of graft cells will strengthen results (see Appendix A). Fabrication of functional "open-channel" devices for cell-seeding was underway at the time of preparation of this dissertation.

Concluding Remarks

Neural prostheses have the potential to restore function to hundreds of thousands of patients who are immobilized by paralysis or neurodegenerative disease. Additionally, these devices may have tremendous impact in neurophysiology research settings. However, stable, long-term recordings must be achieved in these applications. Understanding the reactive tissue response to these devices, and developing effective intervention strategies to improve upon it, may result in enhanced recording quality. In this dissertation, two approaches to improving the tissue integration of synthetic probes were explored: a biohybrid device with further research implications, and a drug-based approach which could be easily applied in a research or clinical setting. Each study

resulted in a measurable improvement of the reactive tissue response and/or impedance associated with neural prostheses, and increased the current understanding of the device-tissue interface. Studying neural stem cell-seeded alginate additionally resulted in stability and scaffolding data which have impacts outside of the field of neural engineering.

Numerous future studies are planned to expand upon these results further. Specifically, it is of primary interest to characterize changes in neuronal function over time following device implantation. If the amplitude and/or firing rate of neurons around devices is reduced due to injury remodeling, then methods of reducing tissue encapsulation and device impedance will be inadequate to improve recording stability. This was illustrated in Chapter 5 data, which showed a drug-induced reduction in microglial activation and impedance, but no improvement in recording quality. Further, the stabilization of neuronal density surrounding devices reported in Chapter 4, and the lack of correlation between neuronal density and recording quality reported in Chapter 5, support this contention. When changes in neuronal function and their associated mechanisms are adequately characterized, then future studies will be conducted to intervene in this response, with the correct factors supplied via cell seeding, scaffolds, or direct drug administration. Combining these strategies with impedance- or glial activation-reducing methods may ultimately be the optimal approach. These research studies, which characterize the electrophysiology, cellular function, and tissue response to a source of brain injury, have the potential to impact not only the field of neural engineering, but also the understanding of, and development of therapies for, central nervous system damage.

Acknowledgements

John Seymour is fabricating the functional open-channel probes, and led the *in situ* probe histology study. Thanks to Debbie Colesa and the Pfingst lab for collaborating on the *in situ* histology project. Chris Bjornsson conducted the multiphoton imaging shown in figure 6.2 at Rensselaer Polytechnic Institute. Soumya Yandamuri is currently conducting preliminary staining for investigating silent synapses around neural probes.

References

Biran, R., D. C. Martin, et al. (2005). "Neuronal cell loss accompanies the brain tissue response to chronically implanted silicon microelectrode arrays." Exp Neurol **195**(1): 115-26.

Bragin, A., J. Hetke, et al. (2000). "Multiple site silicon-based probes for chronic recordings in freely moving rats: implantation, recording and histological verification." J Neurosci Methods **98**(1): 77-82.

Christopherson, K. S., E. M. Ullian, et al. (2005). "Thrombospondins are astrocyte-secreted proteins that promote CNS synaptogenesis." Cell **120**(3): 421-33.

Dancause, N., S. Barbay, et al. (2005). "Extensive cortical rewiring after brain injury." J Neurosci **25**(44): 10167-79.

Edell, D. J., V. V. Toi, et al. (1992). "Factors influencing the biocompatibility of insertable silicon microshafts in cerebral cortex." IEEE Trans Biomed Eng **39**(6): 635-43.

Eysel, U. T. and R. Schmidt-Kastner (1991). "Neuronal dysfunction at the border of focal lesions in cat visual cortex." Neurosci Lett **131**(1): 45-8.

Grossman, S. D., B. B. Wolfe, et al. (1999). "Alterations in AMPA receptor subunit expression after experimental spinal cord contusion injury." J Neurosci **19**(14): 5711-20.

Henze, D. A., Z. Borhegyi, et al. (2000). "Intracellular features predicted by extracellular recordings in the hippocampus in vivo." J Neurophysiol **84**(1): 390-400.

Holecko, M. M., 2nd, J. C. Williams, et al. (2005). "Visualization of the intact interface between neural tissue and implanted microelectrode arrays." J Neural Eng **2**(4): 97-102.

Isaac, J. T. (2003). "Postsynaptic silent synapses: evidence and mechanisms." Neuropharmacology **45**(4): 450-60.

Petralia, R. S., J. A. Esteban, et al. (1999). "Selective acquisition of AMPA receptors over postnatal development suggests a molecular basis for silent synapses." Nat Neurosci **2**(1): 31-6.

Prakash, N., S. Cohen-Cory, et al. (1996). "RAPID and opposite effects of BDNF and NGF on the functional organization of the adult cortex in vivo." Nature **381**(6584): 702-6.

Seymour, J. P. and D. R. Kipke (2007). "Neural probe design for reduced tissue encapsulation in CNS." Biomaterials **28**(25): 3594-607.

Seymour, J. P., E. K. Purcell, et al. (2008). A Method for In Situ Evaluation of Silicon Microelectrode Arrays. Neural Interfaces Conference, Cleveland, OH.

Suner, S., M. R. Fellows, et al. (2005). "Reliability of signals from a chronically implanted, silicon-based electrode array in non-human primate primary motor cortex." IEEE Trans Neural Syst Rehabil Eng **13**(4): 524-41.

Voigt, T., T. Opitz, et al. (2005). "Activation of early silent synapses by spontaneous synchronous network activity limits the range of neocortical connections." J Neurosci **25**(18): 4605-15.

Williams, J. C., J. A. Hippensteel, et al. (2007). "Complex impedance spectroscopy for monitoring tissue responses to inserted neural implants." J Neural Eng **4**(4): 410-23.

Zhang, Y. H., X. X. Chi, et al. (2008). "Brain-derived neurotrophic factor enhances the excitability of rat sensory neurons through activation of the p75 neurotrophin receptor and the sphingomyelin pathway." J Physiol **586**(13): 3113-27.

APPENDIX A
IDENTIFICATION OF GRAFTED NEURAL STEM CELLS IN VIVO

In Chapter 4, mouse-derived neural stem cells were implanted into rats, and the murine-specific marker M2 was used to identify the cells in vivo. M2 "staining" was observed in NSC-seeded probes from several animals at multiple time points, but not in control probes. However, control slides wherein the primary antibody was omitted revealed sufficient background to invalidate these results (Figure A.1) from all animals except for those from the 1 day time point. The positive identification of the cells at this time was further validated by their location within a still intact alginate scaffold. The source of the background problem is believed to be the use of the M2 antibody, which is raised in rat and necessitates the use of an anti-rat IgG secondary on rat tissue experiencing an immune response. While this exact method has been used to detect murine NSCs in a rat model in published literature (Teng, Lavik et al. 2002; Deshpande, Kim et al. 2006), there was no accompanying discussion or evidence of background problems presented, and attempts to contact the authors regarding this issue received no response. Alginate and parylene often brightly autofluoresced in green and blue respectively, which allowed visualization of these structures, but at times further obscured the M2 signal. Several attempts using multiple batches of the M2 antibody were made, with secondary antibodies with different emission spectra, but background staining was an issue in each trial.

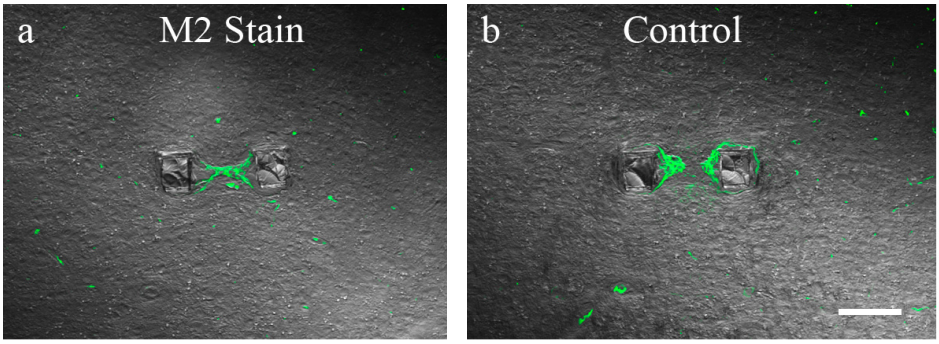

Figure A.1. An example of M2 staining (green) in an animal at the 6 week time point (a), and a control image from a different section in the same animal where the primary antibody was omitted (b). Note the similarity in staining patterns, and the location of staining at the graft site. Images include the DIC channel to facilitate visualization of the probe. Scale = 100 microns.

A search for alternative mouse-specific antibodies did not reveal viable options. The rat anti-mouse thy1.2 antibody, which is specific for most mouse neurons, was tested. Again, an anti-rat secondary was necessitated, and staining appeared similar to controls wherein the antibody was omitted (Figure A.2). There may have been relatively few graft-derived differentiated neurons, which would make detection of these cells with this antibody unlikely.

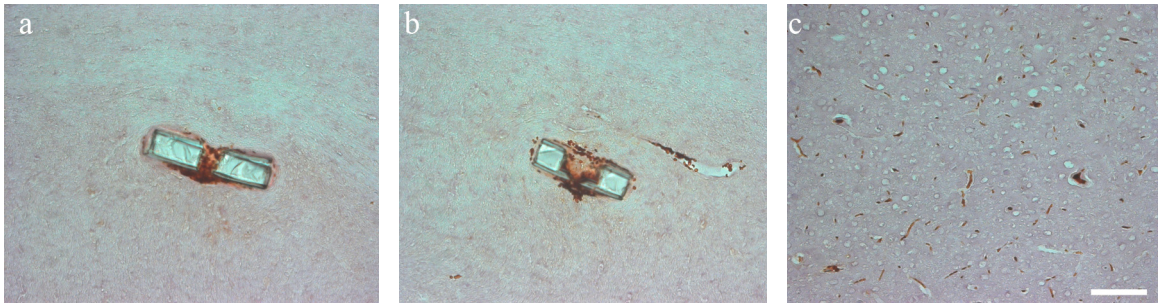

Figure A.2. Thy1.2 staining reveals similar positive (brown) patterns in a probe in which the primary is included (a) and omitted in the place of buffer (b). The cells being labeled are likely part of the immune response to the implant, and stain vascular elements throughout the brain tissue (c). Scale = 100 microns.

Therefore, we cannot claim detection of graft cells at time points later than 1 day post-implantation, and improved methods in the future may more accurately assess their existence and differentiation status *in vivo*. Potential methods in the future (one of which will be used in an upcoming study with functionalized parylene probes seeded with neural stem cells) will pre-label the cells prior to implantation. Genetic engineering with fluorescent proteins, the use of quantum dots, and magnetic resonance imaging of cells labeled with iron oxide nanoparticles are all options (Chapman, Oparka et al. 2005; Sykova and Jendelova 2007).

Acknowledgements

Special thanks to Dr. Jack Parent for his helpful suggestions regarding NSC detection.

References

Chapman, S., K. J. Oparka, et al. (2005). "New tools for in vivo fluorescence tagging." Curr Opin Plant Biol **8**(6): 565-73.

Deshpande, D. M., Y. S. Kim, et al. (2006). "Recovery from paralysis in adult rats using embryonic stem cells." Ann Neurol **60**(1): 32-44.

Sykova, E. and P. Jendelova (2007). "In vivo tracking of stem cells in brain and spinal cord injury." Prog Brain Res **161**: 367-83.

Teng, Y. D., E. B. Lavik, et al. (2002). "Functional recovery following traumatic spinal cord injury mediated by a unique polymer scaffold seeded with neural stem cells." Proc Natl Acad Sci U S A **99**: 3024-9.

APPENDIX B
NEURAL PROSTHESIS SCHEMATICS

Views of the recording neural prostheses used in Chapter 5 are shown below (www.neuronexustech.com):

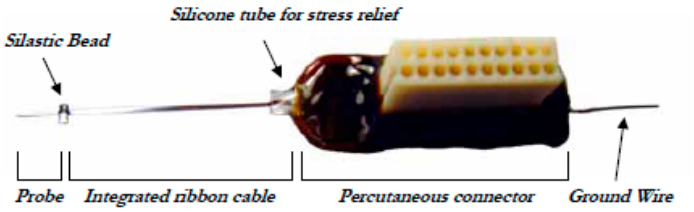

Figure B.1. Chronic neural probe assembly.

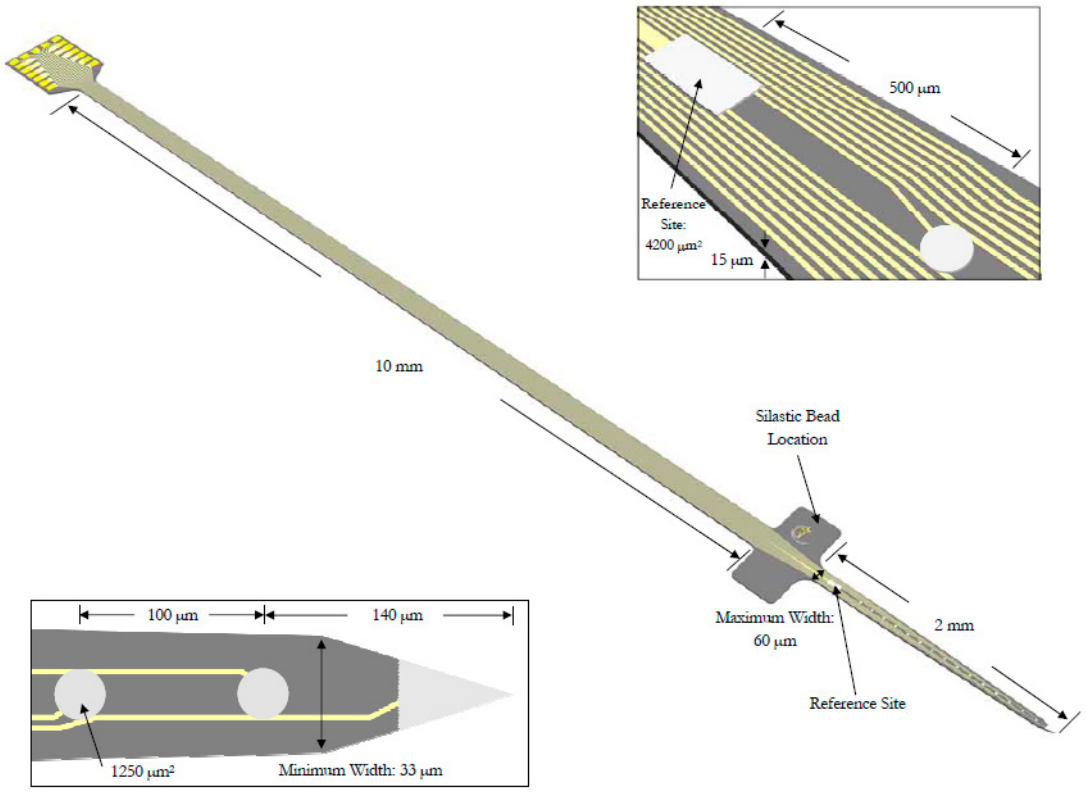

Figure B.2. Probe schematic for devices used in Chapter 5 research. Single shank, sixteen channel probes were used.

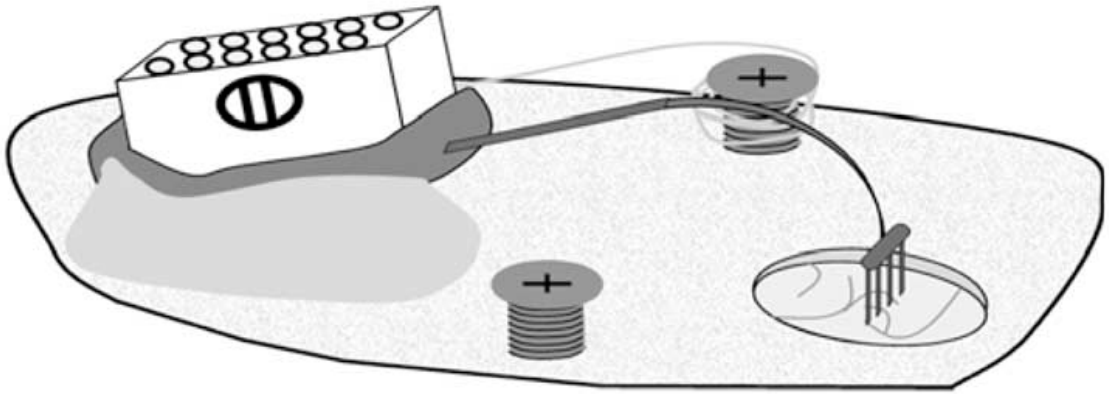

Figure B.3. Illustration of probe insertion (a four shank model is shown) into the craniotomy. The connector is attached to a stainless steel bone screw with dental acrylic, and the ground wire is wrapped around an additional screw. Following GelFoam and silicone closure of the craniotomy, the entire region is encased in dental acrylic, leaving only the connector exposed. From Vetter, Williams et al. 2004.

Reference

Vetter, R. J., J. C. Williams, et al. (2004). "Chronic neural recording using silicon-substrate microelectrode arrays implanted in cerebral cortex." IEEE Trans Biomed Eng **51**(6): 896-904.

APPENDIX C
SELECTED CHAPTER 4 & 5 IMAGES AT HIGHER MAGNIFICATION

Figure C.1. Doublecortin staining, p. 116. Doublecortin (red), NeuN (green), and Hoechst (blue). Scale = 50 microns.

Panel b, neural stem cell (NSC)-seeded.

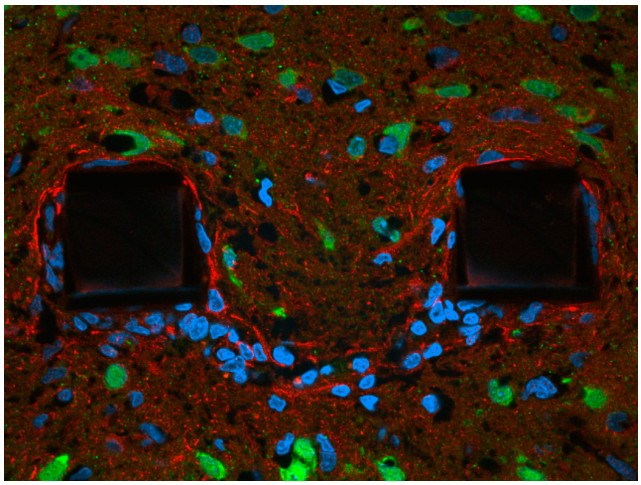

Panel e, control.

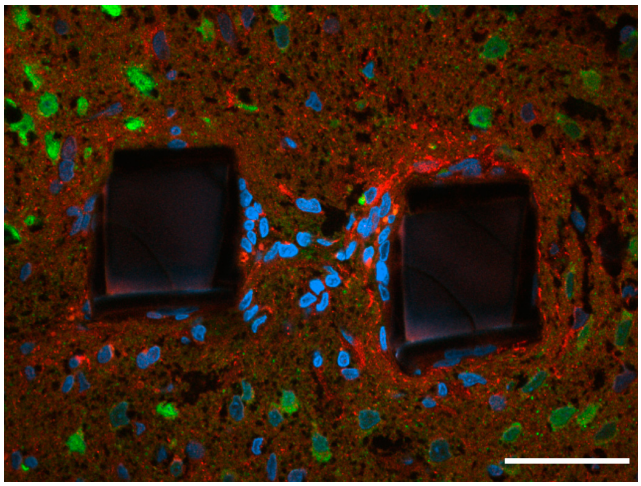

Figure C.2. One week neuronal images, p. 113. NeuN (green), neurofilament (red), and Hoechst (blue). Scale = 50 microns.

NSC-seeded.

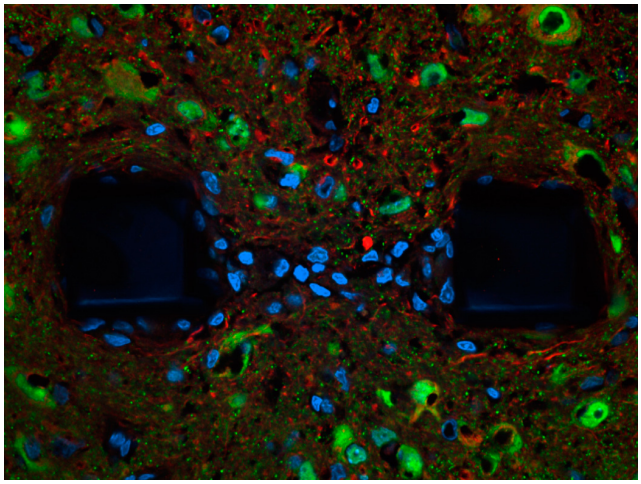

Alginate.

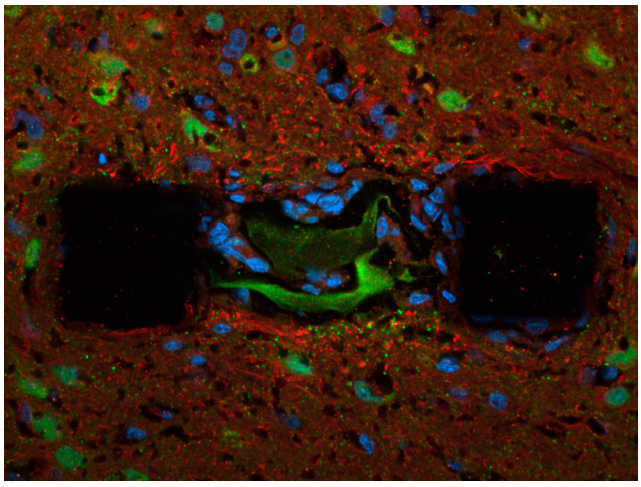

Control probe.

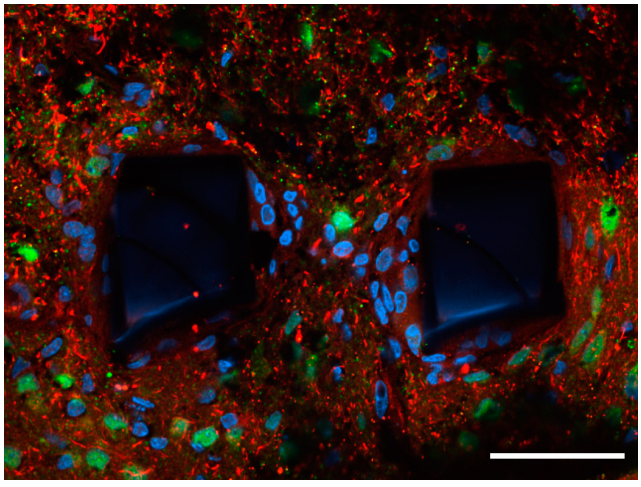

Figure C.3. Three month neuronal images, p. 113. NeuN (green), neurofilament (red), and Hoechst (blue). Scale = 50 microns.

NSC-seeded.

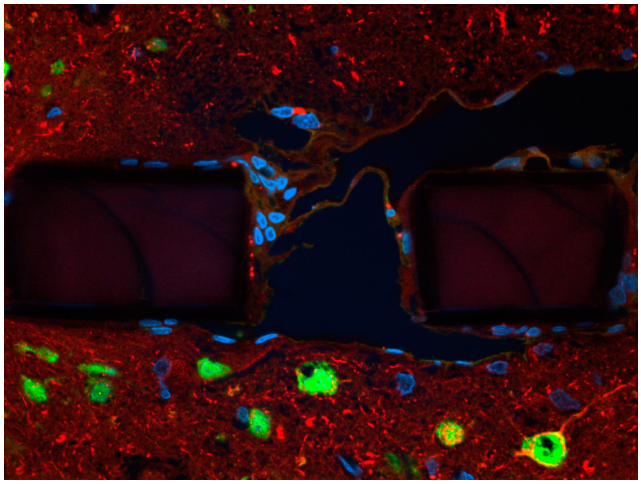

Alginate.

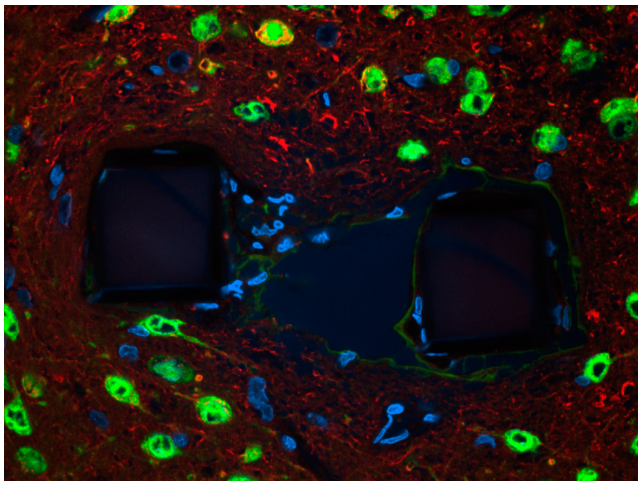

Control probe.

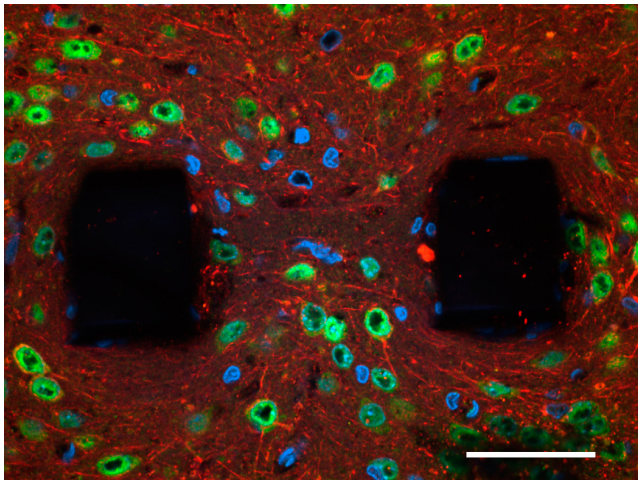

Figure C.4. One week glial images, p. 109. Ox-42 (green), GFAP (red), Hoechst (blue). Scale = 50 microns.

NSC-seeded.

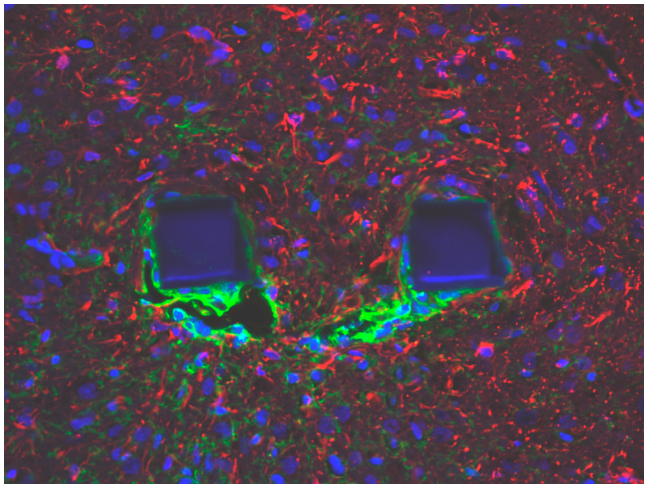

Alginate.

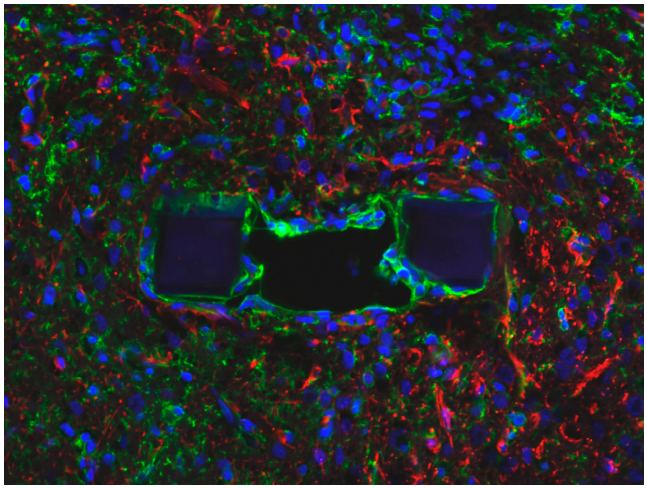

Control probe.

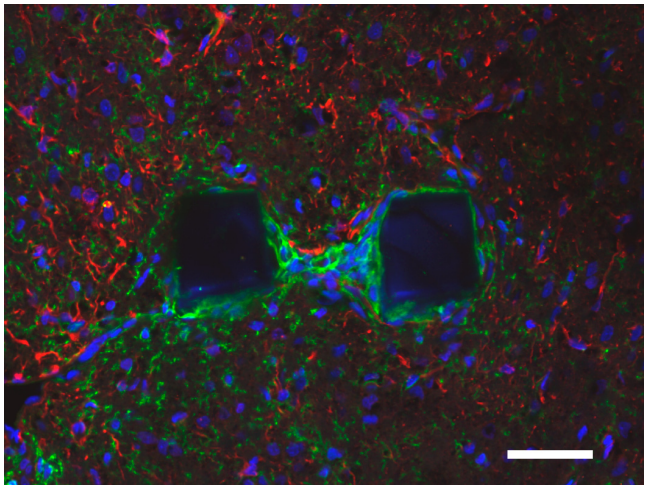

Figure C.5. Three month glial images, p. 109. Ox-42 (green), GFAP (red), Hoechst (blue). Scale = 50 microns.

NSC-seeded.

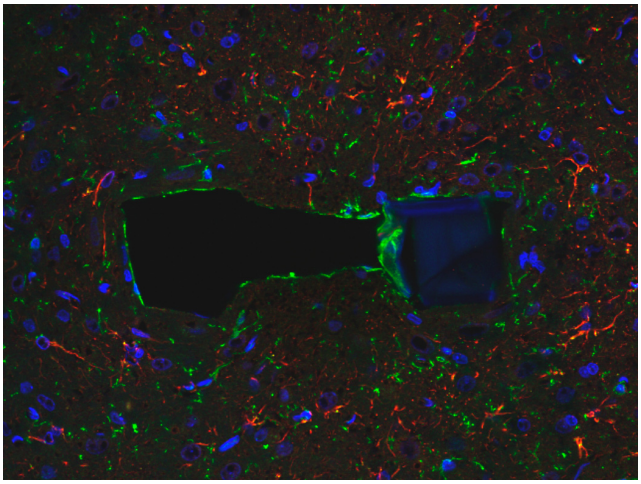

Alginate.

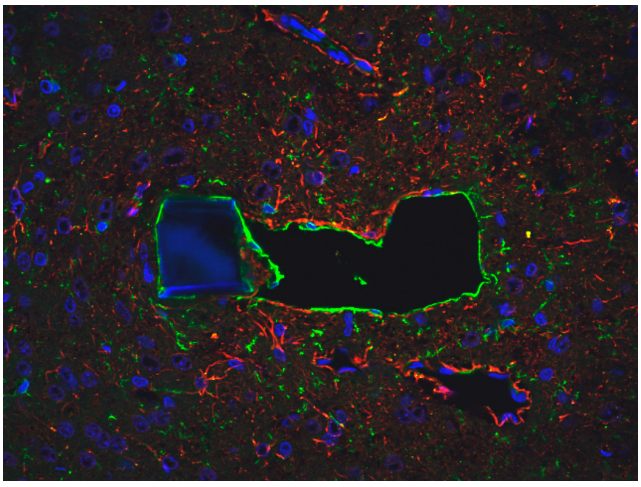

Control probe.